Lawrence Berkeley Laboratory
UNIVERSITY OF CALIFORNIA

Materials & Chemical Sciences Division

Spectroscopy and Reaction Kinetics of HCO

Y. Guo
(Ph.D. Thesis)

January 1989

Prepared for the U.S. Department of Energy under Contract Number DE-AC03-76SF00098.

DISCLAIMER

Spectroscopy and Reaction Kinetics of HCO

By

Yili Guo

B.S. (Fudan University) 1982

DISSERTATION

Submitted in partial satisfaction of the requirements for the degree of

DOCTOR OF PHILOSOPHY

in

CHEMISTRY

in the

GRADUATE DIVISION

of the

UNIVERSITY OF CALIFORNIA at BERKELEY

Approved:

G. Bradley Moore 25 January, 1989
Chair Date

Hugh S. Johnston 26 January 1989

Franklin Hurlbut 27 January 1989

****

SPECTROSCOPY AND REACTION KINETICS OF HCO

Yili Guo

ABSTRACT

The high resolution infrared spectrum of the C-H stretching fundamental of HCO has been studied by means of infrared flash kinetic spectroscopy. HCO was generated by flash photolysis of acetaldehyde or formaldehyde using a 308 nm (XeCl) excimer laser. The transient absorption was probed with an infrared difference frequency laser system. The high resolution spectra obtained were assigned and fitted with rotational, spin-rotational, and centrifugal distortion constants. The υ_1 band origin is 2434.48 cm^{-1}. New ground state constants have been derived from a least-squares fit combining the υ_1 data with previous microwave and FIR LMR measurements. A new set of spectroscopic constants for the (1,0,0) state, the equilibrium rotational constants, and the orientation of the transition dipole moment are also reported.

The kinetics and product branching ratios of the HCO + NO_2 reaction have been studied using visible and infrared laser flash kinetic spectroscopy. The rate constant for the disappearance of HCO radical at 296 K is

$(5.7 \pm 0.9) \times 10^{-11}$ cm^3 $molec^{-1}$ sec^{-1}, and it is independent of the pressure of SF_6 buffer gas up to 700 torr. Less than 10% of the reaction goes through the most exothermic product channel, HNO + CO_2. The product channel, H + CO_2 + NO, is responsible for 52% of the reaction. HONO has been observed, though not quantitatively, as a reaction product corresponding to the HONO + CO channel.

C B Moore

ACKNOWLEDGEMENTS

I am very grateful to Brad for his guidance and support during my time at Berkeley. His enthusiasm for science is most impressive and has constantly inspired me. I especially appreciate the way he helps his students develop fully and prepare for the future.

Many people have provided assistance during the course of this work. Thanks are especially due to Andy Kung and Bill Green for solving laser problems and helpful discussions. Andy has also helped me improve my performance at the bridge table. Thanks go to Dr. Martin Ochsner, Prof. Bob Curl, and Brent Dane, with whom I collaborated for the spectroscopy part of this work.

I have enjoyed playing on the Moorons softball team. Thanks go to Eric, David, Tom, I-Chia, Charles, Young, Art, Ramon, and many people who have left the group for teaching me the game and being good friends.

Chi-Ke is thanked for being such wonderful company for the last four months. Walking between home and school and having dinner together have been very enjoyable, and I have learned a lot from her.

Help given by Jackie on various occasions is much appreciated. Thanks are also due to people who have helped on my English composition, especially Karen, Charles, and Bill.

Ken has helped on numerous things. I am in debt to him for his love, patience, and encouragement. I am most fortunate to have known him at Berkeley and to have him as a lifetime friend.

Lastly, but not at all least, I would like to thank my parents and brothers. I cannot say enough about the support, encouragement, and love they have given me.

TABLE OF CONTENTS

TABLE OF CONTENTS

LIST OF FIGURES

LIST OF TABLES

Part I.

Infrared Flash Kinetic Spectroscopy of HCO

1. Introduction

It is well known that HCO radical plays an important role in atmospheric photochemical reactions[1] and combustion processes[2]. Since the hydrocarbon flame bands between 250 and 410 nm were first observed and HCO was considered to be responsible for these emission bands[3-5], the spectroscopy of HCO in ultraviolet (UV), visible, infrared (IR), far infrared (FIR), and microwave regions has been studied extensively. Three excited electronic states (A, B, and C states) have been characterized[6-8]. It has been shown that the visible absorption of HCO from 900 to 450 nm corresponds to the transition between the bent $\tilde{X}^2A'$ and the linear $\tilde{A}^2A''$ states, which are split by the Renner-Teller interaction[9-12]. The vibrational bands of HCO were first observed in low temperature matrices[7,8,13,14]. Two of these infrared absorption bands (C-O stretching and bending) were studied in the gas phase more recently using laser Stark spectroscopy[15] and laser magnetic resonance (LMR)[16-20]. Pure rotational spectroscopy of HCO has been investigated by a number of groups[21-27], and the rotation constants for HCO in the ground vibronic state have been derived[27]. Most of the rotational and vibrational spectroscopic studies of HCO carried out before 1986 have been reviewed by Hirota[28].

The spectroscopic work on HCO has provided some information needed for determining its molecular constants and for calculating its force fields[7,28-30]. Those investigations have also made it possible to study the reactions of HCO[31] and the dissociations of aldehydes[32] by monitoring HCO spectroscopically. Recently Tjossem et al.[33] have reported resonance-enhanced multiphoton ionization spectra of HCO, which provide a new method for monitoring HCO with high sensitivity in reaction environments. Since the levels with $K_a'>0$ in the $\tilde{A}$ state of HCO predissociate[10,11,34], the fluorescence from $\tilde{A}$ state ($\tilde{A}^2A'' \leftarrow \tilde{X}^2A'$ excitation) cannot be used to monitor the concentration of HCO in states with $K_a' \neq 0$.

HCO is particularly interesting structurally and chemically because of its unsually weak and anharmonic C-H bond. Formaldehyde photodissociation experiments indicate that the C-H bond energy in HCO is only 15.6 kcal mol^{-1} [35]. When Ewing et al. first observed the C-H stretching fundamental at 2493 cm^{-1} in a CO matrix, they could not believe that this C-H streching frequency was so much lower than those in stable molecules, and therefore only mentioned it as a possible assignment. Later Milligan and Jacox observed this band both in CO matrix (2488 cm^{-1}) and Ar matrix (2483 cm^{-1}) and confirmed the assignment.

Recently E.K.C. Lee and coworkers were able to observe the dispersed fluoresence of HCO (Ã state) using visible laser excitation and reported the C-H stretching frequency at 2432 ± 20 cm^{-1}[36]. Lineberger's group has also reported the band center of 2440 ± 20 cm^{-1} for the C-H stretching. by studying the photoelectron spectroscopy of HCO^-[37].

The C-H stretching fundamental has not been previously studied at high resolution in the gas phase, although the high resolution spectroscopy of the other two fundamental vibrations of HCO has been explored to some extent. The bending fundamental (1080.76 cm^{-1}) has been observed by LMR[16] and laser Stark spectroscopy[15] and the C-O stretching fundamental (1868.17 cm^{-1}) has been observed by LMR[18,20]. All of these studies probe only small portions of a vibration-rotation band near a fixed-frequency laser source. The data consequently contain little information on the energy differences between levels with different K_a quantum numbers. A broadly tunable IR difference frequency laser was used in this work to record a large part of the C-H stretching vibration-rotation band at high resolution. The analysis of the spectrum recorded using the IR difference frequency spectrometer (Berkeley) and the diode laser spectrometer (by Dane et al. at Rice University) completes the high resolution determination of the fundamental vibrational

frequencies of HCO and provides improved constants for rotation about the a-axis.

2. Experimental

2.1 Laser System and Optical Arrangement

The difference frequency laser kinetic spectroscopy apparatus is shown in Figure I-1. HCO was generated by photolyzing formaldehyde or acetaldehyde. The photolysis cell (156 cm long, 2.5 cm in diameter) was made of pyrex and the windows were infrasil plates. The photolysis source was an excimer laser (Lambda Physik/EMG 103E) operated on the XeCl (308 nm) line at 60 Hz with a pulse energy of 30-40 mJ. The probe was an IR difference frequency laser system. The output of a single mode, cw Ar^+ laser (Lexel/95-4; 1 W at 524.5 nm) was combined with an Ar^+ laser pumped, tunable, single mode, cw ring dye laser (Spectra-Physics 171-06/380) and focused onto a temperature-phase-matched $LiNbO_3$ crystal. The infrared difference frequency laser thus generated is tunable from about 4.2 to 2.4 μm. The details about the set-up and the operation of the difference frequency laser system have been described in Reference 38. R6G dye was used in the ring dye laser in this experiment. The IR light generated has a linewidth of about 0.0007 cm^{-1}.

The probe and photolysis laser beams were combined

Figure I-1. Schematic diagram of the infrared difference frequency laser spectrometer.

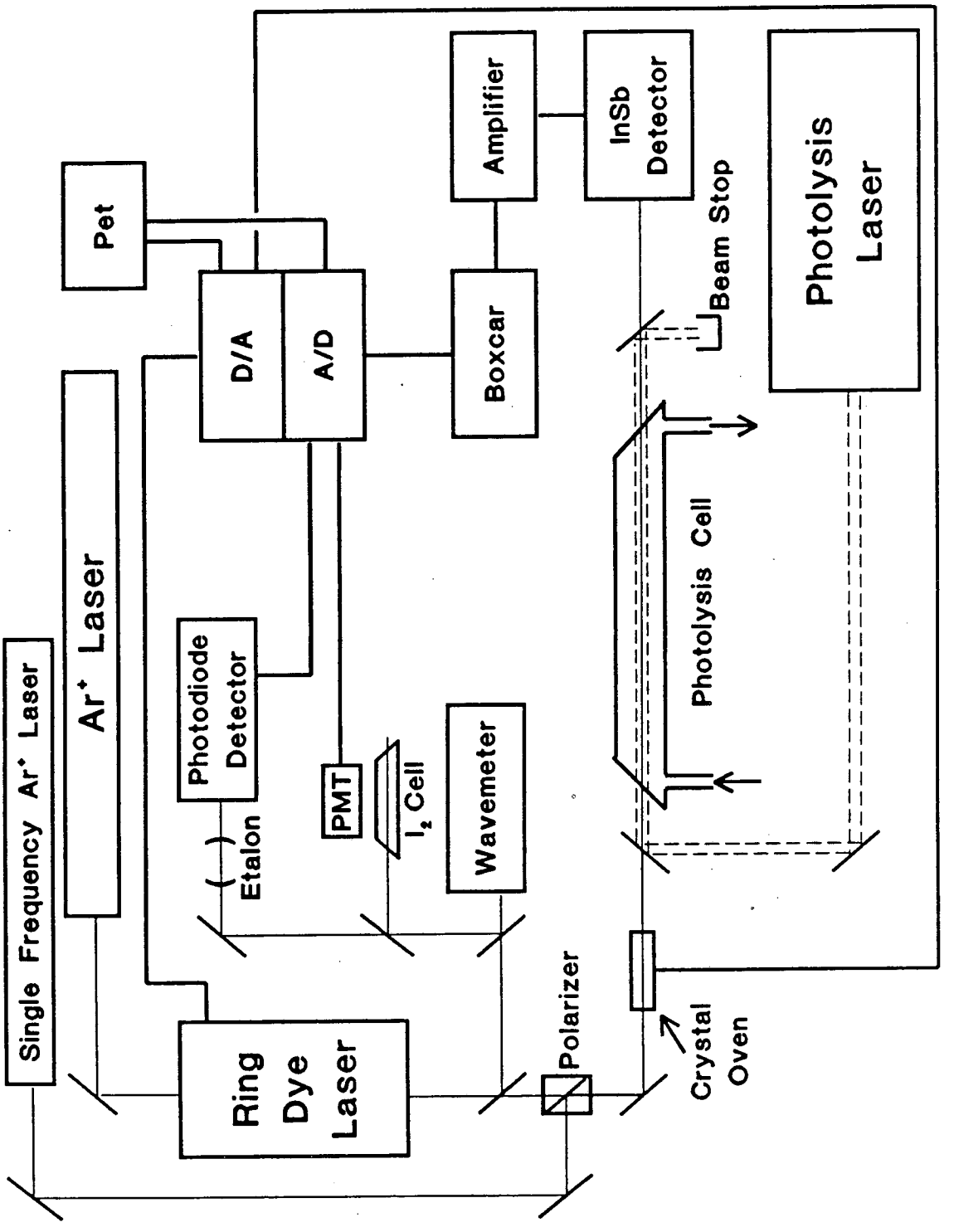
Single Frequency Ar⁺ Laser
Ar⁺ Laser
Ring Dye Laser
Pet
D/A
A/D
Boxcar
Amplifier
InSb Detector
Photolysis Laser
Beam Stop
Photolysis Cell
Photodiode Detector
Etalon
PMT
I₂ Cell
Wavemeter
Polarizer
Crystal Oven

with a UV-reflecting and IR-transmitting sapphire mirror and propagated colinearly through the photolysis cell. Both UV photolysis and IR difference frequency laser beams were focused at the center of the photolysis cell in order to increase the signal amplitude. At the focal point, the diameter of the UV beam was about 2 mm and that of the IR beam was about 1 mm. The photolysis cell was moved away from the beam path when the alignment was carried out. With one aperture placed at the position of each end of the photolysis cell, and one at the center position of the photolysis cell, the UV and the IR laser beams were carefully overlapped. The deviation of the overlapping of the two beams by the infrasil window at the input end when the cell was placed back in the beam was very small. The alignment was optimized by setting the IR laser at the resonance frequency of a known transition of the sample and maximizing the absorption signal. The photolysis and the probe laser beams, after going through the photolysis cell and emerging, were separated by another UV-reflecting IR-transmitting sapphire mirror. A narrow-band IR filter was used to eliminate broad-band IR emission from the excimer discharge.

The absorption coefficients of formaldehyde and acetaldehyde at 308 nm are $(3.2 \pm 0.4) \times 10^{-4}$[39] and $(1.07 \pm 0.02) \times 10^{-3}$ cm^{-1} $torr^{-1}$[40]. The quantum yields

for forming HCO are 0.76[41] and 0.862[39] respectively. Typically 10^{14} to 10^{15} molec cm^{-3} HCO were produced for each photolysis shot. The strongest transitions corresponded to about 10% attenuation of the IR laser power for concentrations approaching 10^{15} cm^{-3}.

2.2 Data Acquisition

The IR probe was detected by an InSb (77 K) detector. The resulting signal was amplified by two low-noise amplification stages (Perry/497 and Keithley/104). The signal was then integrated by a dual channel boxcar integrator (PAR 162/164) with a 60 μsec gate and 50 μsec input time constant. The signal gate (of the boxcar) opened 1 μsec after the reference gate closed. The excimer laser fired during the 1 μs time interval, approximately 500 ns before the opening of the signal gate. After each photolysis pulse the difference between the two boxcar signals was read by a microcomputer A/D and digitally averaged over 25 shots for each frequency increment (0.0015 cm^{-1}). The signal-to-noise ratio was improved by a factor of about 10 by using the dual gate arrangement for the boxcar integrator compared to a single gate.

Under the experimental conditions used in this work, the principal loss mechanism for HCO was the disproportionation of two HCO molecules to produce CO and H_2CO. The decay of HCO monitored at 2531.48 cm^{-1}, which corresponds to the blended $^qR_2$ transitions, is shown in Figure I-2. The diffusion of HCO out of the probe beam was another possible source of signal loss.

Overlapping scans of 3 cm^{-1} each were recorded to give a continuous spectrum of 200 cm^{-1} including some 750 observed absorption lines corresponding to the C-H stretching vibration in HCO. Figure I-3 shows the observed spectrum reconstructed by plotting the line positions and the intensities measured in terms of signal-to-noise ratio.

The fluorescence excitation spectrum of iodine vapor excited by the ring dye laser was measured simultaneously as the HCO spectrum was recorded. The frequencies of the iodine spectrum have been accurately determined and tabulated[42]. The HCO line positions were determined by using the iodine peaks as the reference. The instability of the single frequency Ar^+ laser limits the accuracy to ± 0.01 cm^{-1}.

Figure I-2. Decay of HCO monitored through the absorption of blended $^{q}R_{2}$ lines at 2531.48 cm^{-1}. Acetaldehyde pressure = 4.59 torr. The signal was averaged over 192 shots. Excimer laser pulse energy = 35 mJ.

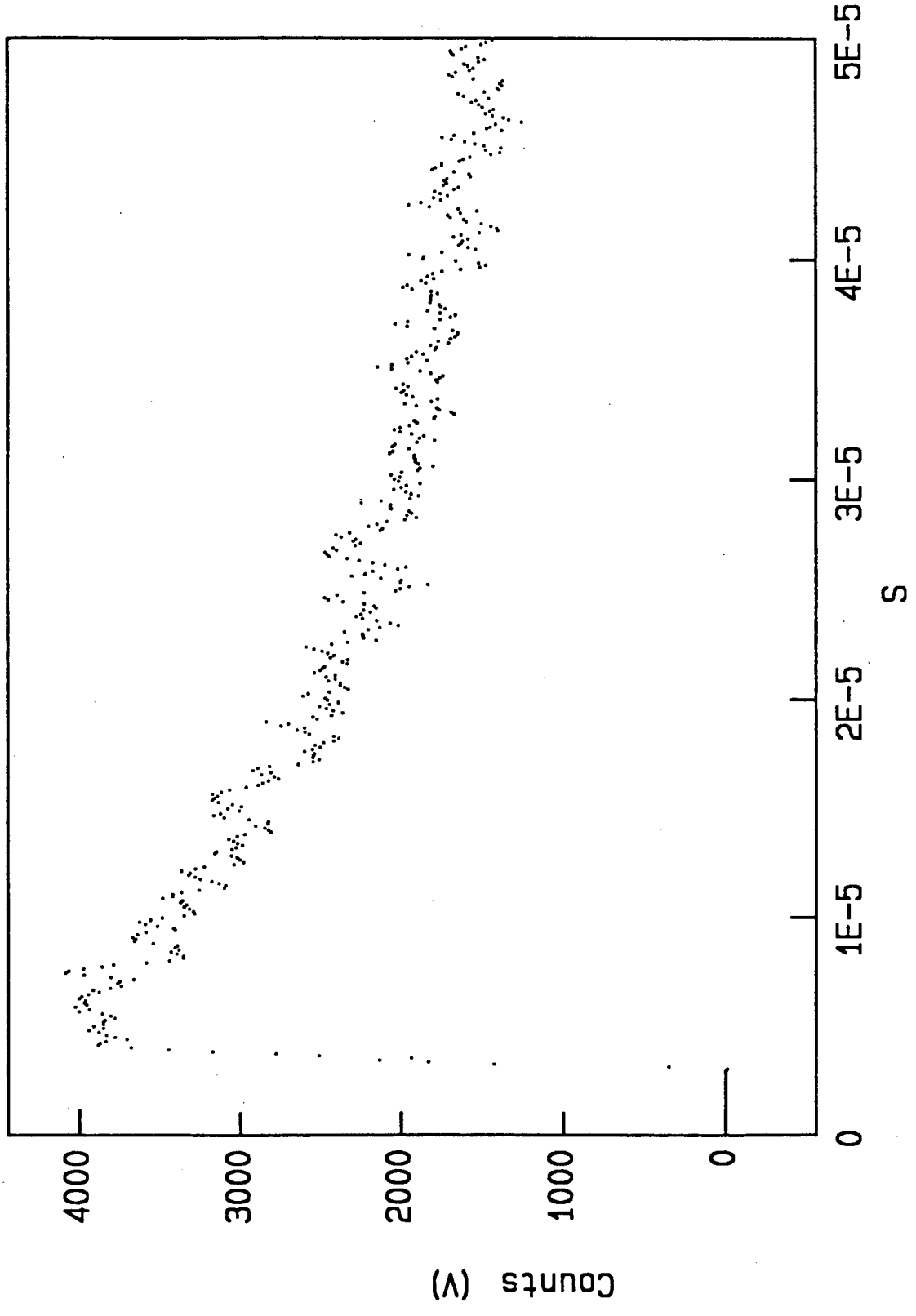
Counts (V)
4000
3000
2000
1000
0
0
1E-5
2E-5
3E-5
4E-5
5E-5
S

Figure I-3. All the observed C-H stretching fundamental transitions using the IR flash kinetic difference frequency laser spectrometer. The plot is a reconstruction of the experimental data; it shows the line positions and the intensities in terms of the signal-to-noise ratio.

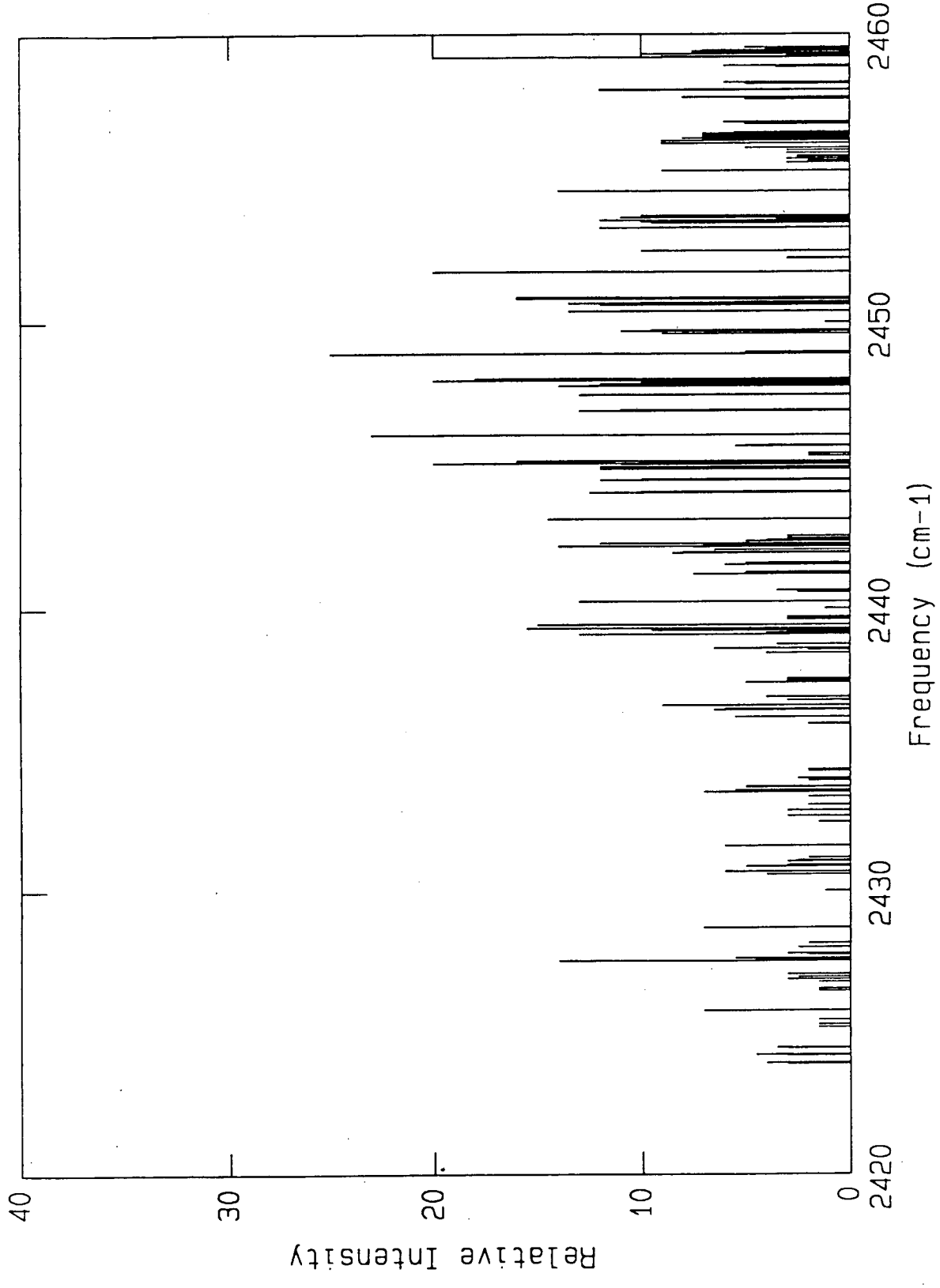
Relative Intensity
0
10
20
30
40
2420
2430
2440
2450
2460
Frequency (cm-1)

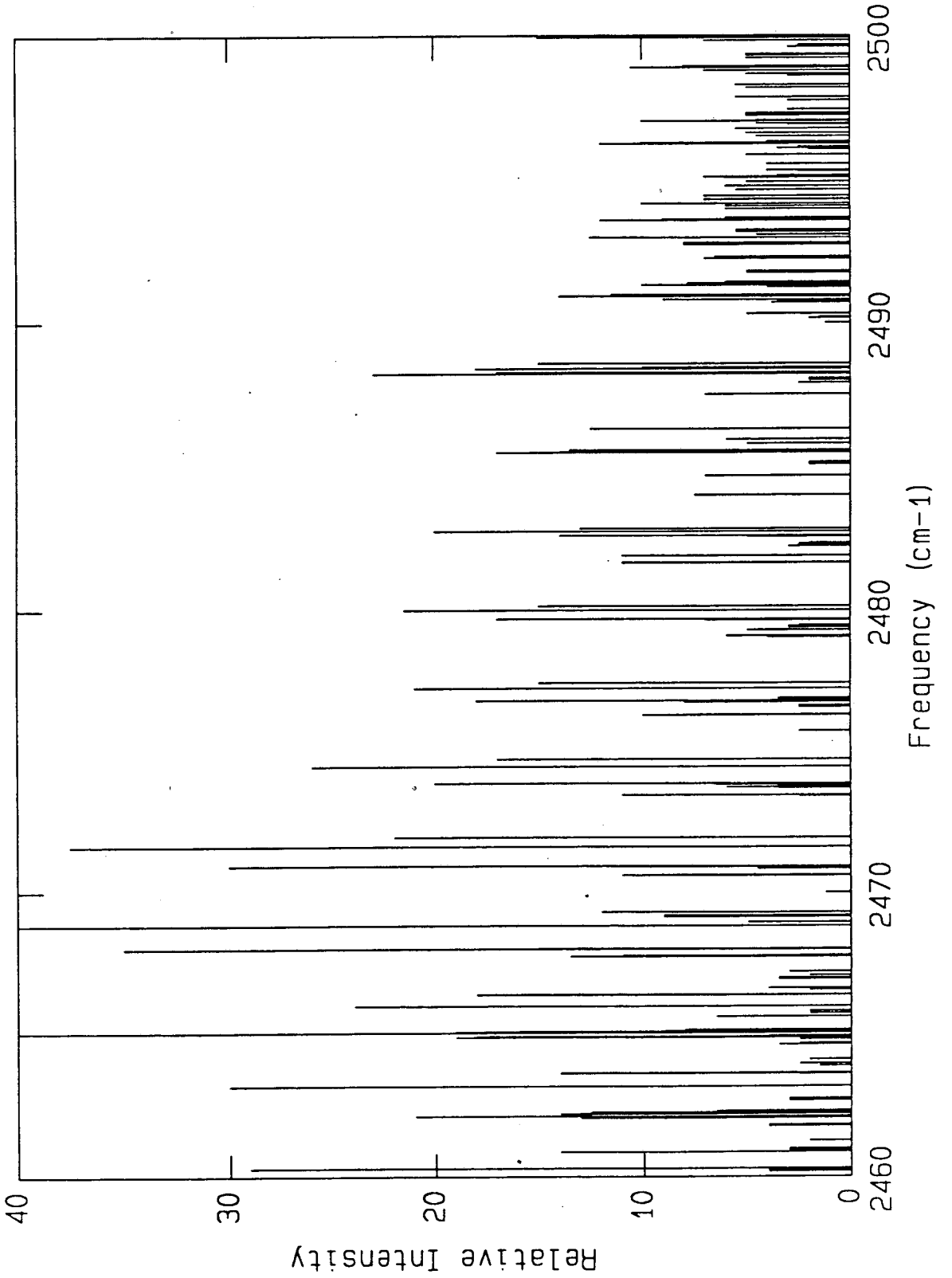
Relative Intensity
0
10
20
30
40
2460
2470
2480
2490
2500
Frequency (cm-1)

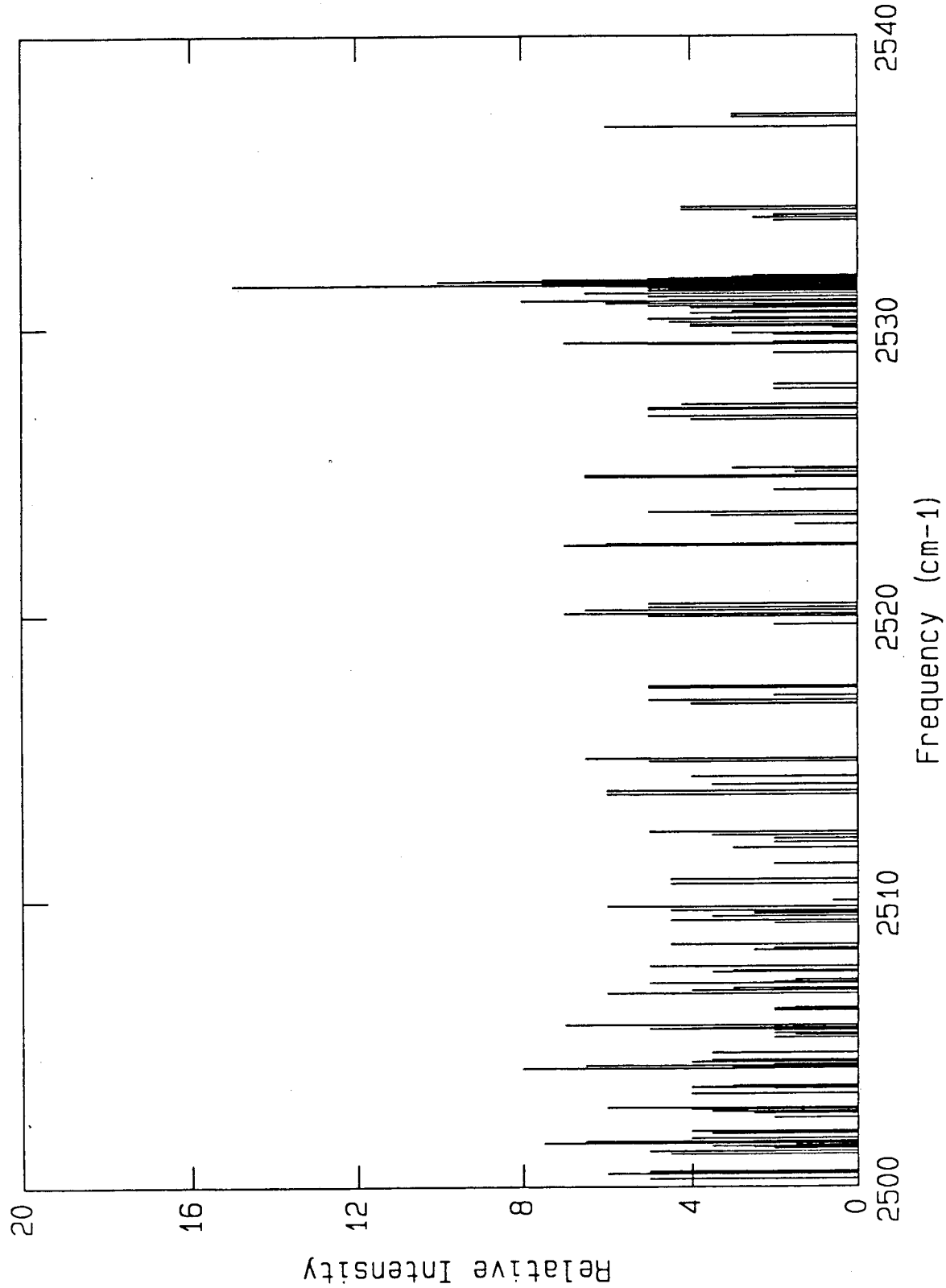
Relative Intensity
20
16
12
8
4
0
2500
2510
2520
2530
2540
Frequency (cm-1)

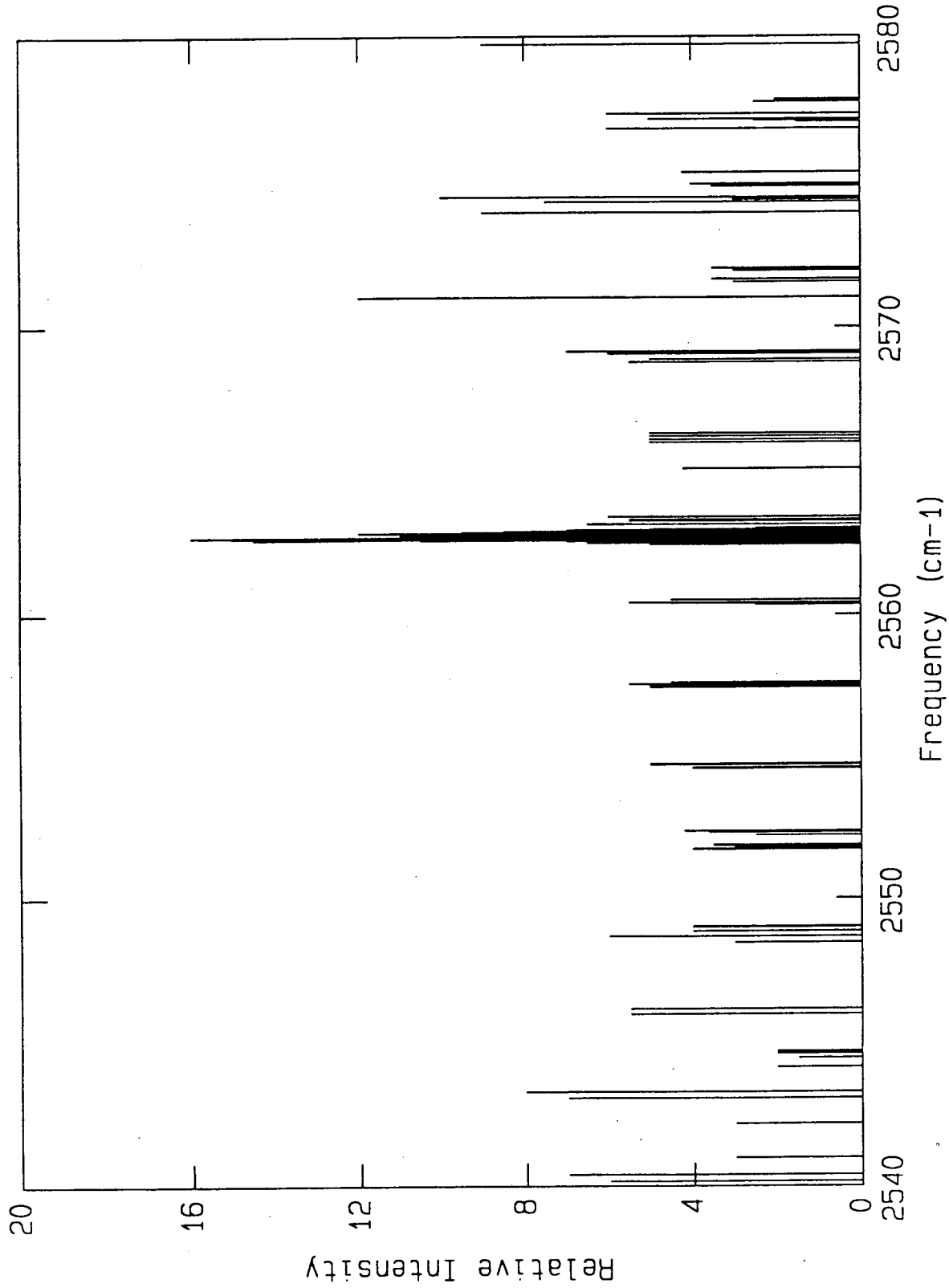
Relative Intensity
20
16
12
8
4
0
2540
2550
2560
2570
2580
Frequency (cm-1)

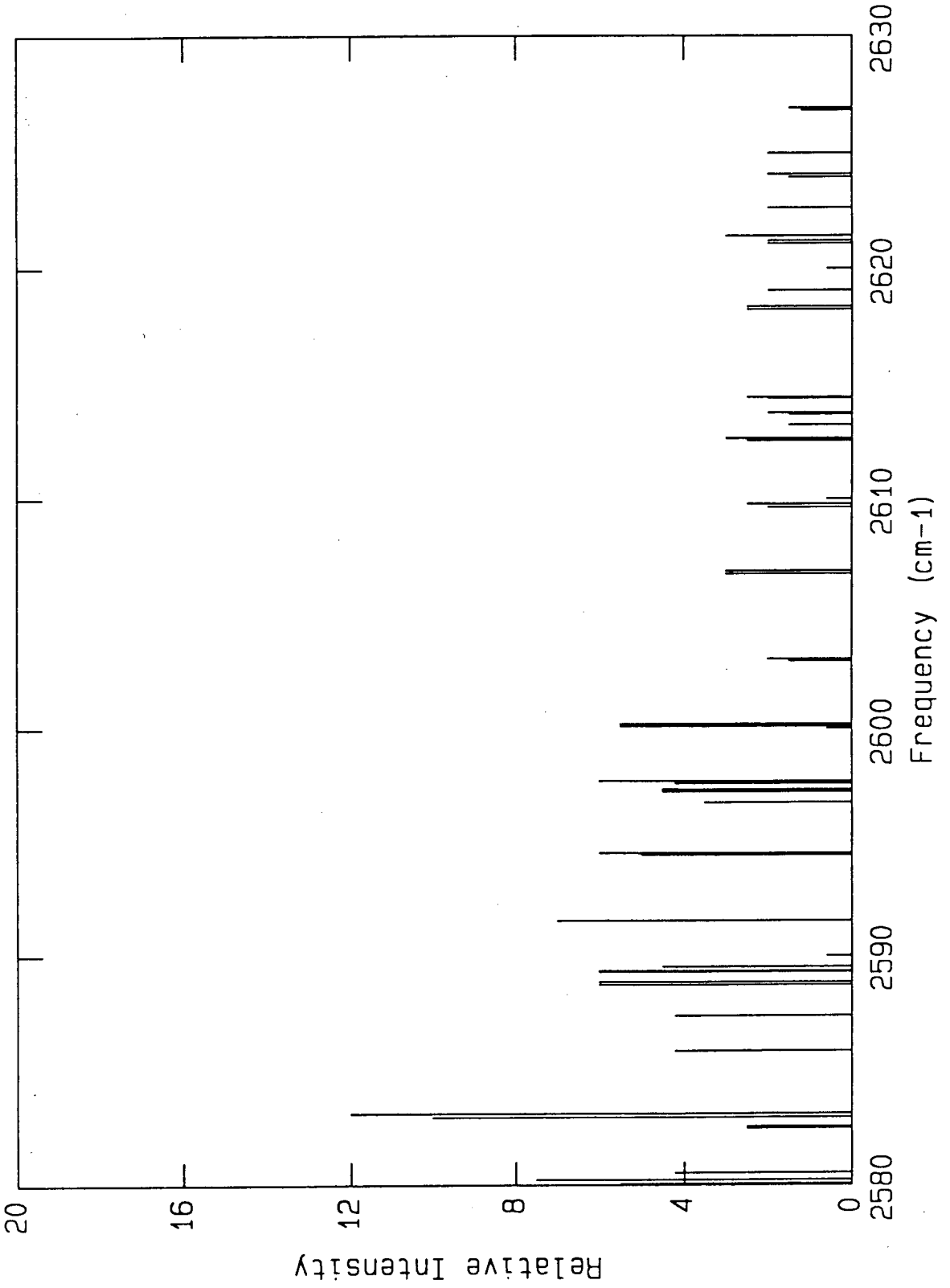
Relative Intensity
0
4
8
12
16
20
2580
2590
2600
2610
2620
2630
Frequency (cm-1)

2.3 Sample Preparation and Handling

Both formaldehyde and acetaldehyde were used as HCO precursors. Formaldehyde was prepared as previously described[43] and stored in a liquid nitrogen trap. Acetaldehyde (Mallinckrodt, min 99%) was purified by several freeze-pump-thaw cycles and kept at 0 °C.

Formaldehyde or acetaldehyde was transferred through a standard vacuum line (background pressure: 10^{-4} to 10^{-5} torr) and continuously flowed through the photolysis cell at about 100 liter/min. Formaldehyde was kept in an ethanol/dry ice cooling bath during the experiments. At -78 °C (dye ice temperature) the vapor pressure of formaldehyde is about 22 torr[44]. The gas pressure in the photolysis cell was 5 or 2.5 torr respectively when formaldehyde or acetaldehyde was used as a precursor. Similar signal-to-noise ratio and identical line positions were obtained for each. A few wavenumbers of the HCO spectrum was obscured by acetaldehyde absorption but observed with formaldehyde.

3. Spectrum Assignment and Fit to Molecular Hamiltonian

3.1 Observations and Spectrum Assignment

The region to be searched for the C-H absorption spectrum in HCO was estimated using the matrix isolation C-H stretching frequency[7] of 2483 cm^{-1} and the C-H stretching frequency estimated from the laser induced fluorescence spectrum[36] of 2432 ± 20 cm^{-1}. The C-H stretching frequency of 2442 cm^{-1} deduced by Jacox after reinterpreting the flame bands was also taken into account[8]. The 2940.09 cm^{-1}[45] transition of singlet methylene produced by photolysis of CH_2CO was used to check and to optimize the optical alignment. A large number of the ^{r}Q-branch and the ^{p}Q-branch transitions of HCO were observed. Unfortunately, the low frequency tuning limit of the difference frequency laser system did not allow the observation of the characteristic a-type Q-branch transitions. This complicated the assignment of the observed spectrum.

Dane et al. at Rice university recorded the spectrum beyond the low frequency end of the difference frequency scans using an IR diode laser system. Although the frequency coverage of diode lasers is very patchy, two

obvious parallel Q-branches were luckily found with the diodes they had. The relative intensity of the second to the first member of each branch suggested that the higher frequency ^{q}Q-branch belonged to K = 3 and the lower frequency one to K = 4. Using the previously measured ground state rotational, spin-rotational, and centrifugal distortion constants[26], P and R-branch lines could be predicted and were identified confirming the K = 3 and 4 parallel Q-branch assignments. The information thus obtained located the approximate positions of the K = 1, 2, and 5 Q-branches. Several lines of the K = 1 Q-branch series and the characteristic four-line patterns of the corresponding P and R-branches were quickly recognized. By fitting Hamiltonian parameters to these lines, many additional lines were predicted and assigned in both difference frequency and diode data. The assignment therefore proved to be quite straightforward. However, since HCO is a doublet and an asymmetric top molecule, the spin and asymmetry splittings made the overall assignments very tedious especially where the lines are congested. The final assignments were checked by combination differences. Figure I-4 shows the K = 3 ← 2 Q-branch region observed with the difference frequency laser system. A complete listing of the observed transition frequencies, assignments, and measured signal-to-noise ratios is given in Table I-1. The absorption lines at

Figure I-4. K = 3 ← 2 perpendicular Q-branches. A total of 25 shots were averaged for each frequency step (0.0015 cm^{-1}). The IR spectrum line widths (0.01 cm^{-1}) are Doppler limited. The subscript + or - in the assignment stands for even or odd K_c" parity respectively. Subscripts are omitted when asymmetry splittings were not resolved.

* Overlapped transitions of 9+, 7-, 15+, 10-, 14-, 11+, 12-, 13+.

** Overlapped transitions of 14-, 13+, 12-, 11+, 10-, 9+, 8-, 7+.

Conditions: Acetaldehyde pressure = 2.5 torr, Photolysis laser pulse energy = 35 mJ, repetition rate = 60 Hz.

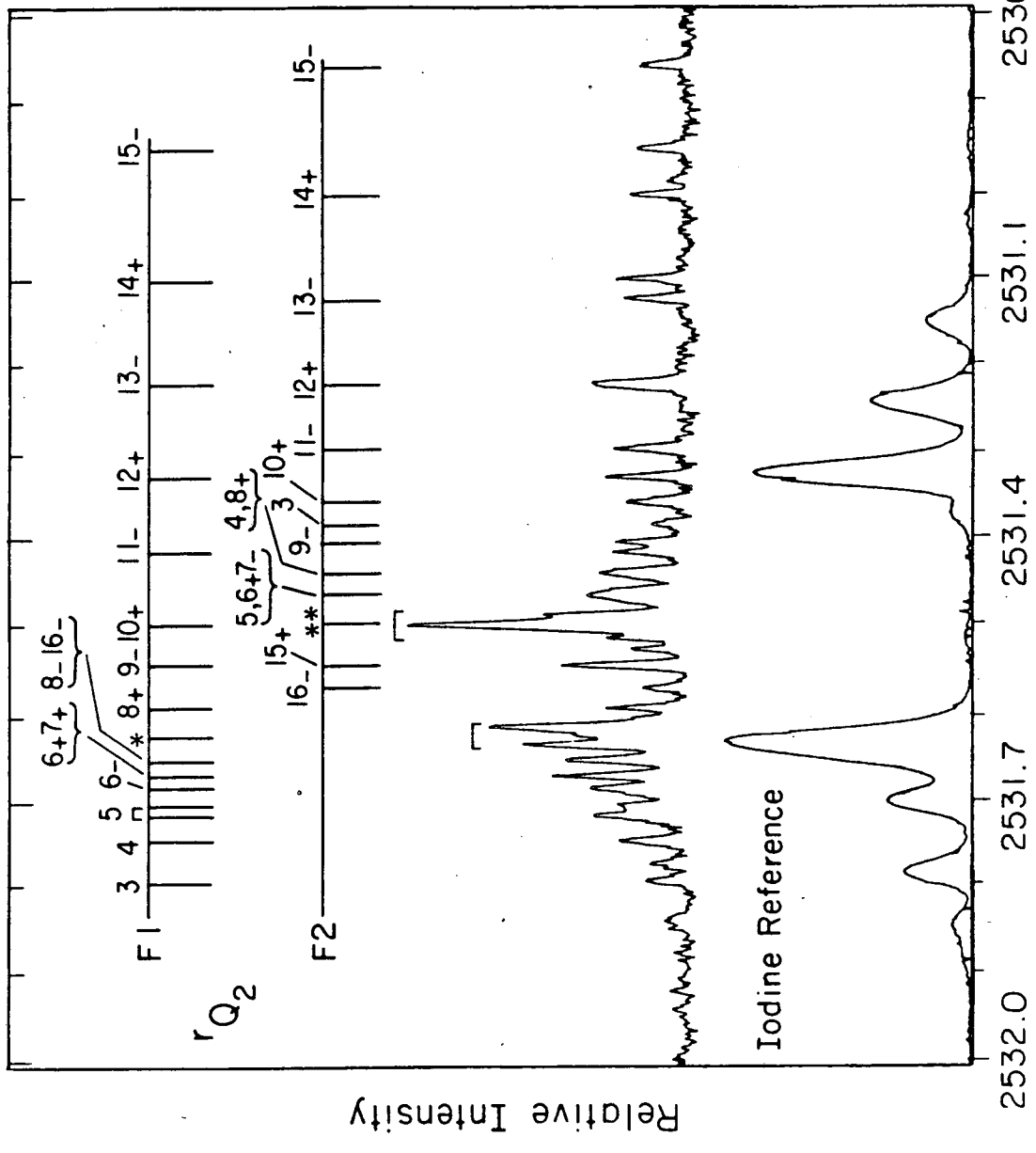
F1
F2
r_{Q_2}
3 4 5 6 7 8 9 10 11 12 13 14 15
6+7+ 8-16-
6- 8+
5,6+7- 4,8+
15+ 3 10+
16- 9- 11-
12+ 13- 14+ 15-
Iodine Reference
Relative Intensity
2532.0 2531.7 2531.4 2531.1 2530.8
IR Difference Frequency (cm^{-1})

Table I-1. Observed IR transition frequencies, assignments†, calculated line strengths, and experimentally observed absorption intensities in terms of the signal-to-noise ratio.

NU	KAU	PU	2*JU	NL	KAL	PL	2*JL	OBS. (CM^{-1})	O-C (CM^{-1})	CAL. INT. ($X10^3$)	OBS. S/N
5	0	-1	9	4	0	1	7	2448.905	7	77	25.0
5	0	-1	11	4	0	1	9	2448.905	9	95	
6	0	1	11	5	0	-1	9	2451.771	2	88	
6	0	1	13	5	0	-1	11	2451.771	4	105	20.0
7	0	-1	13	6	0	1	11	2454.608	-26	97	14.0
7	0	-1	15	6	0	1	13	2454.608	-24	111	
9	0	-1	17	8	0	1	15	2460.311	-32	103	29.0
9	0	-1	19	8	0	1	17	2460.311	-30	115	
10	0	1	19	9	0	-1	17	2463.182	-3	102	30.0
10	0	1	21	9	0	-1	19	2463.182	-1	112	
11	0	-1	21	10	0	1	19	2466.013	-5	98	24.0
11	0	-1	23	10	0	1	21	2466.013	-3	107	
12	0	1	23	11	0	-1	21	2468.837	-3	92	40.0
12	0	1	25	11	0	-1	23	2468.837	-1	100	
13	0	-1	25	12	0	1	23	2471.623	-28	85	37.5
13	0	-1	27	12	0	1	25	2471.623	-25	92	
14	0	1	27	13	0	-1	25	2474.440	-9	77	26.0
14	0	1	29	13	0	-1	27	2474.440	-7	83	
15	0	-1	29	14	0	1	27	2477.227	-6	68	21.0
15	0	-1	31	14	0	1	29	2477.227	-4	73	
16	0	1	31	15	0	-1	29	2480.009	6	59	21.5
16	0	1	33	15	0	-1	31	2480.009	8	63	
17	0	-1	33	16	0	1	31	2482.748	-10	51	20.0
17	0	-1	35	16	0	1	33	2482.748	-7	54	

†N is the quantum number corresponding to angular momentum from end over end rotation of the molecule; KA is the quantum number of angular momentum along the a-axis; P is the parity; J is the total angular momentum ($J = N \pm S$; S represents electron spin angular momentum, 1/2 for HCO). U and L represent upper and lower state, respectively.

18	0	1	35	17	0	-1	33	2485.494	-2	43	17.0
18	0	1	37	17	0	-1	35	2485.494	1	45	
19	0	-1	37	18	0	1	35	2488.219	2	35	23.0
19	0	-1	39	18	0	1	37	2488.219	5	37	
20	0	1	39	19	0	-1	37	2490.922	2	29	14.0
20	0	1	41	19	0	-1	39	2490.922	5	30	
21	0	-1	41	20	0	1	39	2493.605	1	23	12.0
21	0	-1	43	20	0	1	41	2493.605	4	24	
22	0	1	43	21	0	-1	41	2496.273	3	18	12.0
22	0	1	45	21	0	-1	43	2496.273	7	19	
23	0	-1	45	22	0	1	43	2498.917	1	14	10.5
23	0	-1	47	22	0	1	45	2498.917	5	15	
24	0	1	47	23	0	-1	45	2501.541	-1	11	7.5
24	0	1	49	23	0	-1	47	2501.541	2	11	
25	0	-1	49	24	0	1	47	2504.154	5	8	8.0
25	0	-1	51	24	0	1	49	2504.154	9	8	
26	0	1	51	25	0	-1	49	2506.751	14	6	6.0
26	0	1	53	25	0	-1	51	2506.751	18	6	
27	0	-1	53	26	0	1	51	2509.310	5	4	4.5
27	0	-1	55	26	0	1	53	2509.310	9	4	
28	0	1	55	27	0	-1	53	2511.856	1	3	3.0
28	0	1	57	27	0	-1	55	2511.856	5	3	
29	0	-1	57	28	0	1	55	2514.382	-4	2	4.0
29	0	-1	59	28	0	1	57	2514.382	0	2	
30	0	1	59	29	0	-1	57	2516.903	3	2	4.0
30	0	1	61	29	0	-1	59	2516.903	7	2	
1	1	1	3	1	0	-1	3	2455.728	5	67	3.0
2	1	1	5	1	0	-1	3	2461.267	-4	71	2.0
1	1	-1	1	2	0	1	3	2449.597	9	13	9.0
2	1	-1	3	2	0	1	3	2455.663	9	70	2.0
2	1	-1	5	2	0	1	5	2455.795	2	108	2.5
3	1	-1	5	2	0	1	3	2463.900	-8	62	1.5
3	1	-1	7	2	0	1	5	2463.989	-3	88	2.5
3	1	1	5	3	0	-1	5	2455.827	2	106	2.5
3	1	1	7	3	0	-1	7	2455.920	-5	143	3.0
4	1	1	7	3	0	-1	5	2466.589	-16	79	2.0
4	1	1	9	3	0	-1	7	2466.653	-13	102	4.0
4	1	-1	7	4	0	1	7	2456.023	-8	137	3.0
4	1	-1	9	4	0	1	9	2456.107	-5	172	5.0
6	1	-1	11	6	0	1	11	2456.593	12	181	7.0
6	1	-1	13	6	0	1	13	2456.638	-6	211	5.5
7	1	1	13	7	0	-1	13	2456.932	1	193	5.0
7	1	1	15	7	0	-1	15	2456.990	1	221	6.0
8	1	1	15	7	0	-1	13	2476.849	0	112	3.5
8	1	1	17	7	0	-1	15	2476.873	4	127	3.5
9	1	-1	17	8	0	1	15	2479.289	5	112	5.0
9	1	-1	19	8	0	1	17	2479.305	6	125	5.0
9	1	1	17	9	0	-1	17	2457.785	-4	201	5.0
9	1	1	19	9	0	-1	19	2457.842	0	223	8.0
10	1	1	19	9	0	-1	17	2481.673	0	109	11.0
10	1	1	21	9	0	-1	19	2481.682	-2	120	11.0
10	1	-1	19	10	0	1	19	2458.305	4	196	5.0

10	1	-1	21	10	0	1	21	2458.356	3	216	6.0
11	1	-1	21	10	0	1	19	2484.016	-1	103	7.5
11	1	-1	23	10	0	1	21	2484.016	-8	113	
11	1	1	21	11	0	-1	21	2458.878	7	187	3.5
11	1	1	23	11	0	-1	23	2458.938	15	204	6.0
12	1	1	23	11	0	-1	21	2486.314	-5	95	12.5
12	1	1	25	11	0	-1	23	2486.314	-8	103	
12	1	-1	23	12	0	1	23	2459.496	-4	175	4.0
12	1	-1	25	12	0	1	25	2459.552	-1	190	5.0
13	1	-1	25	12	0	1	23	2488.578	-2	86	15.0
13	1	-1	27	12	0	1	25	2488.578	-2	93	
13	1	1	25	13	0	-1	25	2460.192	0	161	4.0
13	1	1	27	13	0	-1	27	2460.238	-8	173	4.0
14	1	1	27	13	0	-1	25	2490.808	6	76	9.0
14	1	1	29	13	0	-1	27	2490.808	8	82	
14	1	-1	27	14	0	1	27	2460.948	0	144	3.0
14	1	-1	29	14	0	1	29	2461.002	-1	155	3.0
15	1	-1	29	14	0	1	27	2493.000	10	66	12.5
15	1	-1	31	14	0	1	29	2493.000	15	71	
15	1	1	29	15	0	-1	29	2461.778	8	128	4.0
15	1	1	31	15	0	-1	31	2461.826	-1	136	4.0
16	1	1	31	15	0	-1	29	2495.141	-3	57	7.0
16	1	1	33	15	0	-1	31	2495.141	4	60	
16	1	-1	31	16	0	1	31	2462.688	27	111	3.0
16	1	-1	33	16	0	1	33	2462.756	37	118	3.0
17	1	-1	33	16	0	1	31	2497.267	-2	47	5.0
17	1	-1	35	16	0	1	33	2497.261	1	50	5.0
17	1	1	33	17	0	-1	33	2463.625	2	94	2.5
18	1	1	35	17	0	-1	33	2499.371	4	39	5.0
18	1	1	37	17	0	-1	35	2499.360	4	41	5.0
18	1	-1	35	18	0	1	35	2464.657	-2	79	3.5
18	1	-1	37	18	0	1	37	2464.716	-4	84	2.5
19	1	-1	37	18	0	1	35	2501.440	-1	31	3.5
19	1	-1	39	18	0	1	37	2501.429	1	33	3.0
19	1	1	37	19	0	-1	37	2465.769	0	65	2.0
19	1	1	39	19	0	-1	39	2465.835	2	69	2.0
20	1	1	39	19	0	-1	37	2503.505	12	25	4.0
20	1	1	41	19	0	-1	39	2503.492	12	26	4.0
20	1	-1	39	20	0	1	39	2466.956	-1	53	3.5
20	1	-1	41	20	0	1	41	2467.018	-5	56	3.5
21	1	-1	41	20	0	1	39	2505.534	5	19	4.0
21	1	-1	43	20	0	1	41	2505.523	8	20	5.0
22	1	1	43	21	0	-1	41	2507.554	4	15	3.0
22	1	1	45	21	0	-1	43	2507.540	6	16	3.0
23	1	-1	45	22	0	1	43	2509.570	11	11	2.5
23	1	-1	47	22	0	1	45	2509.553	10	12	2.5
12	0	1	23	11	1	-1	21	2448.960	6	68	5.0
12	0	1	25	11	1	-1	23	2448.947	7	74	5.0
13	0	-1	25	12	1	1	23	2452.266	1	62	3.0
13	0	-1	27	12	1	1	25	2452.254	-1	67	3.0
14	0	1	27	13	1	-1	25	2455.600	6	56	3.0
14	0	1	29	13	1	-1	27	2455.600	13	60	

16	0	1	31	15	1	-1	29	2462.279	-8	42	
16	0	1	33	15	1	-1	31	2462.279	-6	44	12.5
17	0	-1	33	16	1	1	31	2465.645	1	35	6.5
17	0	-1	35	16	1	1	33	2465.645	1	37	
18	0	1	35	17	1	-1	33	2468.977	-25	29	5.0
18	0	1	37	17	1	-1	35	2468.977	-27	31	
20	0	1	39	19	1	-1	37	2475.713	9	19	2.5
20	0	1	41	19	1	-1	39	2475.713	3	19	
21	0	-1	41	20	1	1	39	2479.047	7	14	4.0
21	0	-1	43	20	1	1	41	2479.047	0	15	
22	0	1	43	21	1	-1	41	2482.364	2	11	
22	0	1	45	21	1	-1	43	2482.364	-5	12	2.0
5	1	1	9	4	1	-1	7	2447.461	0	66	12.0
5	1	1	11	4	1	-1	9	2447.440	3	81	13.0
5	1	-1	9	4	1	1	7	2446.903	0	66	11.0
6	1	1	11	5	1	-1	9	2449.713	2	77	9.5
6	1	1	13	5	1	-1	11	2449.694	4	91	11.0
6	1	-1	11	5	1	1	9	2450.391	-6	77	11.0
6	1	-1	13	5	1	1	11	2450.371	-9	91	13.5
7	1	1	13	6	1	-1	11	2453.335	0	84	10.0
7	1	1	15	6	1	-1	13	2453.319	-2	97	12.0
7	1	-1	13	6	1	1	11	2452.524	9	85	8.0
7	1	-1	15	6	1	1	13	2452.512	15	98	10.0
8	1	1	15	7	1	-1	13	2455.311	-1	90	
8	1	1	17	7	1	-1	15	2455.311	14	102	9.0
8	1	-1	15	7	1	1	13	2456.267	-5	89	9.0
8	1	-1	17	7	1	1	15	2456.251	-10	100	9.0
9	1	1	17	8	1	-1	15	2459.217	9	90	20.0
9	1	1	19	8	1	-1	17	2459.208	9	101	17.0
9	1	-1	17	8	1	1	15	2458.102	-1	92	12.0
9	1	-1	19	8	1	1	17	2458.096	6	103	12.0
10	1	1	19	9	1	-1	17	2460.881	-6	91	12.5
10	1	1	21	9	1	-1	19	2460.872	-4	101	14.0
10	1	-1	19	9	1	1	17	2462.130	-13	89	21.0
10	1	-1	21	9	1	1	19	2462.130	-5	99	
11	1	1	21	10	1	-1	19	2465.065	-11	86	40.0
11	1	1	23	10	1	-1	21	2465.065	-4	94	
11	1	-1	21	10	1	1	19	2463.655	-9	88	14.0
11	1	-1	23	10	1	1	21	2463.648	-6	97	14.0
12	1	1	23	11	1	-1	21	2466.422	-11	83	18.0
12	1	1	25	11	1	-1	23	2466.412	-12	91	18.0
12	1	-1	23	11	1	1	21	2468.008	2	81	35.0
12	1	-1	25	11	1	1	23	2468.008	8	88	
13	1	1	25	12	1	-1	23	2470.928	-5	74	30.0
13	1	1	27	12	1	-1	25	2470.928	0	80	
13	1	-1	25	12	1	1	23	2469.205	11	77	9.0
13	1	-1	27	12	1	1	25	2469.205	19	83	
14	1	1	27	13	1	-1	25	2471.942	-6	70	22.0
14	1	1	29	13	1	-1	27	2471.942	2	75	
14	1	-1	27	13	1	1	25	2473.855	-2	67	20.0
14	1	-1	29	13	1	1	27	2473.855	2	72	
15	1	1	29	14	1	-1	27	2476.778	1	59	18.0

15	1	1	31	14	1	-1	29	2476.778	5	63	
15	1	-1	29	14	1	1	27	2474.701	8	62	17.0
15	1	-1	31	14	1	1	29	2474.701	15	66	
16	1	1	31	15	1	-1	29	2477.414	-14	54	15.0
16	1	1	33	15	1	-1	31	2477.414	-8	58	
16	1	-1	31	15	1	1	29	2479.695	2	51	17.0
16	1	-1	33	15	1	1	31	2479.695	6	55	
17	1	1	33	16	1	-1	31	2482.598	-5	44	14.0
17	1	1	35	16	1	-1	33	2482.598	-2	46	
17	1	-1	33	16	1	1	31	2480.147	-8	47	15.0
17	1	-1	35	16	1	1	33	2480.147	-2	49	
18	1	1	35	17	1	-1	33	2482.848	-25	39	13.0
18	1	1	37	17	1	-1	35	2482.848	-19	41	
18	1	-1	35	17	1	1	33	2485.509	1	37	14.0
18	1	-1	37	17	1	1	35	2485.509	4	39	
19	1	1	37	18	1	-1	35	2488.406	-1	30	18.0
19	1	1	39	18	1	-1	37	2488.406	2	32	
19	1	-1	37	18	1	1	35	2485.570	-10	32	13.5
19	1	-1	39	18	1	1	37	2485.570	-5	34	
20	1	1	39	19	1	-1	37	2488.275	-3	26	17.0
20	1	1	41	19	1	-1	39	2488.275	2	28	
20	1	-1	39	19	1	1	37	2491.318	19	24	10.0
20	1	-1	41	19	1	1	39	2491.318	21	26	
21	1	1	41	20	1	-1	39	2494.187	4	19	10.0
21	1	1	43	20	1	-1	41	2494.187	6	20	
21	1	-1	41	20	1	1	39	2490.964	-1	21	11.5
21	1	-1	43	20	1	1	41	2490.964	4	22	
22	1	1	43	21	1	-1	41	2493.637	-5	17	9.0
22	1	1	45	21	1	-1	43	2493.637	-1	18	
22	1	-1	43	21	1	1	41	2497.062	3	15	10.0
22	1	-1	45	21	1	1	43	2497.062	5	16	
23	1	1	45	22	1	-1	43	2499.932	6	12	15.0
23	1	1	47	22	1	-1	45	2499.932	7	12	
23	1	-1	45	22	1	1	43	2496.303	-5	13	10.0
23	1	-1	47	22	1	1	45	2496.303	-1	14	
24	1	1	47	23	1	-1	45	2498.957	-6	10	8.0
24	1	1	49	23	1	-1	47	2498.957	-2	10	
24	1	-1	47	23	1	1	45	2502.794	10	9	6.0
24	1	-1	49	23	1	1	47	2502.794	12	9	
25	1	1	49	24	1	-1	47	2505.642	12	7	7.0
25	1	1	51	24	1	-1	49	2505.642	14	7	
25	1	-1	49	24	1	1	47	2501.601	-5	8	6.5
25	1	-1	51	24	1	1	49	2501.601	-2	8	
26	1	1	51	25	1	-1	49	2504.243	4	6	6.5
26	1	1	53	25	1	-1	51	2504.243	7	6	
26	1	-1	51	25	1	1	49	2508.475	10	5	4.5
26	1	-1	53	25	1	1	51	2508.475	12	5	
27	1	1	53	26	1	-1	51	2511.300	13	3	2.0
27	1	1	55	26	1	-1	53	2511.300	15	4	
27	1	-1	53	26	1	1	51	2506.862	3	4	4.0
27	1	-1	55	26	1	1	53	2506.862	6	4	
28	1	1	55	27	1	-1	53	2509.469	1	3	3.5

28	1	1	57	27	1	-1	55	2509.469	3	3	
28	1	-1	55	27	1	1	53	2514.108	12	2	3.5
28	1	-1	57	27	1	1	55	2514.108	14	3	
29	1	-1	57	28	1	1	55	2512.053	-12	2	2.0
29	1	-1	59	28	1	1	57	2512.053	-10	2	
30	1	-1	59	29	1	1	57	2519.671	1	1	2.0
30	1	-1	61	29	1	1	59	2519.671	3	1	
31	1	-1	61	30	1	1	59	2517.214	-10	1	2.0
31	1	-1	63	30	1	1	61	2517.214	-6	1	
2	2	1	3	1	1	-1	1	2501.462	3	36	1.5
2	2	1	5	1	1	-1	3	2501.720	0	64	4.0
2	2	-1	3	1	1	1	1	2501.364	-3	36	2.0
2	2	-1	5	1	1	1	3	2501.623	0	64	2.5
2	2	-1	5	2	1	1	5	2496.070	7	33	2.0
3	2	1	5	2	1	-1	3	2504.179	4	47	3.0
3	2	1	7	2	1	-1	5	2504.381	-8	66	4.0
3	2	-1	5	2	1	1	3	2504.452	-4	48	3.5
3	2	-1	7	2	1	1	5	2504.688	10	67	3.5
3	2	1	5	3	1	-1	5	2495.888	3	40	5.0
3	2	1	7	3	1	-1	7	2496.167	8	54	2.5
3	2	-1	5	3	1	1	5	2495.326	0	39	2.5
3	2	-1	7	3	1	1	7	2495.586	-2	53	4.0
4	2	1	7	3	1	-1	5	2507.512	5	55	3.5
4	2	1	9	3	1	-1	7	2507.696	5	71	5.0
4	2	-1	7	3	1	1	5	2506.951	9	54	3.0
4	2	-1	9	3	1	1	7	2507.110	-2	70	5.0
4	2	1	7	4	1	-1	7	2495.174	1	54	3.5
4	2	1	9	4	1	-1	9	2495.369	0	68	4.0
4	2	-1	7	4	1	1	7	2496.115	10	56	3.5
4	2	-1	9	4	1	1	9	2496.316	-2	70	3.0
5	2	1	9	4	1	-1	7	2509.662	12	60	4.5
5	2	1	11	4	1	-1	9	2509.797	7	72	6.0
5	2	-1	9	4	1	1	7	2510.605	5	61	4.5
5	2	-1	11	4	1	1	9	2510.758	2	74	4.5
5	2	1	9	5	1	-1	9	2496.356	3	68	4.0
5	2	1	11	5	1	-1	11	2496.532	3	82	4.5
5	2	-1	9	5	1	1	9	2494.964	7	65	5.0
5	2	-1	11	5	1	1	11	2495.116	3	79	6.0
6	2	1	11	5	1	-1	9	2513.741	4	66	6.0
6	2	1	13	5	1	-1	11	2513.867	-8	77	6.0
6	2	-1	11	5	1	1	9	2512.309	5	63	3.5
6	2	-1	13	5	1	1	11	2512.423	2	74	5.0
6	2	1	11	6	1	-1	11	2494.692	3	73	5.5
6	2	1	13	6	1	-1	13	2494.822	5	86	6.0
6	2	-1	11	6	1	1	11	2496.641	3	78	5.0
6	2	-1	13	6	1	1	13	2496.790	-1	91	5.5
7	2	1	13	6	1	-1	11	2514.911	5	65	5.0
7	2	1	15	6	1	-1	13	2515.010	6	74	6.5
7	2	-1	13	6	1	1	11	2516.931	7	69	4.0
7	2	-1	15	6	1	1	13	2517.049	2	79	5.0
7	2	1	13	7	1	-1	13	2496.966	2	84	4.5
7	2	1	15	7	1	-1	15	2497.099	-1	96	4.5

7	2	-1	13	7	1	1	13	2494.368	-7	78	6.0
7	2	-1	15	7	1	1	15	2494.480	-3	89	7.0
8	2	1	15	7	1	-1	13	2520.167	5	70	6.5
8	2	1	17	7	1	-1	15	2520.268	-7	79	5.0
8	2	-1	15	7	1	1	13	2517.462	8	65	5.0
8	2	-1	17	7	1	1	15	2517.541	3	73	5.0
8	2	1	15	8	1	-1	15	2494.018	-1	79	6.0
8	2	1	17	8	1	-1	17	2494.115	3	89	6.0
8	2	-1	15	8	1	1	15	2497.337	4	87	4.5
8	2	-1	17	8	1	1	17	2497.464	8	99	3.0
9	2	1	17	8	1	-1	15	2519.955	4	63	5.0
9	2	1	19	8	1	-1	17	2520.028	4	70	7.0
9	2	-1	17	8	1	1	15	2523.452	-3	70	3.5
9	2	-1	19	8	1	1	17	2523.572	11	78	5.0
9	2	1	17	9	1	-1	17	2497.774	29	88	3.0
9	2	1	19	9	1	-1	19	2497.889	29	98	5.5
9	2	-1	17	9	1	1	17	2493.624	-2	77	5.5
9	2	-1	19	9	1	1	19	2493.703	-3	86	6.0
10	2	1	19	9	1	-1	17	2526.796	-11	68	4.0
10	2	1	21	9	1	-1	19	2526.902	-6	75	5.0
10	2	-1	19	9	1	1	17	2522.398	0	60	7.0
10	2	-1	21	9	1	1	19	2522.455	-5	66	6.0
9	2	1	17	10	1	-1	19	2464.136	0	27	2.0
10	2	1	19	10	1	-1	19	2493.204	6	73	5.5
10	2	1	21	10	1	-1	21	2493.275	7	81	5.5
10	2	-1	19	10	1	1	19	2498.216	15	86	5.0
10	2	-1	21	10	1	1	21	2498.318	9	95	5.5
11	2	1	21	10	1	-1	19	2524.786	-7	56	6.5
11	2	1	23	10	1	-1	21	2524.841	-6	61	6.5
11	2	-1	21	10	1	1	19	2530.223	2	65	4.5
11	2	-1	23	10	1	1	21	2530.322	4	72	5.0
10	2	1	19	11	1	-1	21	2467.102	-5	32	2.0
10	2	1	21	11	1	-1	23	2467.219	-6	35	3.0
11	2	1	21	11	1	-1	21	2498.702	0	82	5.0
11	2	1	23	11	1	-1	23	2498.812	8	90	7.0
11	2	-1	21	11	1	1	21	2492.744	3	68	8.0
11	2	-1	23	11	1	1	23	2492.807	4	74	8.0
12	2	1	23	11	1	-1	21	2533.701	0	62	2.0
12	2	1	25	11	1	-1	23	2533.799	4	67	2.5
12	2	-1	23	11	1	1	21	2527.139	1	52	5.0
12	2	-1	25	11	1	1	23	2527.186	1	56	5.0
11	2	-1	21	12	1	1	23	2464.835	-15	31	2.5
11	2	-1	23	12	1	1	25	2464.969	7	34	4.0
12	2	1	23	12	1	-1	23	2492.260	2	61	7.0
12	2	1	25	12	1	-1	25	2492.315	2	66	6.5
12	2	-1	23	12	1	1	23	2499.250	2	77	5.0
12	2	-1	25	12	1	1	25	2499.346	1	84	5.0
13	2	1	25	12	1	-1	23	2529.436	3	46	5.0
13	2	1	27	12	1	-1	25	2529.474	0	50	7.0
13	2	-1	25	12	1	1	23	2537.237	-14	57	3.0
13	2	-1	27	12	1	1	25	2537.333	-10	62	3.0
13	2	1	25	13	1	-1	25	2499.835	-3	71	7.0

13	2	-1	25	13	1	1	25	2491.765	11	54	5.0
13	2	-1	27	13	1	1	27	2491.805	3	58	5.0
14	2	1	29	13	1	-1	27	2540.993	27	56	3.0
14	2	1	27	14	1	-1	27	2491.246	13	46	4.0
14	2	1	29	14	1	-1	29	2491.288	11	50	4.0
14	2	-1	27	14	1	1	27	2500.472	-1	63	6.0
14	2	-1	29	14	1	1	29	2500.555	-9	68	5.0
15	2	1	29	14	1	-1	27	2533.881	6	35	2.0
15	2	1	31	14	1	-1	29	2533.905	1	38	2.0
15	2	-1	29	14	1	1	27	2544.588	11	47	2.0
15	2	-1	31	14	1	1	29	2544.672	5	50	2.0
15	2	1	29	15	1	-1	29	2501.162	10	56	4.5
15	2	1	31	15	1	-1	31	2501.256	14	60	5.0
15	2	-1	29	15	1	1	29	2490.708	6	39	3.8
15	2	-1	31	15	1	1	31	2490.744	3	42	3.5
16	2	1	33	15	1	-1	31	2548.456	3	44	3.0
16	2	1	31	16	1	-1	31	2490.165	2	32	2.0
16	2	1	33	16	1	-1	33	2490.201	2	34	1.5
16	2	-1	31	16	1	1	31	2501.881	4	48	3.5
16	2	-1	33	16	1	1	33	2501.973	8	51	4.0
17	2	-1	33	16	1	1	31	2552.230	-5	36	2.5
17	2	-1	35	16	1	1	33	2552.321	-5	38	3.6
17	2	1	33	17	1	-1	33	2502.651	5	41	3.5
17	2	1	35	17	1	-1	35	2502.740	6	44	4.0
18	2	-1	35	18	1	1	35	2503.465	5	34	2.0
18	2	-1	37	18	1	1	37	2503.555	8	36	3.0
19	2	1	37	18	1	-1	35	2542.175	2	17	
19	2	1	39	18	1	-1	37	2542.175	-10	18	3.0
19	2	1	37	19	1	-1	37	2504.299	-20	28	2.0
20	2	-1	39	19	1	1	37	2544.124	-5	13	
20	2	-1	41	19	1	1	39	2544.124	-12	14	2.0
20	2	1	39	20	1	-1	39	2488.074	19	12	2.0
20	2	-1	39	20	1	1	39	2505.217	-6	23	2.0
20	2	-1	41	20	1	1	41	2505.306	-3	24	1.5
21	2	1	41	21	1	-1	41	2506.164	-6	18	2.0
21	2	1	43	21	1	-1	43	2506.252	-5	19	1.5
22	2	-1	43	22	1	1	43	2507.155	-7	14	2.0
22	2	-1	45	22	1	1	45	2507.247	-2	15	1.5
7	2	1	13	6	2	-1	11	2447.802	7	57	12.0
7	2	1	15	6	2	-1	13	2447.745	7	66	10.0
7	2	-1	13	6	2	1	11	2447.828	9	57	12.0
7	2	-1	15	6	2	1	13	2447.770	7	66	12.0
8	2	1	15	7	2	-1	13	2450.693	-4	61	10.0
8	2	1	17	7	2	-1	15	2450.658	7	69	13.5
8	2	-1	15	7	2	1	13	2450.675	16	61	11.5
8	2	-1	17	7	2	1	15	2450.608	-5	69	12.0
9	2	1	17	8	2	-1	15	2453.520	-2	63	9.0
9	2	1	19	8	2	-1	17	2453.483	-1	70	9.5
9	2	-1	17	8	2	1	15	2453.578	0	63	12.0
9	2	-1	19	8	2	1	17	2453.539	-1	70	10.0
10	2	1	19	9	2	-1	17	2456.462	1	63	7.0
10	2	1	21	9	2	-1	19	2456.427	-2	70	8.0

10	2	-1	19	9	2	1	17	2456.388	5	63	7.0
10	2	-1	21	9	2	1	19	2456.347	-2	70	9.0
11	2	1	21	10	2	-1	19	2459.269	30	61	3.0
11	2	1	23	10	2	-1	21	2459.245	35	67	9.0
11	2	-1	21	10	2	1	19	2459.352	4	61	7.5
11	2	-1	23	10	2	1	21	2459.324	4	67	10.0
12	2	1	23	11	2	-1	21	2462.225	-12	58	13.0
12	2	1	25	11	2	-1	23	2462.201	-12	63	14.0
12	2	-1	23	11	2	1	21	2462.083	-9	58	13.0
12	2	-1	25	11	2	1	23	2462.063	-4	63	13.0
13	2	1	25	12	2	-1	23	2464.937	-4	54	18.0
13	2	1	27	12	2	-1	25	2464.913	-5	58	19.0
13	2	-1	25	12	2	1	23	2465.117	-14	53	16.0
13	2	-1	27	12	2	1	25	2465.096	-13	58	19.0
14	2	1	27	13	2	-1	25	2468.040	12	48	5.0
14	2	1	29	13	2	-1	27	2468.026	17	52	15.0
14	2	-1	27	13	2	1	25	2467.777	-8	49	11.0
14	2	-1	29	13	2	1	27	2467.759	-5	52	13.5
15	2	1	29	14	2	-1	27	2470.616	-8	43	10.0
15	2	1	31	14	2	-1	29	2470.597	-8	46	11.0
15	2	-1	31	14	2	1	29	2470.909	-4	46	11.5
16	2	1	31	15	2	-1	29	2473.832	-6	37	6.5
16	2	1	33	15	2	-1	31	2473.817	-6	40	6.5
16	2	-1	31	15	2	1	29	2473.448	-10	38	9.0
16	2	-1	33	15	2	1	31	2473.434	-6	40	11.0
17	2	1	33	16	2	-1	31	2476.284	-2	32	7.5
17	2	1	35	16	2	-1	33	2476.271	1	34	10.0
17	2	-1	33	16	2	1	31	2476.748	-3	32	8.0
17	2	-1	35	16	2	1	33	2476.734	-4	34	8.0
18	2	1	35	17	2	-1	33	2479.666	-5	27	7.0
18	2	1	37	17	2	-1	35	2479.657	-2	28	7.0
18	2	-1	35	17	2	1	33	2479.107	-1	27	6.0
18	2	-1	37	17	2	1	35	2479.092	-1	29	6.0
19	2	1	37	18	2	-1	35	2481.911	-12	22	8.0
19	2	1	39	18	2	-1	37	2481.902	-7	24	11.0
19	2	-1	37	18	2	1	35	2482.583	-14	22	5.0
19	2	-1	39	18	2	1	37	2482.575	-12	23	5.0
20	2	-1	39	19	2	1	37	2484.695	-36	18	7.0
20	2	-1	41	19	2	1	39	2484.695	-24	19	
21	2	1	41	20	2	-1	39	2487.518	-15	14	7.0
21	2	1	43	20	2	-1	41	2487.518	-3	15	
21	2	-1	41	20	2	1	39	2488.459	-11	14	
21	2	-1	43	20	2	1	41	2488.459	-3	15	10.0
22	2	1	43	21	2	-1	41	2491.424	8	11	6.0
22	2	1	45	21	2	-1	43	2491.424	14	12	
22	2	-1	43	21	2	1	41	2490.331	4	11	4.5
22	2	-1	45	21	2	1	43	2490.318	2	12	5.0
23	2	1	45	22	2	-1	43	2493.110	-3	9	4.5
23	2	1	47	22	2	-1	45	2493.099	-4	9	4.5
24	2	1	47	23	2	-1	45	2497.316	-14	7	
24	2	1	49	23	2	-1	47	2497.316	-9	7	5.0
25	2	1	49	24	2	-1	47	2498.653	-8	5	3.0

25	2	1	51	24	2	-1	49	2498.641	-11	5	3.0
25	2	-1	49	24	2	1	47	2500.283	-12	5	5.0
25	2	-1	51	24	2	1	49	2500.283	-8	5	
3	3	1	5	2	2	-1	3	2540.175	-13	51	
3	3	1	7	2	2	-1	5	2540.402	-1	73	
3	3	-1	5	2	2	1	3	2540.175	-13	51	6.0
3	3	-1	7	2	2	1	5	2540.402	0	73	7.0
3	3	-1	5	3	2	1	5	2531.368	-3	17	3.0
3	3	-1	7	3	2	1	7	2531.783	-8	24	3.0
4	3	1	7	3	2	-1	5	2543.066	2	56	7.0
4	3	1	9	3	2	-1	7	2543.279	5	71	8.0
4	3	-1	7	3	2	1	5	2543.066	0	56	
4	3	-1	9	3	2	1	7	2543.279	3	71	
4	3	-1	9	4	2	1	9	2531.735	-6	40	4.5
5	3	1	9	4	2	-1	7	2545.960	2	59	
5	3	1	11	4	2	-1	9	2546.136	-10	71	
5	3	-1	9	4	2	1	7	2545.960	6	59	5.0
5	3	-1	11	4	2	1	9	2546.136	-6	71	5.5
5	3	1	11	5	2	-1	11	2531.693	-9	51	4.5
5	3	-1	11	5	2	1	11	2531.707	-6	51	5.0
6	3	1	11	5	2	-1	9	2548.844	4	60	4.0
6	3	1	13	5	2	-1	11	2549.006	-1	70	4.0
6	3	-1	11	5	2	1	9	2548.854	4	60	4.0
6	3	-1	13	5	2	1	11	2549.016	-1	70	4.0
6	3	1	13	6	2	-1	13	2531.677	-9	59	5.0
6	3	-1	11	6	2	1	11	2531.448	-6	50	6.0
6	3	-1	13	6	2	1	13	2531.659	-7	59	7.5
7	3	1	13	6	2	-1	11	2551.736	-3	60	4.0
7	3	1	15	6	2	-1	13	2551.881	-8	69	3.5
7	3	-1	13	6	2	1	11	2551.716	-3	60	3.5
7	3	-1	15	6	2	1	13	2551.865	-3	69	3.5
7	3	-1	13	7	2	1	13	2531.475	-5	55	7.5
8	3	1	15	7	2	-1	13	2554.587	-2	59	4.0
8	3	1	17	7	2	-1	15	2554.719	-5	67	5.0
8	3	-1	15	7	2	1	13	2554.623	-3	59	4.0
8	3	-1	17	7	2	1	15	2554.755	-6	67	5.0
7	3	1	13	8	2	-1	15	2508.337	0	14	2.0
7	3	-1	13	8	2	1	15	2508.270	-6	14	2.5
7	3	-1	15	8	2	1	17	2508.484	-1	16	1.5
8	3	1	17	8	2	-1	17	2531.640	-4	66	6.5
8	3	-1	15	8	2	1	15	2531.423	1	58	5.5
8	3	1	15	8	2	-1	15	2531.484	2	58	
8	3	-1	17	8	2	1	17	2531.582	-1	66	5.0
9	3	1	17	8	2	-1	15	2557.511	0	57	5.0
9	3	1	19	8	2	-1	17	2557.633	-1	64	4.5
9	3	-1	17	8	2	1	15	2557.450	0	57	5.0
9	3	-1	19	8	2	1	17	2557.572	0	63	5.5
8	3	1	15	9	2	-1	17	2505.366	6	16	2.0
8	3	1	17	9	2	-1	19	2505.549	8	18	3.5
8	3	-1	15	9	2	1	17	2505.461	6	16	2.0
8	3	-1	17	9	2	1	19	2505.642	4	18	
9	3	1	17	9	2	-1	17	2531.387	-1	59	5.0

10	3	1	19	9	2	-1	17	2560.348	48	54	2.5
10	3	1	21	9	2	-1	19	2560.416	4	60	5.5
10	3	-1	19	9	2	1	17	2560.401	5	54	4.5
10	3	-1	21	9	2	1	19	2560.511	1	60	4.5
9	3	1	17	10	2	-1	19	2502.581	10	16	2.5
9	3	-1	17	10	2	1	19	2502.441	13	16	2.0
9	3	-1	19	10	2	1	21	2502.601	13	18	2.5
10	3	1	21	10	2	-1	21	2531.620	6	63	9.0
10	3	-1	19	10	2	1	19	2531.342	0	57	4.5
11	3	1	21	10	2	-1	19	2563.288	6	50	5.5
11	3	1	23	10	2	-1	21	2563.393	6	55	6.0
11	3	-1	21	10	2	1	19	2563.137	0	50	6.5
11	3	-1	23	10	2	1	21	2563.246	6	55	5.5
10	3	1	21	11	2	-1	23	2499.628	3	18	3.0
10	3	-1	19	11	2	1	21	2499.695	6	17	2.5
11	3	1	21	11	2	-1	21	2531.281	0	55	5.0
11	3	1	23	11	2	-1	23	2531.400	2	60	5.0
11	3	-1	21	11	2	1	21	2531.484	0	55	15.0
11	3	-1	23	11	2	1	23	2531.604	0	60	10.0
12	3	1	23	11	2	-1	21	2565.960	0	46	5.0
12	3	1	25	11	2	-1	23	2566.055	0	50	5.0
12	3	-1	23	11	2	1	21	2566.171	1	46	5.0
12	3	-1	25	11	2	1	23	2566.271	4	50	5.0
11	3	1	21	12	2	-1	23	2496.812	3	16	2.0
11	3	1	23	12	2	-1	25	2496.944	2	18	3.0
11	3	-1	23	12	2	1	25	2496.650	1	18	2.0
12	3	-1	25	12	2	1	25	2531.309	-3	55	5.0
13	3	1	25	12	2	-1	23	2569.064	4	42	6.0
13	3	1	27	12	2	-1	25	2569.155	3	45	7.0
13	3	-1	25	12	2	1	23	2568.771	5	41	5.5
13	3	-1	27	12	2	1	25	2568.858	4	45	5.0
13	3	1	25	13	2	-1	25	2531.110	1	46	5.0
13	3	1	27	13	2	-1	27	2531.207	-2	49	6.5
13	3	-1	25	13	2	1	25	2531.500	4	46	4.0
14	3	1	27	13	2	-1	25	2571.572	19	37	3.0
14	3	1	29	13	2	-1	27	2571.659	23	39	3.5
14	3	-1	27	13	2	1	25	2571.963	8	37	3.0
14	3	-1	29	13	2	1	27	2572.050	8	40	3.5
14	3	1	27	14	2	-1	27	2531.511	3	41	3.5
14	3	-1	27	14	2	1	27	2530.989	-6	41	4.5
14	3	-1	29	14	2	1	29	2531.085	-2	44	5.0
15	3	1	29	14	2	-1	27	2574.869	13	32	3.5
15	3	1	31	14	2	-1	29	2574.949	11	34	4.0
15	3	-1	29	14	2	1	27	2574.325	6	32	3.5
15	3	-1	31	14	2	1	29	2574.402	6	34	3.0
15	3	1	29	15	2	-1	29	2530.852	-7	35	6.0
15	3	1	31	15	2	-1	31	2530.942	-3	38	8.0
15	3	-1	29	15	2	1	29	2531.532	6	36	7.5
16	3	1	31	15	2	-1	29	2577.080	19	27	1.5
16	3	1	33	15	2	-1	31	2577.140	7	29	2.5
16	3	-1	31	15	2	1	29	2577.779	16	28	2.5
16	3	-1	33	15	2	1	31	2577.861	20	29	2.0

16	3	1	31	16	2	-1	31	2531.559	7	30	3.0
16	3	-1	31	16	2	1	31	2530.710	11	30	4.0
16	3	-1	33	16	2	1	33	2530.779	1	32	5.0
17	3	1	33	17	2	-1	33	2530.522	9	25	4.0
17	3	1	35	17	2	-1	35	2530.589	3	27	3.0
18	3	1	35	17	2	-1	33	2582.467	5	19	4.2
18	3	1	37	17	2	-1	35	2582.527	3	20	2.5
18	3	-1	35	18	2	1	35	2530.312	15	21	3.5
18	3	-1	37	18	2	1	37	2530.378	12	22	3.5
19	3	1	37	19	2	-1	37	2530.072	21	17	4.0
19	3	1	39	19	2	-1	39	2530.134	19	18	4.0
20	3	1	39	20	2	-1	39	2531.760	8	14	3.0
20	3	1	41	20	2	-1	41	2531.828	3	14	2.5
20	3	-1	39	20	2	1	39	2529.778	6	13	2.0
20	3	-1	41	20	2	1	41	2529.841	9	14	3.0
21	3	1	43	21	2	-1	43	2529.527	14	11	2.0
10	3	1	19	9	3	-1	17	2448.018	11	35	18.0
10	3	1	21	9	3	-1	19	2447.941	6	38	
10	3	-1	19	9	3	1	17	2448.018	10	35	
10	3	-1	21	9	3	1	19	2447.941	5	38	20.0
11	3	1	21	10	3	-1	19	2450.875	3	34	
11	3	1	23	10	3	-1	21	2450.821	11	37	5.5
11	3	-1	21	10	3	1	19	2450.875	4	34	16.0
11	3	-1	23	10	3	1	21	2450.821	13	37	
12	3	1	23	11	3	-1	21	2453.744	11	32	
12	3	1	25	11	3	-1	23	2453.691	13	35	11.0
12	3	-1	23	11	3	1	21	2453.744	9	32	10.0
12	3	-1	25	11	3	1	23	2453.691	11	35	3.5
13	3	1	27	12	3	-1	25	2456.538	-10	33	
13	3	-1	27	12	3	1	25	2456.538	-7	33	4.0
14	3	1	27	13	3	-1	25	2459.464	11	27	
14	3	1	29	13	3	-1	27	2459.424	15	29	7.5
14	3	-1	27	13	3	1	25	2459.464	6	27	7.0
15	3	1	29	14	3	-1	27	2462.319	1	24	6.5
15	3	1	31	14	3	-1	29	2462.274	-5	26	6.5
15	3	-1	29	14	3	1	27	2462.310	-1	24	6.5
15	3	-1	31	14	3	1	29	2462.279	7	26	
16	3	1	31	15	3	-1	29	2465.167	1	21	8.0
16	3	1	33	15	3	-1	31	2465.132	2	23	9.0
16	3	-1	31	15	3	1	29	2465.177	0	21	8.0
16	3	-1	33	15	3	1	31	2465.141	1	23	9.0
18	3	1	35	17	3	-1	33	2470.877	7	15	4.5
18	3	1	37	17	3	-1	35	2470.847	8	16	4.5
18	3	-1	35	17	3	1	33	2470.895	5	15	4.5
18	3	-1	37	17	3	1	35	2470.864	4	16	4.5
19	3	1	37	18	3	-1	35	2473.752	6	13	3.5
19	3	1	39	18	3	-1	37	2473.726	9	13	6.0
19	3	-1	37	18	3	1	35	2473.726	8	13	
19	3	-1	39	18	3	1	37	2473.697	7	13	3.5
20	3	1	39	19	3	-1	37	2476.574	10	10	2.5
20	3	1	41	19	3	-1	39	2476.547	9	11	2.5
20	3	-1	39	19	3	1	37	2476.609	9	10	2.5

20	3	-1	41	19	3	1	39	2476.586	12	11	2.5
21	3	1	41	20	3	-1	39	2479.471	17	8	2.5
21	3	1	43	20	3	-1	41	2479.445	15	9	3.0
21	3	-1	41	20	3	1	39	2479.420	12	8	3.0
21	3	-1	43	20	3	1	41	2479.397	14	9	3.0
22	3	1	43	21	3	-1	41	2482.255	7	7	2.5
22	3	1	45	21	3	-1	43	2482.235	10	7	3.0
22	3	-1	43	21	3	1	41	2482.316	8	7	2.5
22	3	-1	45	21	3	1	43	2482.294	8	7	2.5
23	3	1	45	22	3	-1	43	2485.171	9	5	1.5
23	3	1	47	22	3	-1	45	2485.151	9	5	2.0
23	3	-1	45	22	3	1	43	2485.092	7	5	2.0
23	3	-1	47	22	3	1	45	2485.079	15	5	2.0
24	3	1	47	23	3	-1	45	2487.935	16	4	2.0
24	3	1	49	23	3	-1	47	2487.915	15	4	2.5
24	3	-1	47	23	3	1	45	2488.027	10	4	2.0
24	3	-1	49	23	3	1	47	2488.009	11	4	2.0
4	4	1	7	3	3	-1	5	2574.335	-10	44	7.5
4	4	1	7	3	3	-1	5	2574.335	-10	44	
4	4	1	9	3	3	-1	7	2574.487	-15	56	10.0
4	4	1	9	3	3	-1	7	2574.487	-15	56	
4	4	1	9	4	3	-1	9	2563.010	-11	13	2.5
4	4	1	9	4	3	-1	9	2563.010	-11	13	
5	4	1	9	4	3	-1	7	2577.195	-14	44	5.0
5	4	1	11	4	3	-1	9	2577.375	-6	54	6.0
5	4	1	11	5	3	-1	11	2562.965	-13	23	5.0
5	4	1	11	5	3	-1	11	2562.965	-13	23	
6	4	1	11	5	3	-1	9	2580.074	-14	44	5.5
6	4	1	13	5	3	-1	11	2580.238	-15	52	7.5
6	4	1	13	6	3	-1	13	2562.925	-17	29	
6	4	1	13	6	3	-1	13	2562.925	-17	29	7.0
7	4	1	13	6	3	-1	11	2582.942	-25	43	10.0
7	4	1	15	6	3	-1	13	2583.102	-20	49	12.0
7	4	1	13	7	3	-1	13	2562.660	-24	29	16.0
7	4	1	15	7	3	-1	15	2562.888	-22	33	8.5
7	4	-1	13	7	3	1	13	2562.660	-23	29	
7	4	-1	15	7	3	1	15	2562.888	-22	33	
8	4	-1	15	7	3	1	13	2585.815	-29	42	
8	4	1	15	7	3	-1	13	2585.815	-29	42	4.2
8	4	1	15	8	3	-1	15	2562.649	-31	31	
8	4	1	17	8	3	-1	17	2562.854	-25	35	9.5
8	4	-1	15	8	3	1	15	2562.649	-31	31	12.5
8	4	-1	17	8	3	1	17	2562.854	-25	35	
9	4	1	17	8	3	-1	15	2588.697	-21	40	6.0
9	4	1	19	8	3	-1	17	2588.819	-33	44	6.0
9	4	1	17	9	3	-1	17	2562.635	-35	32	15.0
9	4	1	19	9	3	-1	19	2562.815	-33	36	12.0
9	4	-1	17	9	3	1	17	2562.635	-35	32	
9	4	-1	19	9	3	1	19	2562.815	-32	36	
10	4	1	19	9	3	-1	17	2591.547	-41	37	
10	4	-1	19	9	3	1	17	2591.547	-41	37	7.0
10	4	1	19	10	3	-1	19	2562.611	-43	32	14.0

10	4	1	21	10	3	-1	21	2562.773	-42	35	
10	4	-1	19	10	3	1	19	2562.611	-44	32	
10	4	-1	21	10	3	1	21	2562.773	-42	35	10.5
11	4	1	21	10	3	-1	19	2594.447	-6	34	
11	4	1	23	10	3	-1	21	2594.515	-55	37	
11	4	-1	21	10	3	1	19	2594.447	-7	34	5.0
11	4	-1	23	10	3	1	21	2594.515	-56	37	6.0
11	4	1	21	11	3	-1	21	2562.582	-53	31	14.5
11	4	1	23	11	3	-1	23	2562.729	-53	34	11.0
11	4	-1	21	11	3	1	21	2562.582	-52	31	
11	4	-1	23	11	3	1	23	2562.729	-51	34	
12	4	1	23	11	3	-1	21	2597.251	-65	31	
12	4	1	25	11	3	-1	23	2597.359	-67	33	
12	4	-1	23	11	3	1	21	2597.251	-64	31	4.5
12	4	-1	25	11	3	1	23	2597.359	-65	33	4.5
12	4	1	23	12	3	-1	23	2562.551	-58	29	10.5
12	4	1	25	12	3	-1	25	2562.685	-58	31	11.0
12	4	-1	23	12	3	1	23	2562.551	-60	29	
12	4	-1	25	12	3	1	25	2562.685	-61	31	
13	4	1	25	12	3	-1	23	2600.118	-53	28	
13	4	1	27	12	3	-1	25	2600.212	-62	30	
13	4	-1	25	12	3	1	23	2600.118	-56	28	5.5
13	4	-1	27	12	3	1	25	2600.212	-65	30	5.5
13	4	1	25	13	3	-1	25	2562.512	-71	27	7.0
13	4	-1	25	13	3	1	25	2562.512	-67	27	
14	4	1	27	13	3	-1	25	2602.960	-68	24	
14	4	1	29	13	3	-1	27	2603.056	-68	26	
14	4	-1	27	13	3	1	25	2602.960	-63	24	1.5
14	4	-1	29	13	3	1	27	2603.056	-64	26	2.0
14	4	1	27	14	3	-1	27	2562.459	-86	24	6.5
14	4	-1	27	14	3	1	27	2562.459	-92	24	
15	4	1	31	15	3	-1	31	2562.525	-99	22	5.0
15	4	-1	31	15	3	1	31	2562.525	-89	22	
16	4	1	33	16	3	-1	33	2562.471	-93	19	6.0
16	4	-1	33	16	3	1	33	2562.471	-105	19	
17	4	-1	33	16	4	1	31	2456.483	-107	10	2.0
17	4	1	35	17	3	-1	35	2562.418	-111	16	4.0
17	4	-1	35	17	3	1	35	2562.405	-103	16	5.0
20	4	1	41	19	4	-1	39	2464.953	-128	6	1.5
21	4	1	43	20	4	-1	41	2467.793	-132	5	1.0
21	4	1	41	20	4	-1	39	2467.808	-160	5	1.0
6	5	1	11	5	4	-1	9	2606.767	-8	26	3.0
6	5	1	13	5	4	-1	11	2606.897	2	30	3.0
6	5	-1	11	5	4	1	9	2606.767	-8	26	
6	5	-1	13	5	4	1	11	2606.897	2	30	
6	5	1	13	6	4	-1	13	2589.617	-1	10	1.2
6	5	-1	13	6	4	1	13	2589.617	-1	10	
7	5	1	13	6	4	-1	11	2609.636	-6	25	2.0
7	5	1	15	6	4	-1	13	2609.770	2	28	2.5
7	5	-1	13	6	4	1	11	2609.636	-6	25	
7	5	-1	15	6	4	1	13	2609.770	2	28	
7	5	1	15	7	4	-1	15	2589.582	0	13	2.5

7	5	-1	15	7	4	1	15	2589.582	0	13	
8	5	1	15	7	4	-1	13	2612.520	9	24	2.5
8	5	1	17	7	4	-1	15	2612.631	-5	27	3.0
8	5	-1	15	7	4	1	13	2612.520	9	24	
8	5	-1	17	7	4	1	15	2612.631	-5	27	
8	5	1	17	8	4	-1	17	2589.551	3	15	
8	5	-1	17	8	4	1	17	2589.551	3	15	2.5
9	5	1	17	9	4	-1	17	2589.329	10	14	5.0
9	5	1	19	9	4	-1	19	2589.515	1	16	3.0
9	5	-1	17	9	4	1	17	2589.329	10	14	
9	5	-1	19	9	4	1	19	2589.515	1	16	
10	5	1	19	9	4	-1	17	2618.236	-8	20	2.5
10	5	1	21	9	4	-1	19	2618.359	0	22	2.5
10	5	-1	19	9	4	1	17	2618.236	-8	20	
10	5	-1	21	9	4	1	19	2618.359	0	22	
10	5	1	19	10	4	-1	19	2589.305	1	14	
10	5	1	21	10	4	-1	21	2589.482	3	16	
10	5	-1	19	10	4	1	19	2589.305	1	14	2.5
10	5	-1	21	10	4	1	21	2589.482	3	16	3.0
11	5	1	21	10	4	-1	19	2621.103	-3	19	
11	5	1	23	10	4	-1	21	2621.215	-1	20	
11	5	-1	21	10	4	1	19	2621.103	-2	19	2.0
11	5	-1	23	10	4	1	21	2621.215	-1	20	2.0
11	5	1	21	11	4	-1	21	2589.285	2	14	4.0
11	5	1	23	11	4	-1	23	2589.446	3	15	2.5
11	5	-1	21	11	4	1	21	2589.285	2	14	
11	5	-1	23	11	4	1	23	2589.446	3	15	
12	5	1	23	11	4	-1	21	2623.959	-5	17	1.5
12	5	1	25	11	4	-1	23	2624.068	-1	18	2.0
12	5	-1	23	11	4	1	21	2623.959	-5	17	
12	5	-1	25	11	4	1	23	2624.068	-1	18	
12	5	1	23	12	4	-1	23	2589.259	0	13	
12	5	1	25	12	4	-1	25	2589.411	5	14	
12	5	-1	23	12	4	1	23	2589.259	0	13	2.5
12	5	-1	25	12	4	1	25	2589.411	5	14	2.5
13	5	1	25	12	4	-1	23	2626.809	-9	15	
13	5	1	27	12	4	-1	25	2626.913	-5	16	
13	5	-1	25	12	4	1	23	2626.809	-9	15	1.2
13	5	-1	27	12	4	1	25	2626.913	-5	16	1.5
13	5	1	25	13	4	-1	25	2589.236	6	12	2.0
13	5	1	27	13	4	-1	27	2589.370	4	13	2.5
13	5	-1	25	13	4	1	25	2589.236	6	12	
13	5	-1	27	13	4	1	27	2589.370	4	13	
14	5	1	27	14	4	-1	27	2589.198	0	11	
14	5	-1	27	14	4	1	27	2589.198	0	11	1.5
15	5	1	29	15	4	-1	29	2589.163	2	10	1.5
15	5	-1	29	15	4	1	29	2589.163	2	10	
16	5	1	31	16	4	-1	31	2589.135	13	8	
16	5	-1	31	16	4	1	31	2589.135	14	8	1.2

14	3	1	27	14	4	-1	27	2263.989	1	1237
13	3	-1	25	13	4	1	25	2264.002	-6	1382
13	3	1	25	13	4	-1	25	2264.013	-1	1382
11	3	-1	21	11	4	1	21	2264.056	2	1610
11	3	1	21	11	4	-1	21	2264.056	0	1610
10	3	-1	19	10	4	1	19	2264.081	0	1670
10	3	1	19	10	4	-1	19	2264.081	2	1670
9	3	1	17	9	4	-1	17	2264.109	1	1678
9	3	-1	17	9	4	1	17	2264.109	1	1678
8	3	-1	15	8	4	1	15	2264.138	-1	1622
8	3	1	15	8	4	-1	15	2264.138	-1	1622
7	3	-1	13	7	4	1	13	2264.175	-1	1491
7	3	1	13	7	4	-1	13	2264.175	-2	1491
6	3	-1	11	6	4	1	11	2264.221	0	1274
6	3	1	11	6	4	-1	11	2264.221	0	1274
5	3	-1	9	5	4	1	9	2264.283	1	960
5	3	1	9	5	4	-1	9	2264.283	1	960
4	3	-1	7	4	4	1	7	2264.378	2	537
4	3	1	7	4	4	-1	7	2264.378	2	537
11	5	-1	21	11	5	1	21	2393.626	0	282
11	5	1	21	11	5	-1	21	2393.626	0	282
10	5	-1	19	10	5	1	19	2393.650	-1	358
10	5	1	19	10	5	-1	19	2393.650	-1	358
9	5	-1	17	9	5	1	17	2393.676	0	452
9	5	1	17	9	5	-1	17	2393.676	0	452
8	5	1	15	8	5	-1	15	2393.700	0	568
8	5	-1	15	8	5	1	15	2393.700	0	568
7	5	-1	13	7	5	1	13	2393.726	1	712
7	5	1	13	7	5	-1	13	2393.726	1	712
6	5	1	11	6	5	-1	11	2393.753	1	893
6	5	-1	11	6	5	1	11	2393.753	1	893
5	5	1	9	5	5	-1	9	2393.785	-1	1118
5	5	-1	9	5	5	1	9	2393.785	-1	1118
13	0	-1	27	14	0	1	29	2393.863	-2	8108
13	0	-1	25	14	0	1	27	2393.863	4	7544
8	1	1	17	9	1	-1	19	2406.965	-4	10926
8	1	1	15	9	1	-1	17	2406.965	1	9767
12	0	1	25	12	1	-1	25	2407.457	0	20323
3	3	1	5	4	3	-1	7	2407.499	1	1155
3	3	-1	5	4	3	1	7	2407.499	1	1155
12	0	1	23	12	1	-1	23	2407.513	1	18744
4	4	1	9	4	4	-1	9	2407.627	-10	2903
4	4	-1	9	4	4	1	9	2407.627	-10	2903
9	4	-1	17	9	4	1	17	2407.649	-34	744
9	4	1	17	9	4	-1	17	2407.649	-34	744
8	4	-1	15	8	4	1	15	2407.677	-27	937
8	4	1	15	8	4	-1	15	2407.677	-27	937
7	4	1	13	7	4	-1	13	2407.704	-21	1176
7	4	-1	13	7	4	1	13	2407.704	-21	1176
6	4	-1	11	6	4	1	11	2407.731	-16	1476
6	4	1	11	6	4	-1	11	2407.731	-16	1476
5	4	1	9	5	4	-1	9	2407.760	-12	1858

5	4	-1	9	5	4	1	9	2407.760	-12	1858
4	4	1	7	4	4	-1	7	2407.796	-8	2344
4	4	-1	7	4	4	1	7	2407.796	-8	2344
6	0	1	13	6	1	-1	13	2410.531	-2	22799
6	0	1	11	6	1	-1	11	2410.601	0	19519
7	5	-1	13	6	5	1	11	2414.072	1	397
7	5	1	13	6	5	-1	11	2414.072	1	397
6	0	1	13	7	0	-1	15	2414.200	-1	12229
6	0	1	11	7	0	-1	13	2414.200	3	10570
12	1	1	23	13	0	-1	25	2414.249	0	7043
12	1	1	25	13	0	-1	27	2414.259	-1	7610
5	1	1	9	6	1	-1	11	2415.118	3	8531
5	1	1	11	6	1	-1	13	2415.118	-1	10122
8	5	-1	17	7	5	1	15	2416.641	0	594
8	5	1	17	7	5	-1	15	2416.641	0	594
8	5	-1	15	7	5	1	13	2416.905	0	520
8	5	1	15	7	5	-1	13	2416.905	0	520
5	0	-1	9	6	0	1	11	2417.098	0	9847
5	0	-1	11	6	0	1	13	2417.098	-4	11674
2	2	1	3	3	2	-1	5	2418.812	1	1858
2	2	-1	3	3	2	1	5	2418.812	0	1858
2	2	-1	5	3	2	1	7	2418.933	-2	2775
2	2	1	5	3	2	-1	7	2418.933	-1	2775
8	3	1	15	8	3	-1	15	2419.114	0	1115
8	3	-1	15	8	3	1	15	2419.114	-1	1115
7	3	1	13	7	3	-1	13	2419.133	-1	1401
7	3	-1	13	7	3	1	13	2419.133	-1	1401
6	3	1	11	6	3	-1	11	2419.151	-1	1762
6	3	-1	11	6	3	1	11	2419.151	-1	1762
5	3	-1	9	5	3	1	9	2419.169	-2	2225
5	3	1	9	5	3	-1	9	2419.169	-2	2225
4	3	1	7	4	3	-1	7	2419.191	-2	2830
4	3	-1	7	4	3	1	7	2419.191	-2	2830
3	3	-1	5	3	3	1	5	2419.221	-2	3605
3	3	1	5	3	3	-1	5	2419.221	-2	3605
3	1	1	5	4	1	-1	7	2420.980	1	6041
3	1	1	7	4	1	-1	9	2420.991	0	7865
10	1	1	19	11	0	-1	21	2421.074	1	8502
10	1	1	21	11	0	-1	23	2421.090	-1	9321
3	1	-1	5	4	1	1	7	2421.321	1	6069
3	1	-1	7	4	1	1	9	2421.337	-1	7898
4	0	1	7	3	1	-1	5	2423.511	1	5053
2	1	-1	3	3	1	1	5	2423.904	1	4228
2	1	-1	5	3	1	1	7	2423.932	0	6104
2	1	1	3	3	1	-1	5	2424.169	0	4238
2	1	1	5	3	1	-1	7	2424.201	0	6118
9	1	-1	17	10	0	1	19	2424.432	1	8992
9	1	-1	19	10	0	1	21	2424.452	-1	9953
5	0	-1	11	4	1	1	9	2426.479	-2	8112
5	0	-1	9	4	1	1	7	2426.558	1	6578
15	2	1	31	15	2	-1	31	2426.612	0	156
15	2	1	29	15	2	-1	29	2426.626	-2	148

1	1	1	1	2	1	-1	3	2426.785	0	2014
14	2	-1	29	14	2	1	29	2426.809	-1	205
14	2	-1	27	14	2	1	27	2426.823	-2	195
1	1	1	3	2	1	-1	5	2426.881	-2	3791
1	1	-1	1	2	1	1	3	2426.968	1	2014
13	2	1	25	13	2	-1	25	2426.990	0	254
1	1	-1	3	2	1	1	5	2427.067	-1	3794
12	2	-1	25	12	2	1	25	2427.112	1	349
12	2	-1	23	12	2	1	23	2427.127	0	328
2	2	-1	5	2	2	1	5	2427.548	2	5492
2	2	1	5	2	2	-1	5	2427.548	1	5492
3	2	-1	5	3	2	1	5	2427.604	-1	2836
3	2	1	5	3	2	-1	5	2427.604	2	2836
2	2	-1	3	2	2	1	3	2427.630	2	3618
2	2	1	3	2	2	-1	3	2427.630	1	3618
11	2	-1	23	11	2	1	23	2427.685	1	450
11	2	-1	21	11	2	1	21	2427.694	-1	421
8	1	1	15	9	0	-1	17	2427.752	3	9241
8	1	1	17	9	0	-1	19	2427.775	-1	10350
13	2	-1	25	13	2	1	25	2427.856	-4	254
13	2	-1	27	13	2	1	27	2427.856	2	269
15	2	-1	31	15	2	1	31	2428.135	-1	156
15	2	-1	29	15	2	1	29	2428.135	-3	148
12	5	1	25	11	5	-1	23	2428.165	0	702
12	5	-1	25	11	5	1	23	2428.165	0	702
12	5	-1	23	11	5	1	21	2428.306	0	646
12	5	1	23	11	5	-1	21	2428.306	0	646
16	2	1	33	16	2	-1	33	2428.326	-2	117
16	2	1	31	16	2	-1	31	2428.326	-2	112
4	3	1	9	3	3	-1	7	2430.579	-1	1662
4	3	-1	9	3	3	1	7	2430.579	-1	1662
6	1	1	13	6	1	-1	13	2430.634	1	527
6	1	1	11	6	1	-1	11	2430.662	-1	467
8	4	-1	17	7	4	1	15	2430.686	-27	1879
8	4	1	17	7	4	-1	15	2430.686	-27	1879
8	4	-1	15	7	4	1	13	2430.861	-26	1650
8	4	1	15	7	4	-1	13	2430.861	-26	1650
4	3	-1	7	3	3	1	5	2430.916	-1	1238
4	3	1	7	3	3	-1	5	2430.916	-1	1238
13	5	-1	27	12	5	1	25	2431.032	-2	663
13	5	1	27	12	5	-1	25	2431.032	-2	663
7	1	-1	15	8	0	1	17	2431.061	1	10449
3	1	-1	7	3	1	1	7	2432.132	0	1254
3	1	-1	5	3	1	1	5	2432.157	-1	998
2	1	1	5	2	1	-1	5	2432.430	0	1887
2	1	1	3	2	1	-1	3	2432.459	-1	1338
1	1	-1	3	1	1	1	3	2432.627	-1	3441
1	1	-1	1	1	1	1	1	2432.671	0	1434
7	0	-1	15	6	1	1	13	2432.735	-2	10054
7	0	-1	13	6	1	1	11	2432.785	1	8680
1	1	1	3	1	1	-1	3	2432.826	-1	3443
1	1	1	1	1	1	-1	1	2432.858	0	1435

5	3	1	9	4	3	-1	7	2433.719	-1	2250
5	3	-1	9	4	3	1	7	2433.719	-1	2250
14	5	1	29	13	5	-1	27	2433.898	0	610
14	5	-1	29	13	5	1	27	2433.898	0	610
14	5	-1	27	13	5	1	25	2434.012	1	568
14	5	1	27	13	5	-1	25	2434.012	1	568
5	1	1	9	5	1	-1	9	2434.164	1	598
5	1	1	11	5	1	-1	11	2434.176	0	686
6	1	1	11	7	0	-1	13	2434.256	-2	8806
6	1	1	13	7	0	-1	15	2434.302	2	10197
6	1	-1	11	6	1	1	11	2434.731	0	473
6	1	-1	13	6	1	1	13	2434.750	0	529
7	1	1	13	7	1	-1	13	2435.395	1	376
7	1	1	15	7	1	-1	15	2435.416	-1	421
17	2	1	33	18	1	-1	35	2435.538	1	1286
17	2	1	35	18	1	-1	37	2435.562	0	1360
8	0	1	17	7	1	-1	15	2435.918	-1	10473
8	0	1	15	7	1	-1	13	2435.958	2	9220
3	2	1	7	2	2	-1	5	2436.161	1	2919
3	2	-1	7	2	2	1	5	2436.161	-1	2919
6	3	1	11	5	3	-1	9	2436.563	1	3037
6	3	-1	11	5	3	1	9	2436.563	1	3037
15	5	1	31	14	5	-1	29	2436.759	0	548
15	5	-1	31	14	5	1	29	2436.759	0	548
15	5	-1	29	14	5	1	27	2436.861	0	513
15	5	1	29	14	5	-1	27	2436.861	0	513
1	0	-1	3	0	0	1	1	2437.367	0	3249
5	1	-1	9	6	0	1	11	2437.442	-2	8042
5	1	-1	11	6	0	1	13	2437.498	1	9554
4	2	1	9	3	2	-1	7	2439.077	-1	4863
4	2	-1	9	3	2	1	7	2439.077	3	4863
9	0	-1	19	8	1	1	17	2439.134	2	10546
9	0	-1	17	8	1	1	15	2439.160	-1	9419
4	2	1	7	3	2	-1	5	2439.223	-1	3696
4	2	-1	7	3	2	1	5	2439.223	3	3696
7	3	1	15	6	3	-1	13	2439.295	1	4195
7	3	-1	15	6	3	1	13	2439.295	1	4195
11	4	-1	23	10	4	1	21	2439.304	-49	2030
11	4	1	23	10	4	-1	21	2439.304	-49	2030
7	3	1	13	6	3	-1	11	2439.416	-1	3615
7	3	-1	13	6	3	1	11	2439.416	-1	3615
16	5	-1	33	15	5	1	31	2439.616	0	481
16	5	1	33	15	5	-1	31	2439.616	0	481
16	5	-1	31	15	5	1	29	2439.709	-1	453
16	5	1	31	15	5	-1	29	2439.709	-1	453
2	0	1	3	1	0	-1	1	2440.255	-2	3210
2	0	1	5	1	0	-1	3	2440.255	0	5775
4	1	1	7	5	0	-1	9	2440.578	-2	6895
4	1	1	9	5	0	-1	11	2440.649	2	8499
3	1	-1	7	2	1	1	5	2441.222	0	6422
3	1	-1	5	2	1	1	3	2441.286	-1	4450
12	4	1	23	11	4	-1	21	2442.263	-55	1787

12	4	-1	23	11	4	1	21	2442.263	-55	1787
8	3	1	15	7	3	-1	13	2442.281	1	4000
8	3	-1	15	7	3	1	13	2442.281	1	4000
10	0	1	21	9	1	-1	19	2442.377	2	10311
10	0	1	19	9	1	-1	17	2442.398	-1	9316
17	5	-1	35	16	5	1	33	2442.470	0	415
17	5	1	35	16	5	-1	33	2442.470	0	415
17	5	-1	33	16	5	1	31	2442.555	0	391
17	5	1	33	16	5	-1	31	2442.555	0	391
15	2	1	29	16	1	-1	31	2442.955	1	1867
15	2	1	31	16	1	-1	33	2442.986	-2	1990
3	0	-1	5	2	0	1	3	2443.139	-2	5627
3	0	-1	7	2	0	1	5	2443.139	0	8034
6	2	-1	13	5	2	1	11	2444.859	1	7382
6	2	1	13	5	2	-1	11	2444.873	0	7381
6	2	-1	11	5	2	1	9	2444.932	2	6209
6	2	1	11	5	2	-1	9	2444.945	0	6209
13	4	-1	27	12	4	1	25	2445.027	-65	1812
13	4	1	27	12	4	-1	25	2445.027	-65	1812
9	3	1	19	8	3	-1	17	2445.062	2	4713
9	3	-1	19	8	3	1	17	2445.062	3	4713
13	4	1	25	12	4	-1	23	2445.111	-65	1678
13	4	-1	25	12	4	1	23	2445.111	-65	1678
9	3	1	17	8	3	-1	15	2445.146	2	4208
9	3	-1	17	8	3	1	15	2445.146	3	4208
18	5	1	37	17	5	-1	35	2445.320	0	350
18	5	-1	37	17	5	1	35	2445.320	0	350
18	5	1	35	17	5	-1	33	2445.400	0	332
18	5	-1	35	17	5	1	33	2445.400	0	332
11	0	-1	23	10	1	1	21	2445.648	2	9816
11	0	-1	21	10	1	1	19	2445.665	0	8953
4	0	1	7	3	0	-1	5	2446.020	-2	7720
4	0	1	9	3	0	-1	7	2446.020	0	10002
4	0	1	7	3	0	-1	5	2446.032	10	7720
4	0	1	9	3	0	-1	7	2446.032	12	10002
14	2	-1	27	15	1	1	29	2446.598	1	2182

lower frequencies than 2446 cm^{-1} were recorded using the IR diode laser spectrometer at Rice University. There are 35 observed lines that are unassigned; those transitions are listed in Appendix I-1.

3.2 Spectrum Fit to Molecular Hamiltonian

An attempt was made at first to fit the spectrum by using Watson's A-reduced Hamiltonian and adding spin-rotation interaction as a perturbation. It was soon proved to be not sufficient. The program used in analyzing the spectra was written by T.J. Sears. Watson's A-reduced Hamiltonian[46] and the spin-rotation formulation of Brown and Sears[47] are used in this program:

$$H = H_R + H_{CD} + H_{SR} + H_{SRCD}$$

H_R and H_{CD} are the Hamiltonians representing the rotational energy and its centrifugal distortion correction, respectively. H_{SR} and H_{SRCD} refer to spin-rotation interaction and its centrifugal distortion correction, respectively.

$$H_R = AN_z^2 + BN_x^2 + CN_y^2$$

$$
\begin{aligned}
H_{CD} = & -\Delta_K N_z^4 - \Delta_{NK}\mathbf{N}^2 N_z^2 - \Delta_N \mathbf{N}^4 \\
& - 2\delta_N \mathbf{N}^2 (N_+^2 + N_-^2) - \delta_K [N_+^2 + N_-^2, N_z^2]_+ \\
& + \Phi_K N_z^6 + \Phi_K \mathbf{N}^2 N_z^4 + \Phi_{NK} \mathbf{N}^4 N_z^2 + \Phi_N \mathbf{N}^6 \\
& + 2\phi_N \mathbf{N}^4 (N_+^2 + N_-^2) + \phi_{NK} \mathbf{N}^2 [N_z^2, N_+^2 + N_-^2]_+ \\
& + \phi_K [N_z^2, N^2 + N_-^2] \\
& - L_K N_z^8
\end{aligned}
$$

Δ, Φ, and ϕ are the effective quartic, sextic and octic centrifugal distortion parameters.

$$
\begin{aligned}
H_{SR} = & \epsilon_{aa} N_z S_z + \epsilon_{bb} N_x S_x + \epsilon_{cc} N_y S_y \\
& + (1/2)\epsilon_{ab} \{[N_x, S_z]_+ + [N_z, S_x]_+\} \\
& + (1/2)\epsilon_{ac} \{[N_y, S_z]_+ + [N_z, S_y]_+\} \\
& + (1/2)\epsilon_{bc} \{[N_x, S_y]_+ + [N_y, S_x]_+\}
\end{aligned}
$$

ϵ_{ij}'s are spin-rotation interaction parameters.

$$
\begin{aligned}
H_{SRCD} = & \Delta_K^S N_z^3 S_z + \Delta_{KN}^S N_z^2 \mathbf{N}\cdot\mathbf{S} + (1/2)\Delta_{NK}^S \{\mathbf{N}^2 N_z S_z + N_z S_z \mathbf{N}^2\} \\
& + \Delta_N^S \mathbf{N}^2 (\mathbf{N}\cdot\mathbf{S}) + \delta_N^S (N_+^2 + N^2)\mathbf{N}\cdot\mathbf{S} \\
& + (1/2)\delta_K^S \{(N_+^2 + N^2) N_z S_z + N_z S_z (N_+^2 + N^2)\} \\
& + \Phi_K^S N_z^5 S_z
\end{aligned}
$$

Δ^S, δ, and Φ are the effective spin-rotation centrifugal distortion parameters.

Sears' program was designed for fitting the spectra of asymmetric top molecules. By choosing the options, it can be used either to analyze magnetic resonance spectra or zero-field spectra. The program also allows simultaneous fits to rotational and rovibrational transitions from the same vibrational state. The instructions for using the program have been given in Reference 48. The detailed theory behind the program has been discussed by Sears[49]. Some minor changes had to be made to Sears' original program (SEARS.FORTRAN). The program was then combined with matrix diaganolization routines from EISPACK and LINPACK to fit the HCO spectra. The present version of the program is named HCO.FORTRAN. The sample input file is saved as TOT.TOT. All these files are stored in the UCB CMSA system under the account MOORONS2.

3.2.1. Coriolis Interaction between (1,0,0,)† and (0,0,2) States in HCO

†In HCO, υ_1 refers to C-H stretching, υ_2 C-O stretching, and υ_3 bending.

Initially, the observed transitions were least-squares fitted with a band origin and upper state rotational, spin-rotational, and centrifugal distortion constants. When such a fitting was carried out, it was found that the K' = 4 and K' = 5 infrared transitions appeared to be incompatible with each other. When transitions involving levels from both stacks were included, the standard deviation became about 2.5 times that expected from the estimated errors in the measurements, almost tripling in comparison with the standard deviation obtained when only either K' = 4 or K' = 5 transitions were included in the fit. This could not be remedied by including additional centrifugal distortion constants of higher order in K even though K' = 5 is the highest K' observed and assigned. It seems that the apparent perturbation in the upper state can be ascribed primarily to the K' = 4 levels. If K' = 4 lines are included, there are systematic deviations in the K' = 3 levels and several of the upper state centrifugal distortion and spin-rotational centrifugal distortion constants change by unusually large amounts from the ground state. However, as discussed later, there are still significant changes in Δ_{NK} and Φ_{KN} even when the K' = 4 lines were omitted. Fits for which both K' = 4 and K' = 5 were included or for which only K' = 4 was included were carried out. The resulting spectroscopic parameters

and the residuals grouped with respect to different K' stacks are given in Appendix I-1.

It was suspected that the K' = 4 transitions may be affected by Coriolis interaction with the K' = 5 levels of the bending overtone. The band center of the (0,0,2) ← (0,0,0) transition has been reported to be 2129 cm^{-1} from the HCO^- photoelectron spectroscopic study by linberger's group[37]. The A rotational constant of the bending overtone is expected to be much larger than the A value of the C-H stretch excited state. The estimation of the A constant for the first excited bending overtone state is shown below:

$$A(v) = A_e - \Sigma\alpha_i(v_i + 1/2) \quad [50]$$

For the ground state, $A(0,0,0) = A_e - (1/2)\Sigma\alpha_i$

Thus, $A(0,0,1) = A(0,0,0) - \alpha_3$

Since $A(0,0,1) = 26.5\ cm^{-1}$[15] and
$A(0,0,0) = 24.3\ cm^{-1}$[27],

Therefore, $\alpha_3 = -2.2\ cm^{-1}$
$A(0,0,2) = 28.6\ cm^{-1}$

The A constant of the (1,0,0) state is only 22.6 cm^{-1} as shown in Table I-2. As a result even though the bending overtone is near 2129 cm^{-1}, the energies of a level of given K will catch up with the K-1 and eventually with the K levels of the 2434 cm^{-1} C-H stretch as K increases. Figure I-5 depicts an estimate of the relative locations of the (1,0,0) and (0,0,2) K stacks. The A', B', and C' rotational constants needed for calculating the energy levels of the (0,0,2) states were estimated based upon the bending vibration-rotation interaction constants[15] as shown above. The calculated energy difference between the K' = 4 level of the (1,0,0) state and the K' = 5 level of the (0,0,2) state is only 31 cm^{-1}. The estimated uncertainty is ±40 cm^{-1} due primarily to the uncertainties in the determination of the band origin for the bending overtone and in the estimation of the A', B', and C' constants for the (0,0,2) state.

The K' = 4 levels appear to be pushed down by increasing amounts with increasing N' with a maximum displacement of about 0.2 cm^{-1} near the largest observed N' of 23 as seen in the residuals from the least-squares fit presented in Figure I-6. Such a displacement could result from a Coriolis interaction between (0,0,2) K' = 5 and (1,0,0) K' = 4. The slow onset is readily explained by the fact that (B+C)/2 for (1,0,0) is, in fact, expected

Table I-2. Parameters resulting from least-squares fit of the infrared, FIR LMR, and microwave data for HCO.

Parameter (cm^{-1})	(0,0,0)[a]	(0,0,0)[b]	(1,0,0)[c]
υ_0			2434.47790(24)
A-(B+C)/2	22.882726(11)	22.8832961(86)[d]	21.14225(37)[d]
(B+C)/2	1.4463102(4)	1.44630991(28)	1.4451800(26)
10^2 (B-C)/4	2.3824(16)	2.3821(11)	2.52491(64)
10^6 Δ_N	3.952(19)	3.953(13)	4.0113(71)
10^5 Δ_{NK}	1.520(13)	1.5244(96)	-0.490(56)
10^2 Δ_K	3.06891(96)	3.14115(83)	2.696(14)
10^7 δ_N	3.911(43)	3.841(33)	4.298(48)
10^4 δ_K	1.50(16)[e]	1.47(11)	1.404(53)
10^9 Φ_{NK}		2.7(12)	f
10^7 Φ_{KN}	-4.718(87)	-4.860(98)	-9.80(21)
10^4 Φ_K		1.472(11)	1.29(14)
10^7 L_K		6.82(35)	0.24(38)
10 $\varepsilon_{aa}+\varepsilon_{bb}+\varepsilon_{cc}$	3.81448(40)	3.8140(27)	3.2942(34)
10 $2\varepsilon_{aa}-\varepsilon_{bb}-\varepsilon_{cc}$	7.81705(67)	7.81606(45)	6.7665(70)
10^3 $(\varepsilon_{bb}-\varepsilon_{cc})/2$	3.7439(24)	3.7462(18)	3.700(78)
10^3 ε_{ab}	6.72(8)	6.504(53)	f
10^7 Δ_N^s	2.10(33)	2.34(27)	f
10^6 Δ_{NK}^s	-3.32(73)	-1.65(53)	f
10^3 Δ_K^s	-1.637(12)	-1.6033(75)	-1.295(17)
10^6 Φ_K^s	4.45(88)	1.56(54)	f
$\sigma_{weighted}$[g]		1.1	0.9

[a]Reference 27.

[b]This work.

[c]This work.

[d]Uncertainties are one estimated standard deviation in last two reported digits.

For the (1,0,0) level the uncertainty applies to the difference between (1,0,0) and (0,0,0) constants.

[e]Corrected uncertainty by T.J. Sears, Private communication.

[f]Constrained to ground state value.

[g]The weighting is such that the expected standard deviation is 1.0.

Figure I-5. Estimated locations of the hypothetical N = 0 energy levels for the $2\upsilon_3$ and υ_1 states. It is believed that the K = 4 level of υ_1 is being perturbed by an anharmonic Coriolis interaction with K = 5 of $2\upsilon_3$ as is indicated by the double-headed arrow. The uncertainty in the estimation of the $2\upsilon_3$ levels is about ± 40 cm^{-1}.

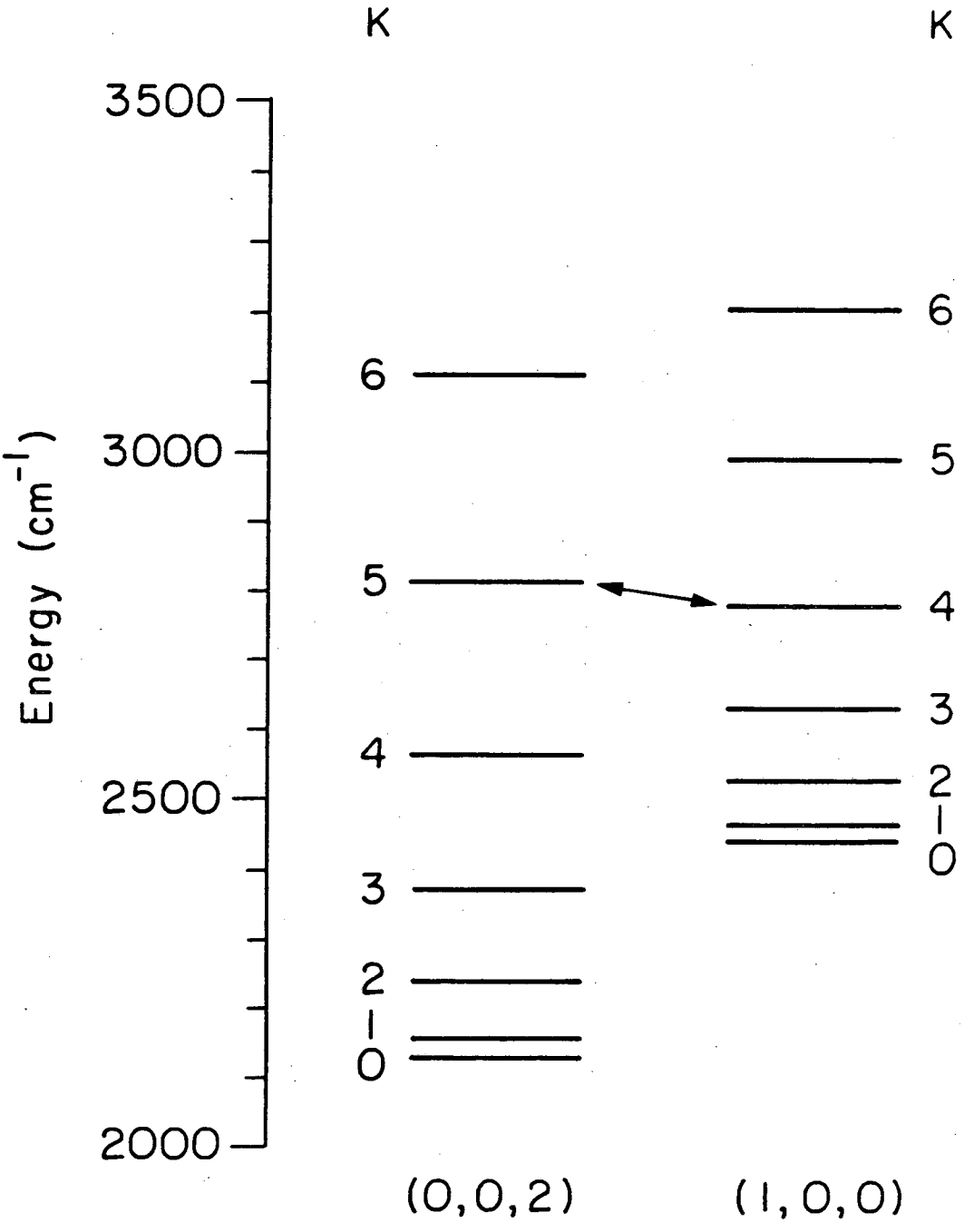
K
K
3500
3000
2500
2000
Energy (cm⁻¹)
6
5
4
3
2
1
0
6
5
4
3
2
1
0
(0,0,2)
(1,0,0)

Figure I-6. Residuals of the observed transitions involving the K' = 4 rotational levels calculated from the results of the least-squares fit presented in Table I-2. The circles represent difference frequency laser observations and the squares diode laser observations.

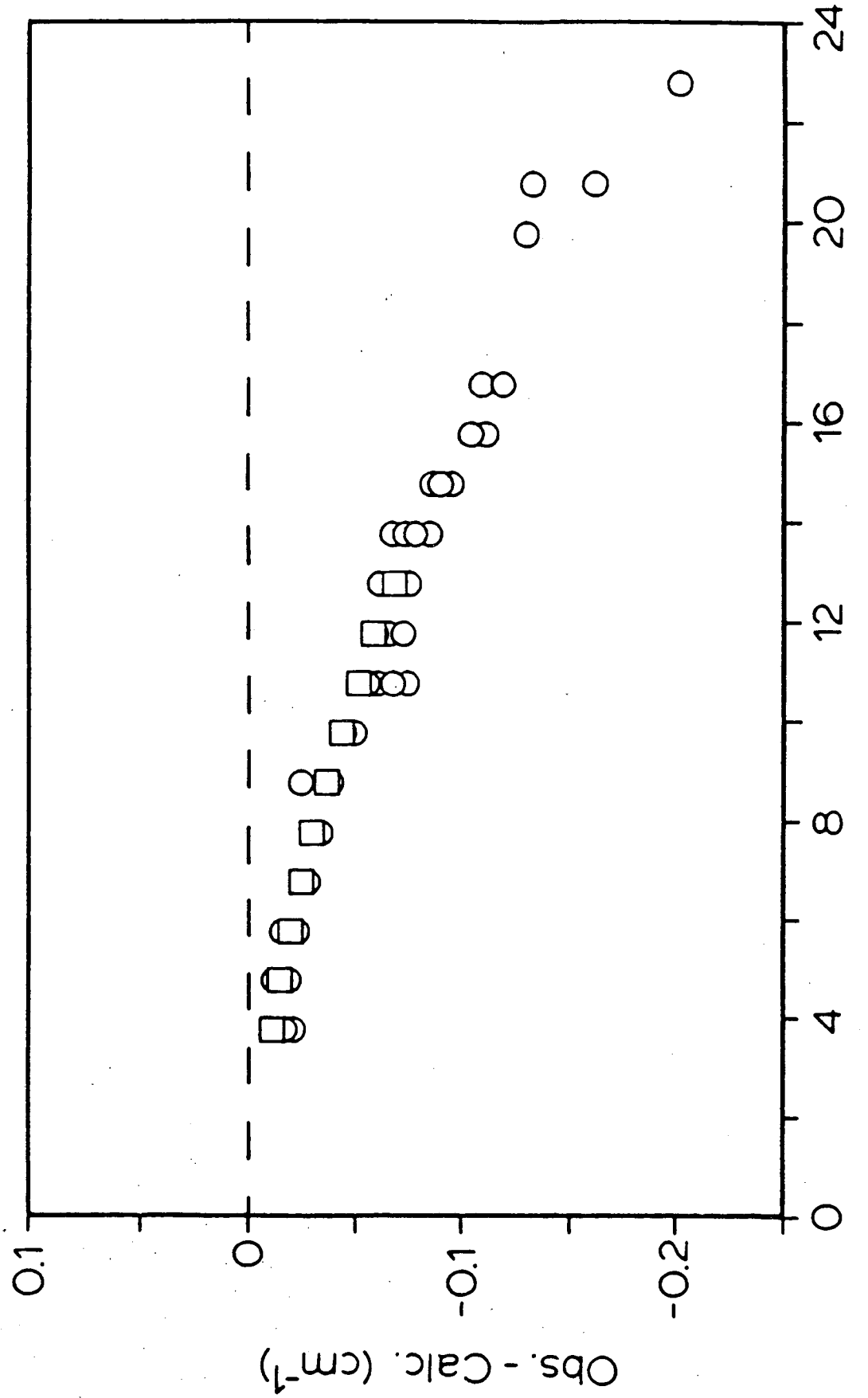
0.1
0
-0.1
-0.2
Obs. - Calc. (cm⁻¹)
0
4
8
12
16
20
24
Excited State N (K'=4)

to be slightly smaller than (B+C)/2 for (0,0,2). Thus by N = 20 the separation between the two levels is expected to increase by almost 0.5 cm^{-1} from its smallest value at N = 5. Therefore it is believed that the increasing size of the perturbation with N results because the Coriolis matrix element[51] is proportional to $[(N(N + 1) - 20]^{1/2}$† and the energy difference between the two interacting levels is almost independent of N.

3.2.2. Derivation of the Spectroscopic Constants for the Ground State of HCO

Previous to this work, the ground state rotational, spin-rotational, and centrifugal distortion constants had been obtained from fits of EPR[24], microwave[26], and FIR LMR[49] data by Sears[49]. Although up to K" = 6 parallel transitions were measured in these experiments, only 1 ← 0, 0 ← 1, and 2 ← 1 perpendicular K-stack lines were observed. With the large access to the different rotational levels of the ground vibrational states in the IR data recorded in this work, the ground state constants

† The selection rules for Coriolis interactions are $\Delta K = 0, 1,$ and 2. The matrix element $\langle J,K,v| H_{Coriolis} |J,K\pm1,v\rangle$ is proportional to $[(N(N + 1) - K(K \pm 1)]^{1/2}$.

could be improved. One obvious choice is to least-squares fit the ground and the excited state constants simultaneously by combining all the rotational and rovibrational data. However, having recognized that some of the upper state levels are possibly perturbed, it seemed appropriate to fit the ground state and excited state separately.

The first step was to fit the ground state and thereby improve the ground state constants. Since fitting combination differences of the IR data can introduce the problem[52] of observational correlation, a method was derived by Curl et al. at Rice University[53] to obtain the ground state constants. In this method, an additional parameter was introduced for each upper state level to take into account the inadequacy of the upper state Hamiltonian. This parameter was represented by the average frequency of all the observed lines ending on the same upper state level and a combination of the parameters correlated with the ground state constants (rotational, centrifugal distortion, and spin-rotational). Therefore, instead of fitting linear combinations of observations as done in fitting combination differences or term values, a fit using a linear combination of parameters was made. The details of this method have been discussed in reference[53]. Although in principle this method

eliminated the problems due to correlations between observations, in the present fit there are no differences between the ground state constants for HCO obtained by using the method of Reference 53 and by fitting combination differences. Presumably observational correlations are smaller than inadequacies in the form of the Hamiltonian.

In the present fit, 40 microwave lines from Black et al.'s work[26], 37 FIR LMR line reported by Sears[49], and 900 υ_1 infrared lines were used involving 332 upper state levels. (There appear to be more υ_1 lines used than were given as measured and assigned because unresolved spin and asymmetry doublets were each treated as two lines at half weight in the fit.) Each data point was weighted by the squared reciprocal of the estimated measurement uncertainty (microwave = 1×10^{11}, FIR LMR = 1×10^{8}, difference frequency = 1×10^{4}, and diode = 1×10^{6}).

In the Hamiltonian used there were 23 parameters for a given vibrational state corresponding to 3 rotational constants, 5 quartic, 4 sextic, and 1 octic centrifugal distortion parameters (the 3 off-diagonal in K sextic constants are omitted and only the K^8 octic term was included), 4 spin-rotation interaction constants, 5 quartic spin-rotation centrifugal distortion constants

(Δ^S_{NK} is omitted), and 1 sextic spin-rotation distortion constant (Φ^S_K). Even the large number of lines used in the fit is not sufficient to determine all of these parameters. The diagnostic least-squares method[54] was used to identify the poorly determined parameters (Φ_N, δ^S_N, δ^S_K). The resulting ground state rotational, centrifugal distortion, and spin-rotational parameters are listed in Table I-2.

The weighted standard deviation of this fit is 1.1 which is what is expected from the estimated errors in the observations. However, it must be pointed out that the residuals are not distributed very smoothly. Sears [49] recognized that several of the FIR LMR lines have large residuals when fitting ground state parameters with all the available rotational transitions. Moreover, the fit of the microwave data is poorer than the expected experimental error. In the present spectrum analysis, the υ_1 data is actually fitted somewhat better than the estimated experimental error, perhaps due to the over estimation of the error for the difference frequency data. One pair of FIR LMR lines (N = 11 ← 10, K = 6) have by far the largest weighted residuals and appear to have a spin-rotation splitting which is too small. However, eliminating these two lines is not sufficient to make the distribution of residuals smooth. It is believed that the

ground state parameters given in Table I-2 are the best synthesis of the information currently available.

3.2.3. Derivation of the Spectroscopic Constants for the (1,0,0) State of HCO

The ground state parameters were fixed at the values obtained as described in the previous section. The excited state rotational, centrifugal distortion, and spin-rotational constants as well as the band origin were then determined by fitting the infrared transition frequencies. Once again the diagnostic least squares procedure was used to decide which parameters are determinable, guiding the truncation of the Hamiltonian. In this fit K' = 4 lines were omitted because of the suspected perturbation mentioned in Section 3.2.1. In the final fit, 705 transitions were used: 555 difference frequency laser and 150 diode laser measurements. Table I-2 presents the resulting excited state constants and the band origin. It was noticed that there are rather large changes in Δ_{NK} and Φ_{KN} from the ground state. Similar changes were found even if the K' = 5 lines were omitted, i.e. if only lines of K' = 0, 1, 2, and 3 are included. It is possible that some of the K' = 3 levels are slightly perturbed. The differences between the calculated IR

transition frequencies using the parameters derived in this work and the observed ones are listed in Table I-1.

4. Other Results

4.1 Equilibrium Constants

The rotational and centrifugal distortion constants obtained here have been combined with those obtained in previous high resolution studies of the bending and C-O stretching fundamentals to calculate the vibration-rotation interaction constants. These constants are listed in Table I-3. The ground state rotational constants resulting from fitting the bending and C-O stretching fundamentals are somewhat different from the values given in Table I-2. For this reason the differences between the ground and excited state constants obtained in these studies were used rather than the absolute values of the excited state constants since these differences are believed to be better determined.

From the vibration-rotation interaction constants, the centrifugal distortion constants, and rotational g-factors, equilibrium rotational constants and moments of inertia of HCO may be calculated and are listed in Table I-4. The corrections to the apparent rotational constants (A, B, C) presently derived were carried out to obtain the equilibrium rotational constants A_e, B_e, and C_e[50,55]:

Table I-3. α constants and $\frac{1}{2}\sum_s \alpha_s^i$ of HCO (cm^{-1}).

s	α_s^A	α_s^B	α_s^C
1[a]	1.7422(4)[b]	-0.00173(2)	0.00399(2)
2[c]	0.1012(2)	0.01253(6)	0.01152(6)
3[d]	-2.2463(1)	0.00633(5)	0.00610(7)
$\frac{1}{2}\sum_s \alpha_s^i$	-2.015(2)	0.00224(4)	0.01081(5)

[a]This work.

[b]Values in parentheses correspond to one standard deviation.

[c]Reference 16.

[d]Reference 20.

Table I-4. Calculation of equilibrium rotational constants (cm^{-1}) and moments of inertia ($\mu\AA$) of HCO.

A_1^a	24.1282(2)	A_2^b	24.1282	A_3^c	24.1280	A_e^d	24.3153
B_1	1.49620(4)	B_2	1.49606	B_3	1.49583	B_e	1.49585
C_1	1.40947(5)	C_2	1.40961	C_3	1.40995	C_e	1.41015

Equilibrium moments of inertia:

I_a^e	0.693290
I_b^e	11.2695
I_c^e	11.9545
Δ_e	-0.0084

[a]Equilibrium A,B,C from the α's of Table I-3 and the ground state rotational constants of Table I-2.

[b]Ground state $R_6 = -3.3 \times 10^{-8}$ cm^{-1} and with the equilibrium centrifugal distortion constants assumed equal to the ground state.

[c]Ground state $\tau_{abab} = -4.5 \times 10^{-8}$ cm^{-1} and equilibrium assumed equal to ground state.

[d]Rotational g-values calculated from the formula $g_{ii} = -\psi\varepsilon_{ii}|/\zeta$ (Reference 56) with ζ assumed equal to 50 cm^{-1} (Reference 57).

(1). Corrections for the rotation-vibration interactions

$$A_1 = A - 1/2(\alpha_1^A + \alpha_2^A + \alpha_3^A)$$
$$B_1 = A - 1/2(\alpha_1^B + \alpha_2^B + \alpha_3^A)$$
$$C_1 = A - 1/2(\alpha_1^C + \alpha_2^C + \alpha_3^C)$$

(2). Corrections for the centrifugal distortion effect

$$A_2 = A_1 - 16R_6$$
$$B_2 = B_1 + 16R_6(A-C)/(B-C)$$
$$C_2 = C_1 - 16R_6(A-C)/(B-C)$$

$$A_3 = A_2 - \hbar^4\tau_{abab}/2$$
$$B_3 = B_2 - \hbar^4\tau_{abab}/2$$
$$C_3 = C_2 - 3\hbar^4\tau_{abab}/4$$

(3). Corrections for the electron slippage

$$A_e = A_3(1 - g_{aa}/1836)$$
$$B_e = B_3(1 - g_{bb}/1836)$$
$$C_e = C_3(1 - g_{cc}/1836)$$

The two centrifugal distortion constants needed to correct the rotational constants for centrifugal distortion effects, R_6 and τ_{abab}, were calculated from the constants

listed in Table I-2 using the expressions for Δ_N, Δ_{NK}, Δ_K, δ_N, and δ_K in terms of the four independent planar centrifugal distortion constants, τ_{aaaa}, τ_{bbbb}, τ_{aabb}, and τ_{abab} then least-squares fitting the five Δ's with the four τ's; the expressions can be found in Gordy and Cook's book[50]. The resulting R_6 and τ_{abab} are -3.3×10^{-8} cm^{-1} and -4.5×10^{-4} cm^{-1}, respectively. The rotational g-factors needed for the electron slippage correction were estimated from the spin-rotation interaction constants using the equation $g_{ii} = -|\varepsilon_{ii}|/\zeta$[56], with $\zeta = 50$ cm^{-1} [57]. The inadequacy of this method for finding approximate values of the g_{ii}'s is probably the reason that the equilibrium inertial defect is so large ($\Delta_e = -0.0084$). In order to determine the equilibrium structure of HCO, a similar treatment of DCO is required. Such a treatment is not possible at this time because the bending fundamental of DCO has not been observed under high resolution.

4.2 Transition Dipole Orientation

The orientation of the transition dipole moment for υ_1 with respect to the principal axes was obtained by measuring the relative intensities of parallel and perpendicular rotational components and comparing them

with the theoretically calculated ratios:

$$I\ (\Delta K = 0) \propto \mu_A^2$$
$$I\ (\Delta K = 1) \propto \mu_B^2$$

I: transition strength

μ: transition dipole moment

If I_A' and I_B' are calculated line strengths for parallel and perpendicular transitions from the same rotation level of the ground vibrational state respectively, and I_A and I_B are experimentally observed relative line intensities correspond to the same transitions, then

$$I_A/I_B = (I_A'/I_B')(\mu_A^2/\mu_B^2)$$

The angle (α) of the transition dipole moment relative to the b-axis can be calculated:

$$\alpha = \tan^{-1}(\mu_A/\mu_B)$$

The theoretical calculations of the line strengths[48] for unit vibrational transition dipole moments are included in Sears' spectrum analysis program. The intensities of 90 pairs of difference frequency laser absorption lines with common ground state rotational

levels were compared as shown in Table I-5. Although there is considerable scatter in these relative intensity measurements, the scatter in the angle which the transition dipole moment makes with the axes is relatively small because the arc tangent of the square root of the intensity ratio is involved. The result is that the transition dipole moment makes an angle of 63 ± 6° with the b-axis. The quoted error is 1 σ value. The equilibrium structure calculated by Hirota[28] gives 41° as the orientation of the C-H bond with respect to the b-axis. Thus the transition dipole makes an angle of 22° (or with the less reasonable choice of signs 76°) with the C-H bond, as illustrated in Figure I-7. As the H atom moves away from the C atom, there must be significant motion of the electron density along the C-O bond.

Table I-5. List of 90 pairs of absorption lines used to calculate the angle of the transition dipole moment relative to the b-axis.

NU	KAU	PU	2*JU	NL	KAL	PL	2*JL	OBS. (CM-1)	CAL. INT.	OBS. S/N	ANGLE (°)
10	0	1	21	9	0	-1	19	2463.182	112	30.0	66
10	1	1	21	9	0	-1	19	2481.682	120	11.0	
11	0	-1	21	10	0	1	19	2466.013	98	24.0	64
11	1	-1	21	10	0	1	19	2484.016	103	7.5	
11	1	-1	21	10	1	1	19	2463.655	88	14.0	62
11	0	-1	21	10	1	1	19	2445.665	73	5.5	
11	0	-1	23	10	0	1	21	2466.013	107	24.0	64
11	1	-1	23	10	0	1	21	2484.016	113	7.5	
12	0	1	23	11	0	-1	21	2468.837	92	40.0	67
12	1	1	23	11	0	-1	21	2486.314	95	12.5	
14	0	1	27	13	0	-1	25	2474.440	77	26.0	66
14	1	1	27	13	0	-1	25	2490.808	76	9.0	
15	0	-1	29	14	0	1	27	2477.227	68	21.0	58
15	1	-1	29	14	0	1	27	2493.000	66	12.5	
16	0	1	33	15	0	-1	31	2480.009	63	21.5	66
16	1	1	33	15	0	-1	31	2495.141	60	7.0	
17	0	-1	33	16	0	1	31	2482.748	51	20.0	70
17	1	-1	33	16	0	1	31	2497.267	47	5.0	
21	0	-1	41	20	0	1	39	2493.605	23	12.0	68
21	1	-1	41	20	0	1	39	2505.534	19	4.0	
22	0	1	45	21	0	-1	43	2496.273	19	12.0	68
22	1	1	45	21	0	-1	43	2507.540	16	3.0	
5	1	-1	11	4	1	1	9	2446.876	82	13.0	77
5	0	-1	11	4	1	1	9	2426.479	66	1.5	
9	1	-1	17	8	1	1	15	2458.102	92	12.0	68
9	0	-1	17	8	1	1	15	2439.160	77	3.0	
10	1	1	19	9	1	-1	17	2460.881	91	12.5	65
10	0	1	19	9	1	-1	17	2442.398	76	4.0	
10	1	1	21	9	1	-1	19	2460.872	101	14.0	63
10	0	1	21	9	1	-1	19	2442.377	84	5.0	
12	1	1	25	11	1	-1	23	2466.412	91	18.0	66
12	0	1	25	11	1	-1	23	2448.947	74	5.0	
13	1	-1	25	12	1	1	23	2469.205	77	9.0	64
13	0	-1	25	12	1	1	23	2452.266	62	3.0	
13	1	-1	27	12	1	1	25	2469.205	83	9.0	64
13	0	-1	27	12	1	1	25	2452.254	67	3.0	

14	1	1	27	13	1	-1	25	2471.942	70	22.0	75
14	0	1	27	13	1	-1	25	2455.600	56	3.0	
16	1	1	33	15	1	-1	31	2477.414	58	12.0	49
16	0	1	33	15	1	-1	31	2462.279	44	12.5	
17	1	-1	33	16	1	1	31	2480.147	47	15.0	59
17	0	-1	33	16	1	1	31	2465.645	35	6.5	
18	1	1	37	17	1	-1	35	2482.848	41	13.0	60
18	0	1	37	17	1	-1	35	2468.977	31	5.0	
20	1	1	39	19	1	-1	37	2488.275	26	17.0	73
20	0	1	39	19	1	-1	37	2475.713	19	2.5	
21	1	-1	41	20	1	1	39	2490.964	21	11.5	61
21	0	-1	41	20	1	1	39	2479.047	14	4.0	
22	1	1	43	21	1	-1	41	2493.637	17	9.0	66
22	0	1	43	21	1	-1	41	2482.364	11	2.0	
3	1	-1	5	2	1	1	3	2441.286	36	5.0	60
3	2	-1	5	2	1	1	3	2504.452	48	3.5	
3	1	-1	7	2	1	1	5	2441.222	52	7.5	62
3	2	-1	7	2	1	1	5	2504.688	67	3.5	
6	1	-1	11	5	1	1	9	2450.391	77	11.0	67
6	2	-1	11	5	1	1	9	2512.309	63	3.5	
6	1	-1	13	5	1	1	11	2450.371	91	13.5	62
6	2	-1	13	5	1	1	11	2512.423	74	5.0	
6	1	1	11	5	1	-1	9	2449.713	77	9.5	55
6	2	1	11	5	1	-1	9	2512.309	63	6.0	
6	1	1	13	5	1	-1	11	2449.694	91	11.0	57
6	2	1	13	5	1	-1	11	2512.423	74	6.0	
7	1	-1	15	6	1	1	13	2452.512	98	10.0	57
7	2	-1	15	6	1	1	13	2517.049	79	5.0	
8	1	-1	15	7	1	1	13	2456.267	89	9.0	54
8	2	-1	15	7	1	1	13	2517.462	65	5.0	
8	1	-1	17	7	1	1	15	2456.251	100	9.0	54
8	2	-1	17	7	1	1	15	2517.541	73	5.0	
9	1	1	17	8	1	-1	15	2459.217	90	20.0	66
9	2	1	17	8	1	-1	15	2519.955	63	5.0	
9	1	1	19	8	1	-1	17	2459.208	101	17.0	50
9	2	1	19	8	1	-1	17	2520.028	70	7.0	
11	1	-1	21	10	1	1	19	2463.655	88	14.0	63
11	2	-1	21	10	1	1	19	2530.223	65	4.5	
12	1	1	23	11	1	-1	21	2466.422	83	18.0	76
12	2	1	23	11	1	-1	21	2533.701	62	2.0	
15	1	-1	29	14	1	1	27	2474.701	62	17.0	76
15	2	-1	29	14	1	1	27	2544.588	47	2.0	
15	1	1	29	14	1	-1	27	2476.778	59	18.0	74
15	2	1	29	14	1	-1	27	2533.881	35	2.0	
19	1	1	37	18	1	-1	35	2488.406	30	18.0	68
19	2	1	37	18	1	-1	35	2542.175	17	3.0	
20	1	-1	39	19	1	1	37	2491.318	24	10.0	65
20	2	-1	39	20	1	1	39	2505.217	23	2.0	
3	2	-1	7	2	2	1	5	2436.161	24	5.5	64
3	3	-1	7	2	2	1	5	2540.402	73	7.0	
4	2	-1	9	3	2	1	7	2439.077	40	13.0	66
4	3	-1	9	3	2	1	7	2543.279	71	8.0	

4	2	1	7	3	2	-1	5	2439.223	30	9.5	64
4	3	1	7	3	2	-1	5	2543.066	56	7.0	
6	2	-1	11	5	2	1	9	2444.932	50	12.0	69
6	3	-1	11	5	2	1	9	2548.854	60	4.0	
6	2	1	11	5	2	-1	9	2444.945	50	12.0	69
6	3	1	11	5	2	-1	9	2548.844	60	4.0	
7	2	-1	13	6	2	1	11	2447.828	57	12.0	69
7	3	-1	13	6	2	1	11	2551.716	60	3.5	
7	2	-1	15	6	2	1	13	2447.770	66	12.0	69
7	3	-1	15	6	2	1	13	2551.865	69	3.5	
7	2	1	13	6	2	-1	11	2447.802	57	12.0	67
7	3	1	13	6	2	-1	11	2551.736	60	4.0	
8	2	-1	15	7	2	1	13	2450.675	61	11.5	66
8	3	-1	15	7	2	1	13	2554.623	59	4.0	
8	2	-1	17	7	2	1	15	2450.608	69	12.0	63
8	3	-1	17	7	2	1	15	2554.755	67	5.0	
8	2	1	15	7	2	-1	13	2450.693	61	10.0	64
8	3	1	15	7	2	-1	13	2554.587	59	4.0	
8	2	1	17	7	2	-1	15	2450.658	69	13.5	65
8	3	1	17	7	2	-1	15	2554.719	67	5.0	
9	2	1	17	8	2	-1	15	2453.520	63	9.0	58
9	3	1	17	8	2	-1	15	2557.511	57	5.0	
9	2	-1	17	8	2	1	15	2453.578	63	12.0	62
9	3	-1	17	8	2	1	15	2557.450	57	5.0	
9	2	1	19	8	2	-1	17	2453.483	70	9.5	60
9	3	1	19	8	2	-1	17	2557.633	64	4.5	
9	2	-1	19	8	2	1	17	2453.539	70	10.0	58
9	3	-1	19	8	2	1	17	2557.572	63	5.5	
10	2	1	19	9	2	-1	17	2456.462	63	7.0	65
10	3	1	19	9	2	-1	17	2560.348	54	2.5	
10	2	1	21	9	2	-1	19	2456.427	70	8.0	54
10	3	1	21	9	2	-1	19	2560.416	60	5.5	
10	2	-1	19	9	2	1	17	2456.388	63	7.0	56
10	3	-1	19	9	2	1	17	2560.401	54	4.5	
11	2	-1	21	10	2	1	19	2459.352	61	7.5	49
11	3	-1	21	10	2	1	19	2563.137	50	6.5	
11	2	-1	23	10	2	1	21	2459.324	67	10.0	56
11	3	-1	23	10	2	1	21	2563.246	55	5.5	
11	2	1	21	10	2	-1	19	2459.269	61	3.0	38
11	3	1	21	10	2	-1	19	2563.288	50	5.5	
11	2	1	23	10	2	-1	21	2459.245	67	9.0	53
11	3	1	23	10	2	-1	21	2563.393	55	6.0	
12	2	-1	25	11	2	1	23	2462.063	63	13.0	61
12	3	-1	25	11	2	1	23	2566.271	50	5.0	
12	2	1	25	11	2	-1	23	2462.201	63	14.0	62
12	3	1	25	11	2	-1	23	2566.055	50	5.0	
13	2	-1	25	12	2	1	23	2465.117	53	16.0	63
13	3	-1	25	12	2	1	23	2568.771	41	5.5	
13	2	-1	27	12	2	1	25	2465.096	58	19.0	64
13	3	-1	27	12	2	1	25	2568.858	45	5.0	
13	2	1	25	12	2	-1	23	2464.937	54	18.0	63
13	3	1	25	12	2	-1	23	2569.064	42	6.0	

13	2	1	27	12	2	-1	25	2464.913	58	19.0	62
13	3	1	27	12	2	-1	25	2569.155	45	7.0	
15	2	-1	31	14	2	1	29	2470.909	46	11.5	66
15	3	-1	31	14	2	1	29	2574.402	34	3.0	
15	2	1	29	14	2	-1	27	2470.616	43	10.0	66
15	3	1	29	14	2	-1	27	2574.869	32	3.5	
15	2	1	31	14	2	-1	29	2470.597	46	11.0	61
15	3	1	31	15	2	-1	31	2530.942	38	8.0	
16	2	1	31	15	2	-1	29	2473.832	37	6.5	67
16	3	1	31	15	2	-1	29	2577.080	27	1.5	
16	2	1	33	15	2	-1	31	2473.817	40	6.5	60
16	3	1	33	15	2	-1	31	2577.140	29	2.5	
18	2	1	35	17	2	-1	33	2479.666	27	7.0	61
18	3	1	35	17	2	-1	33	2582.467	19	4.2	
18	2	1	37	17	2	-1	35	2479.657	28	7.0	61
18	3	1	37	17	2	-1	35	2582.527	20	2.5	
4	3	1	7	3	3	-1	5	2430.916	10	3.0	57
4	4	1	7	3	3	-1	5	2574.335	44	7.5	
4	3	1	9	3	3	-1	7	2430.580	14	4.0	58
4	4	1	9	3	3	-1	7	2574.487	56	10.0	
6	3	1	11	5	3	-1	9	2436.563	25	9.0	66
6	4	1	11	5	3	-1	9	2580.074	44	5.5	
7	3	1	15	6	3	-1	13	2439.295	34	9.5	68
7	4	1	15	6	3	-1	13	2583.102	49	12.0	
11	3	1	21	10	3	-1	19	2450.875	34	16.0	68
11	4	1	21	10	3	-1	19	2594.447	34	5.0	
11	3	1	23	10	3	-1	21	2450.821	37	16.0	65
11	4	1	23	10	3	-1	21	2594.515	37	6.0	
12	3	-1	23	11	3	1	21	2453.744	32	10.0	62
12	4	-1	23	11	3	1	21	2597.251	31	4.5	
12	3	-1	25	11	3	1	23	2453.691	35	3.5	63
12	4	-1	25	11	3	1	23	2597.359	33	4.5	
13	3	-1	27	12	3	1	25	2456.538	33	4.0	47
13	4	-1	27	12	3	1	25	2600.212	30	5.5	

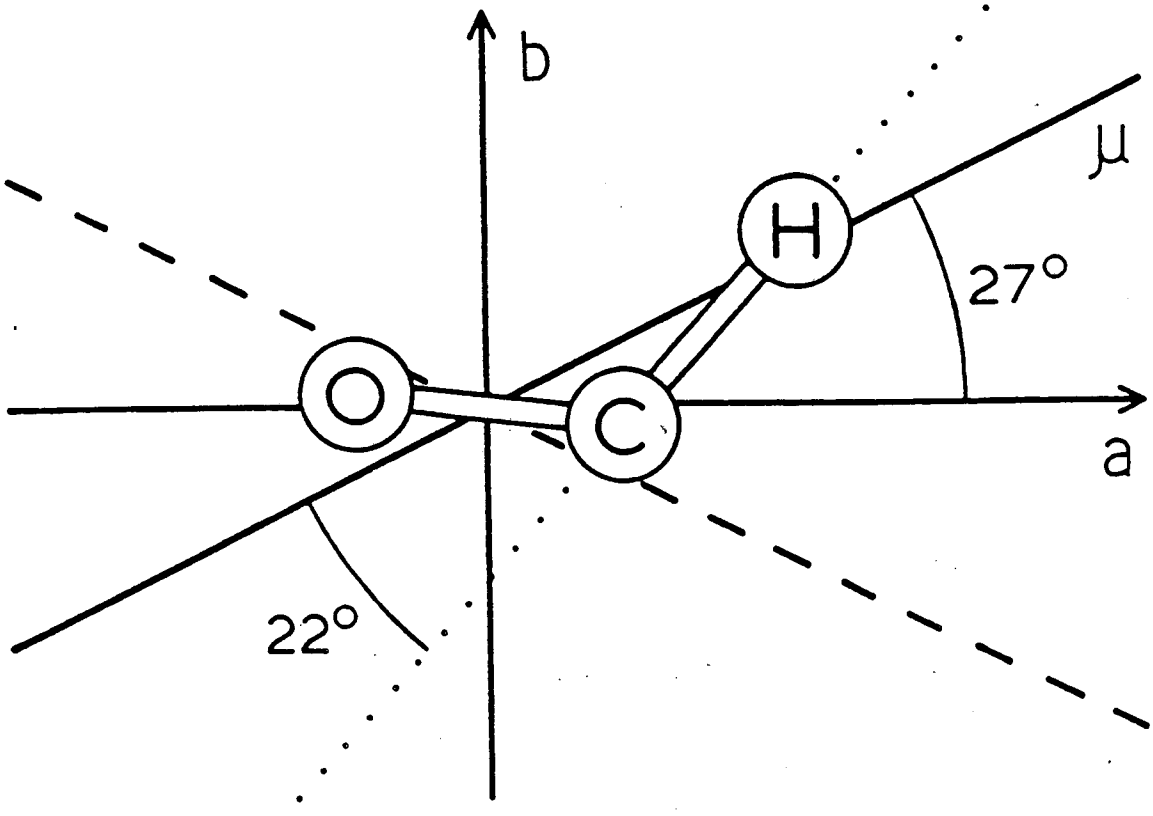

Figure I-7. Orientation of the transition dipole moment for υ_1 in the molecule. The line marked μ is the most reasonable orientation; the dashed line is the orientation which results from the other choice of the relative signs of the a and b components of the transition dipole.

5. Discussion

The C-H stretching frequency determined here, 2434.48 cm^{-1}, is well within the range of 2432 ± 20 cm^{-1} determined by LIF[36] and of 2440 ± 20 cm^{-1} by photoelectron spectroscopy[37]. The ab initio value of 2448 cm^{-1} is too high by only 0.6%[58]. The much higher frequency observed in an Ar matrix[14] implies a matrix shift of 48 cm^{-1} to the blue. Jacox has suggested that this anomalously large stiffening of the C-H stretch is a consequence of the unusually low dissociation energy, low vibrational frequency, and large anharmonicity[8].

Because the C-H bond of HCO is unusually weak and anharmonic, there is considerable interest in mapping out the complete potential energy surface of the molecule. A high quality ab initio surface has been developed[58]. Hirota has determined quadratic and cubic force constants from the fundamental frequencies and high resolution vibration-rotation constants available in 1985[28]. The improved centrifugal distortion constants for the ground state and especially the new constants for υ_1 reported here should permit a significantly improved force field to be defined. An even better determined force field should result from the investigation of combination bands especially the Fermi resonance between $2\upsilon_3$ and υ_1, or even

better, between $\upsilon_1 + 2\upsilon_3$ and $2\upsilon_1$ which would directly determine the cubic force constant linear in the C-H stretch and quadratic in the bend. The υ_3 band of DCO also remains to be studied at high resolution. In HCO the high resolution study of $2\upsilon_1$ and possibly combinations thereof with υ_3 and υ_2 should produce valuable information about the nature of the potential surface and nuclear motions on that surface near the C-H dissociation threshold.

The photoelectron spectroscopy of HCO^- studied by Lineberger's group[37] gave the band center for different vibrational bands of HCO up to 10268 cm^{-1} which corresponds to the (2,2,2) ← (0,0,0) transition. Attempts have been made to study the absorption spectra of (1,0,1) ← (0,0,0) (3468 cm^{-1}), (1,0,2) ← (0,0,0) (4533 cm^{-1}), and (2,0,0) ← (0,0,0) (4533 cm^{-1}) bands. Unfortunately, H_2CO absorbs at those frequency regions and CH_3CHO absorbs even more. Negative peaks were observed as a result of the depletion of H_2CO (or CH_3CHO) by the UV photolysis. Some positive peaks were also observed. Many positive peaks were seen when the IR laser was scanned through the (0,1,1) ← (0,0,0) or the (0,0,3) ← (0,0,0) band center region (Both of them appeared at 2936 cm^{-1} in Lineberger's work). It was later realized that at least some of those positive peaks were from rotationally or rovibrationally

hot H_2CO absorptions. Those H_2CO were either formed through the HCO recombination reaction or through energy transfer when room temperature H_2CO collided with hot HCO and H after UV photolysis. A careful examination is necessary to see if any of those observed lines were from HCO absorptions. This is not trivial to do since the absorption spectrum of H_2CO at such high frequency has not been studied. This work has not been finished in the present study.

Appendix I-1. List of unassigned lines.

Frequency (cm^{-1})	S/N
2460.303	4.5
2485.814	5.0
2485.962	6.0
2494.348	7.0
2499.669	2.0
2505.572	2.0
2520.399	5.0
2523.142	1.5
2525.079	1.5
2527.316	4.2
2534.068	4.2
2534.166	4.2
2536.893	6.0
2544.448	1.5
2548.672	6.0
2552.367	4.2
2565.057	4.2
2571.030	12.0
2575.338	4.2
2576.857	6.0
2579.745	9.0
2582.552	2.5
2587.344	4.2
2589.076	2.0
2597.632	4.2
2597.727	6.0
2604.101	4.5
2604.111	5.5
2613.230	1.5
2613.692	1.5
2613.767	2.0
2614.391	2.0
2614.439	2.0
2621.422	3.0
2622.640	2.0
2624.982	2.0

Appendix I-2.

As discussed in Section 3.2.1., the K' = 4 levels of the (1,0,0) state in HCO are perturbed by the K' = 5 levels of the (0,0,2) state through Coriolis interaction. The spectroscopic parameters and the residuals resulting from the least-squares fits for which both K' = 4 and K' = 5 were included (Table I-6 and Figures I-8 to I-13) or for which only K' = 4 was included (Table I-7 and Figures I-14 to I-19) are given in this Appendix. The residuals are the difference between the observed and the calculated transition frequencies (Obs - Calc). The circles represent difference frequency laser observations and the squares diode laser observations.

Table I-6. Parameters resulting from the least-squares fit of IR data when K' = 1, 2, 3, 4 and 5 levels were included.

Parameter (cm^{-1})	(0,0,0)[a]	(1,0,0)[b]
υ_0		2434.477600(8)
A-(B+C)/2	22.8832961(86)[c]	21.14143(32)
(B+C)/2	1.44630991(28)	1.4452019(52)
10^2 (B-C)/4	2.3821(11)	2.526205(18)
10^6 Δ_N	3.953(13)	3.993(21)
10^5 Δ_{NK}	1.5244(96)	1.04(11)
10^2 Δ_K	3.14115(83)	2.6192(77)
10^7 δ_N	3.841(33)	4.13(13)
10^4 δ_K	1.47(11)	1.47(16)
10^9 Φ_{NK}	2.7(12)	d
10^7 Φ_{KN}	-4.860(98)	-4.51(43)
10^4 Φ_K	1.472(11)	0.391(56)
10^7 L_K	6.82(35)	-23.9(12)
10 $\varepsilon_{aa}+\varepsilon_{bb}+\varepsilon_{cc}$	3.8140(27)	3.2905(83)
10 $2\varepsilon_{aa}-\varepsilon_{bb}-\varepsilon_{cc}$	7.81606(45)	6.764(17)
10^3 $(\varepsilon_{bb}-\varepsilon_{cc})/2$	3.7462(18)	3.55(20)
10^3 ε_{ab}	6.504(53)	d
10^7 Δ_N^s	2.34(27)	d
10^6 Δ_{NK}^s	-1.65(53)	d
10^3 Δ_K^s	-1.6033(75)	-1.278(44)

$10^6 \Phi_K^S$	1.56(54)	d
$\sigma_{weighted}$	1.1	2.5

[a]Ground state parameters.

[b]Both K' = 4 and 5 levels were included in the fit.

[c]Uncertainties are one standard deviation in last two reported digits.

[d]Constrained to ground state value.

Figure I-8

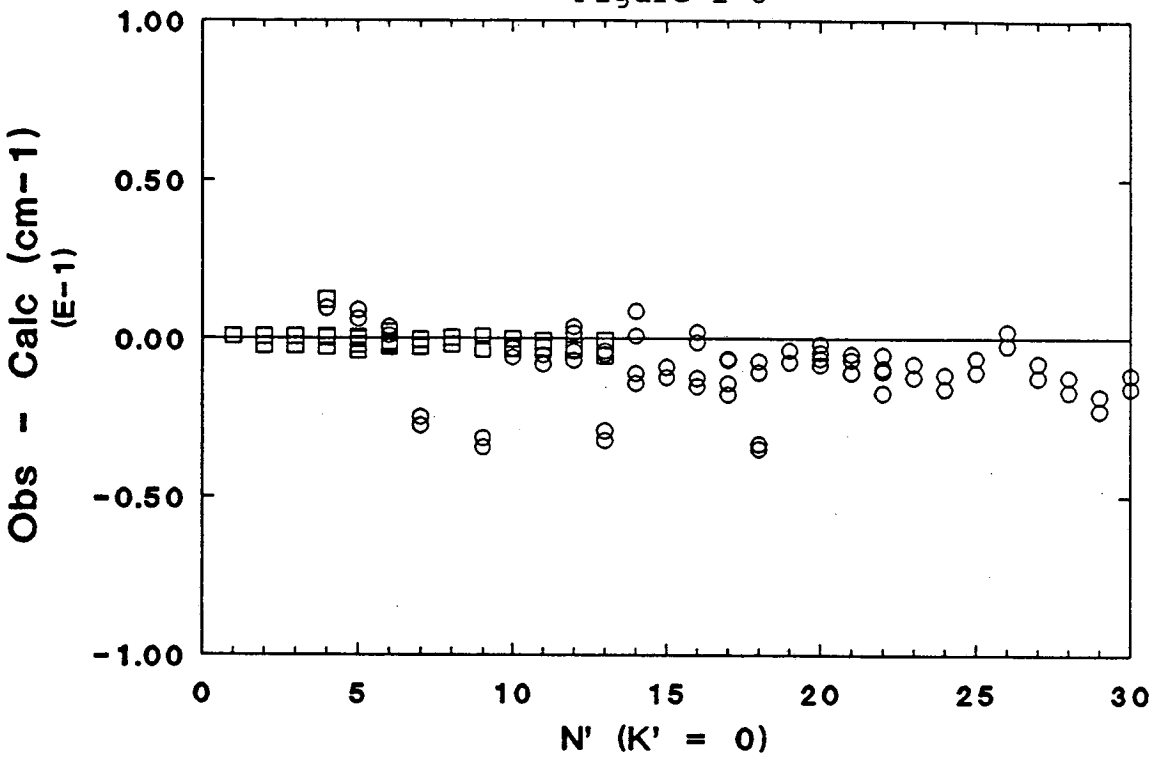

Figure I-9

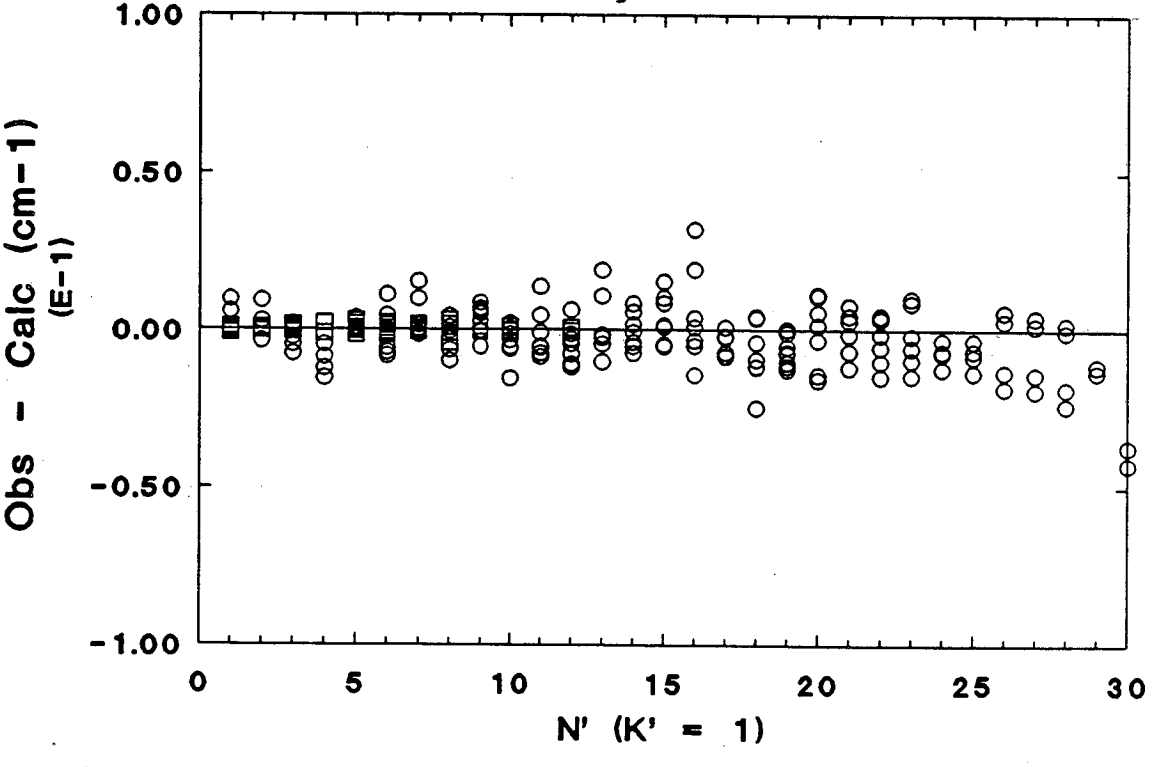

Figure I-10

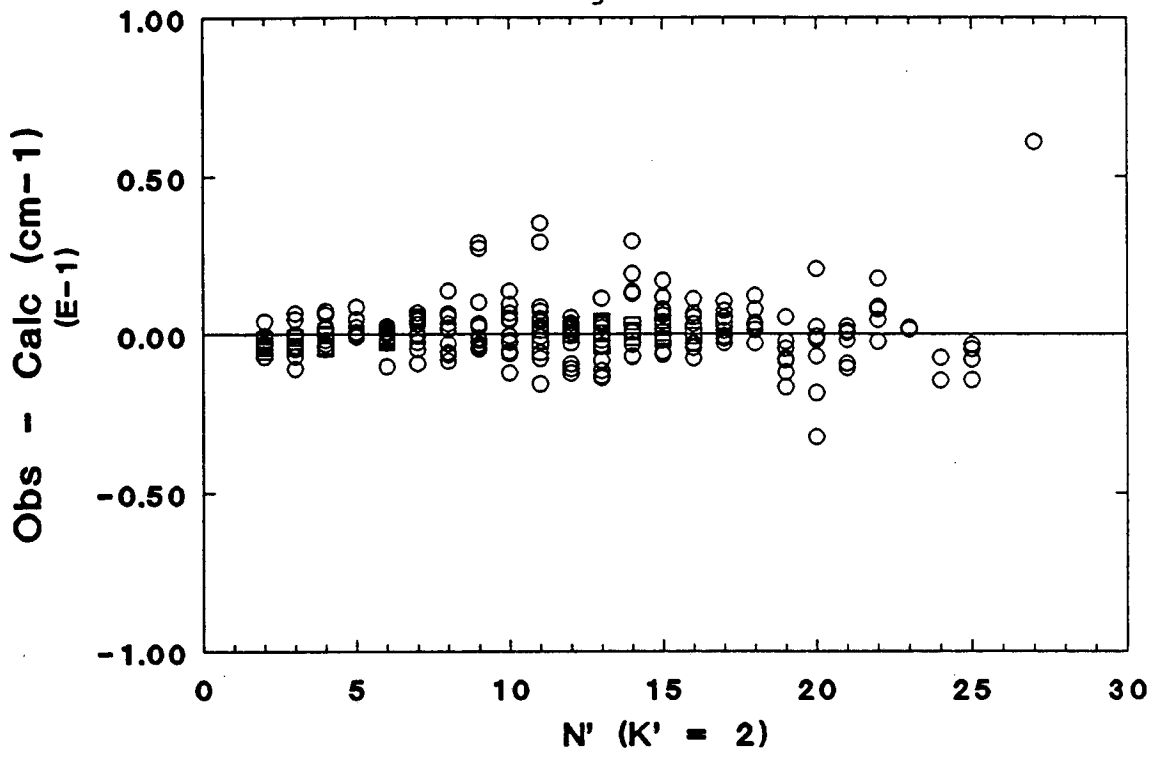

Figure I-11

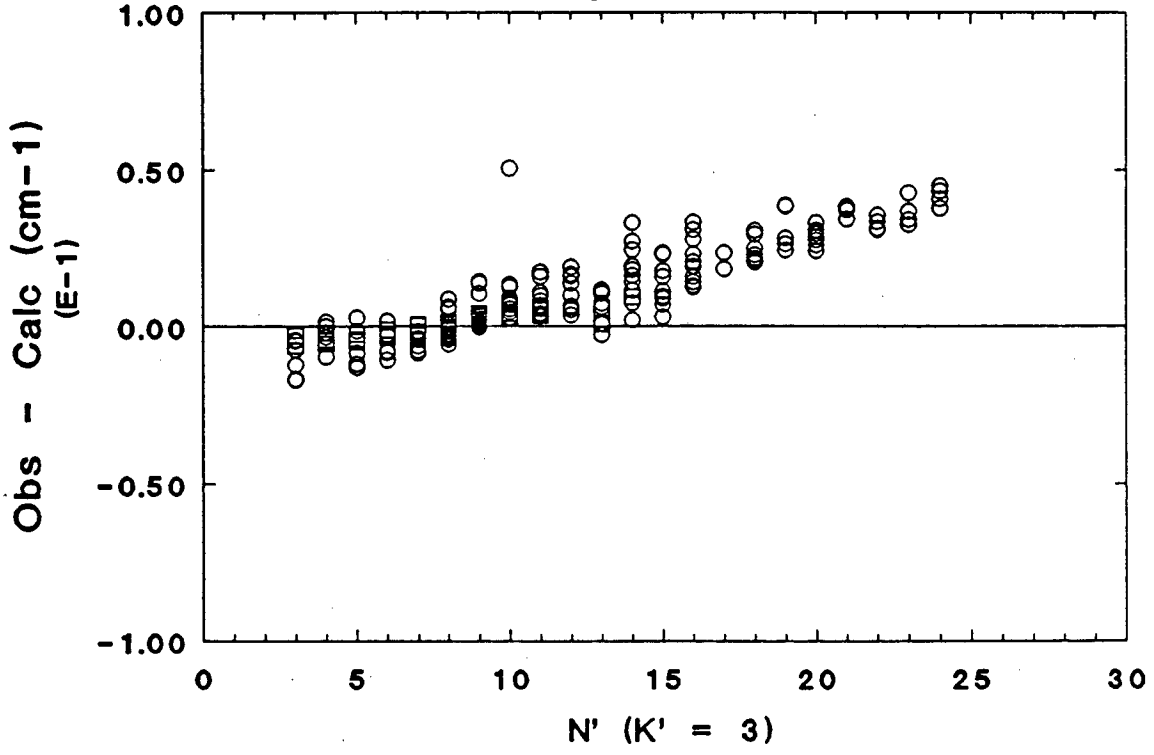

Figure I-12

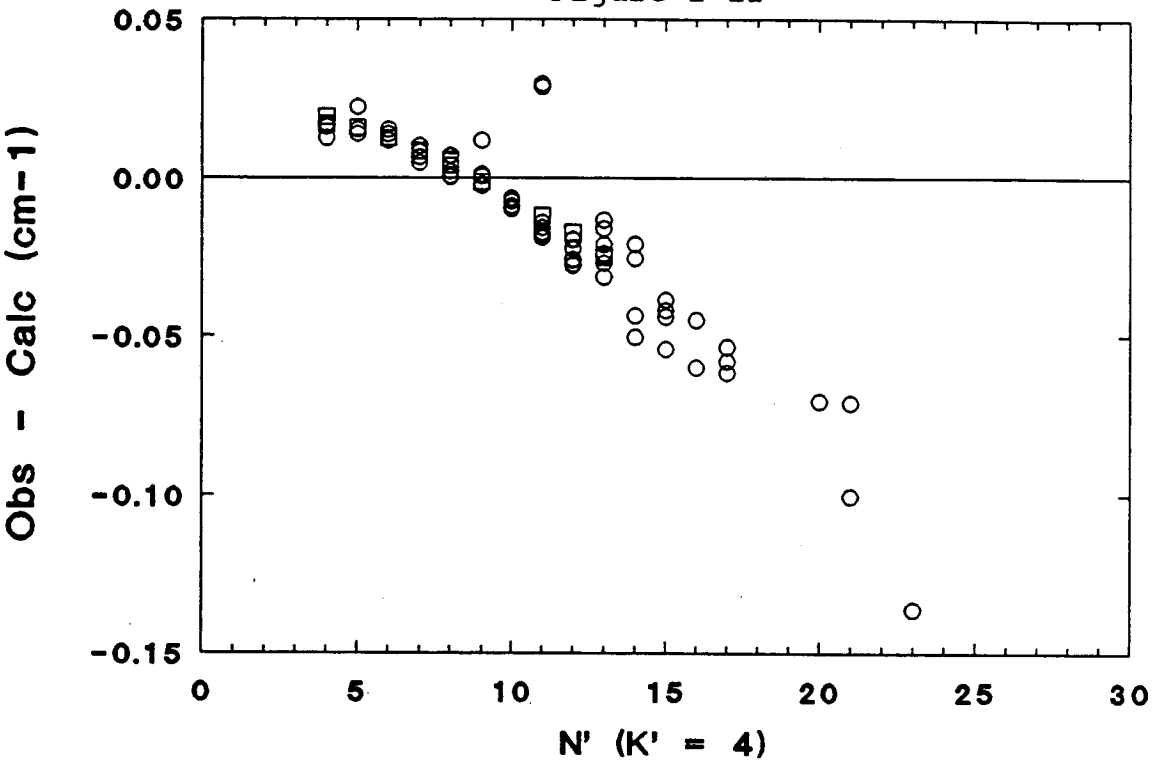

Figure I-13

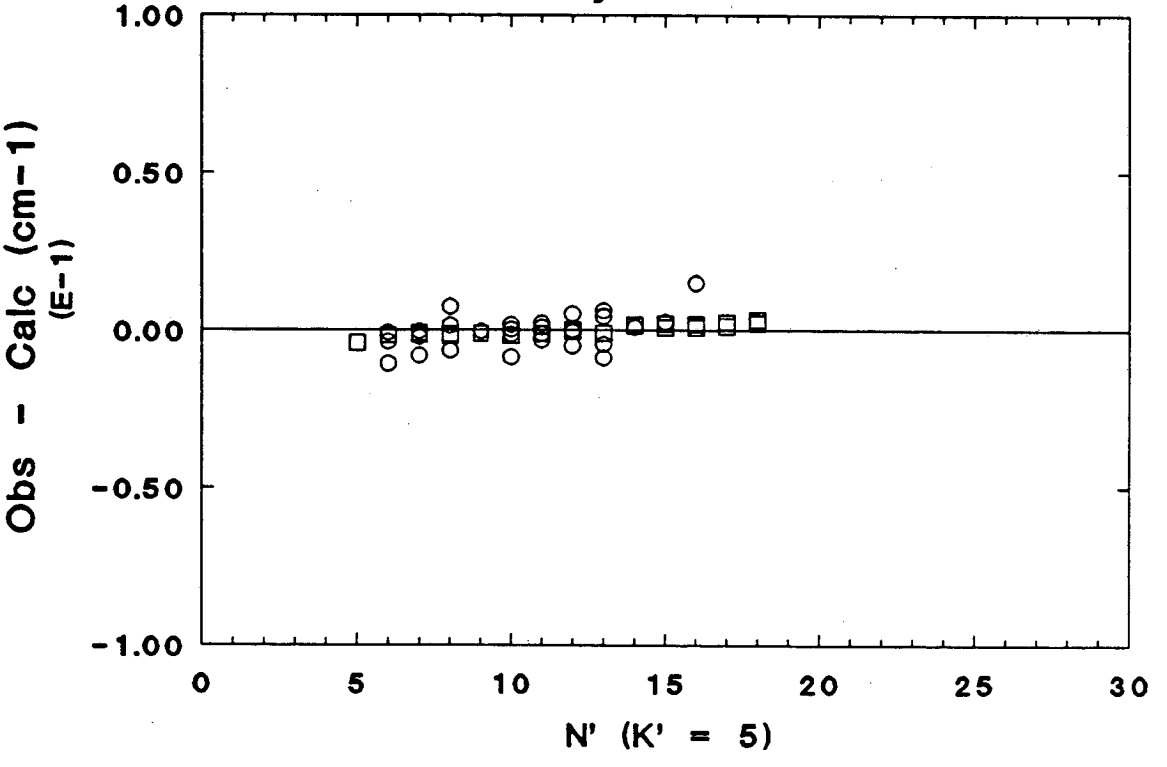

Table I-7. Parameters resulting from the least squares fit of IR data when K' = 0, 1, 2, 3, and 4 levels were included.

Parameter (cm^{-1})	(0,0,0)[a]	(1,0,0)[b]
υ_0		2434.47760(36)
A-(B+C)/2	22.8832961(86)[c]	21.14295(28)
(B+C)/2	1.44630991(28)	1.4451649(30)
10^2 (B-C)/4	2.3821(11)	2.5219(11)
10^6 Δ_N	3.953(13)	3.936(10)
10^5 Δ_{NK}	1.5244(96)	-2.200(91)
10^2 Δ_K	3.14115(83)	2.726(15)
10^7 δ_N	3.841(33)	4.114(72)
10^4 δ_K	1.47(11)	0.866(89)
10^9 Φ_{NK}	2.7(12)	d
10^7 Φ_{KN}	-4.860(98)	-32.38(63)
10^4 Φ_K	1.472(11)	2.44(19)
10^7 L_K	6.82(35)	47.8(69)
10 $\varepsilon_{aa}+\varepsilon_{bb}+\varepsilon_{cc}$	3.8140(27)	3.3040(60)
10 $2\varepsilon_{aa}-\varepsilon_{bb}-\varepsilon_{cc}$	7.81606(45)	6.789(12)
10^3 $(\varepsilon_{bb}-\varepsilon_{cc})/2$	3.7462(18)	3.63(11)
10^3 ε_{ab}	6.504(53)	d
10^7 Δ_N^S	2.34(27)	d
10^6 Δ_{NK}^S	-1.65(53)	d
10^3 Δ_K^S	-1.6033(75)	-1.378(48)

$10^6 \Phi_K^S$	1.56(54)	d
$\sigma_{weighted}$	1.1	1.5

[a]Ground state parameters derived in this work.

[b]Only K' = 4 levels were included in the fit.

[c]Uncertainties are one standard deviation in last two reported digits.

[d]Constrained to ground state value.

Figure I-14

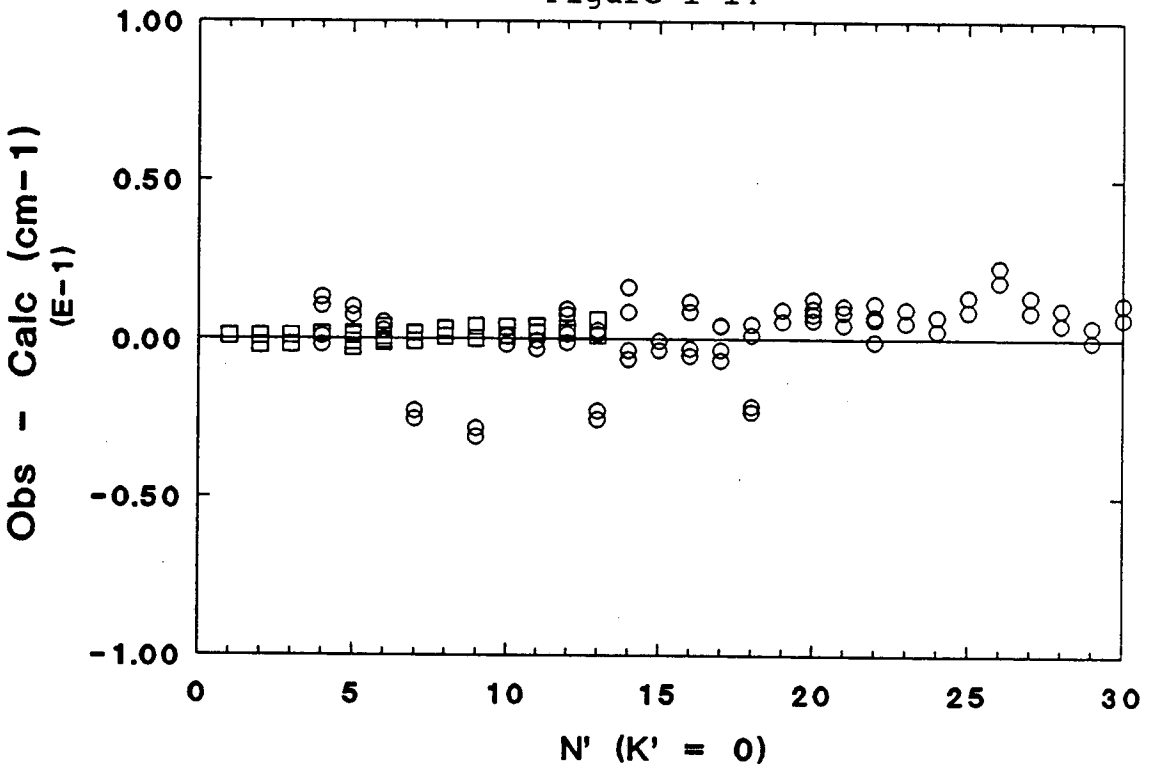

Figure I-15

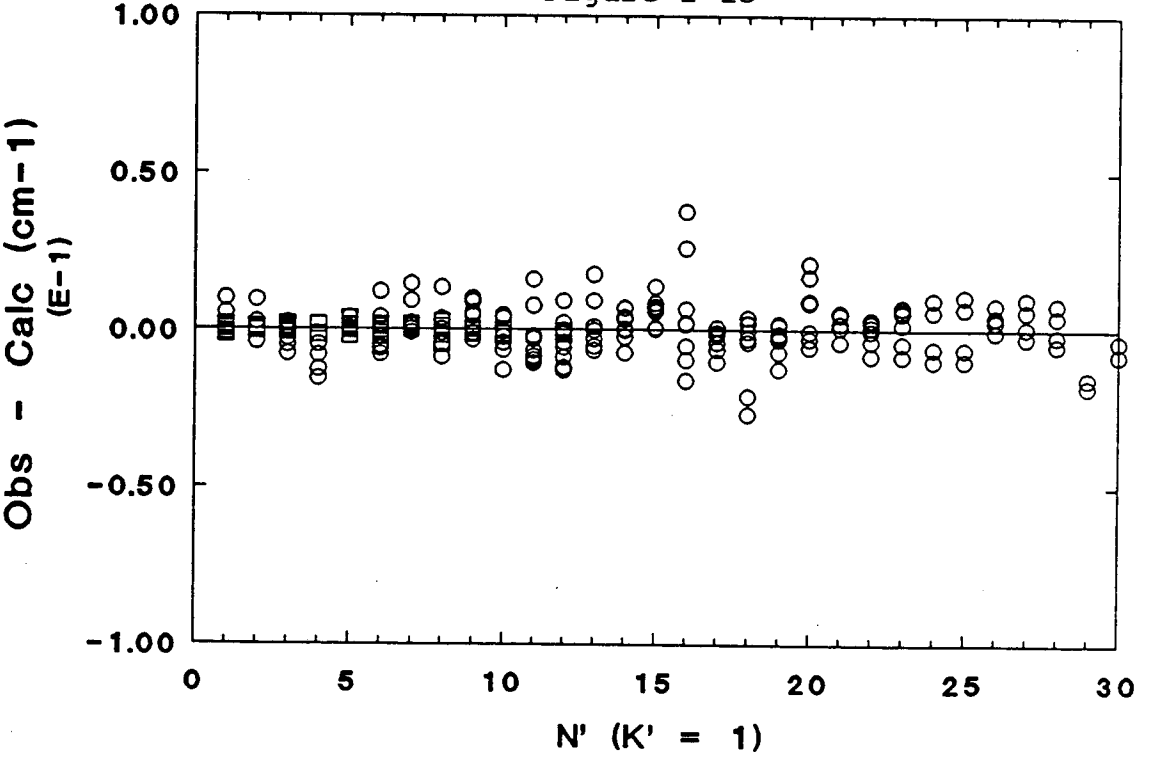

Figure I-16

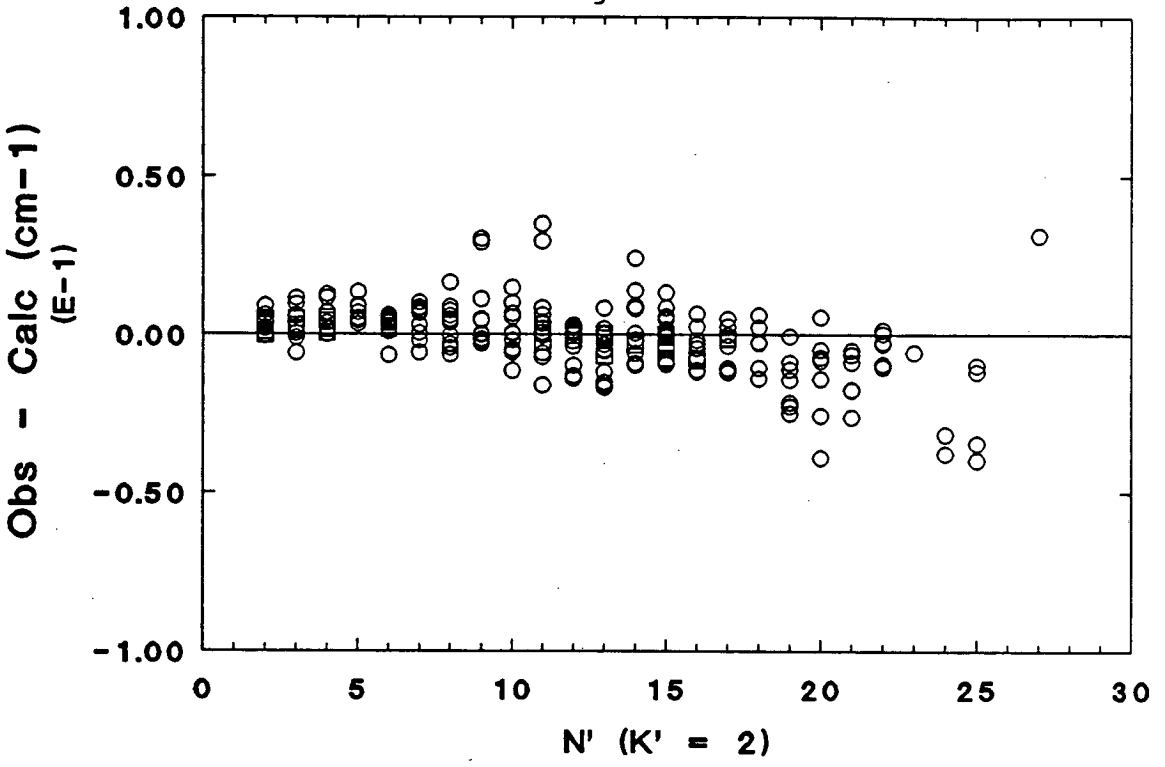

Figure I-17

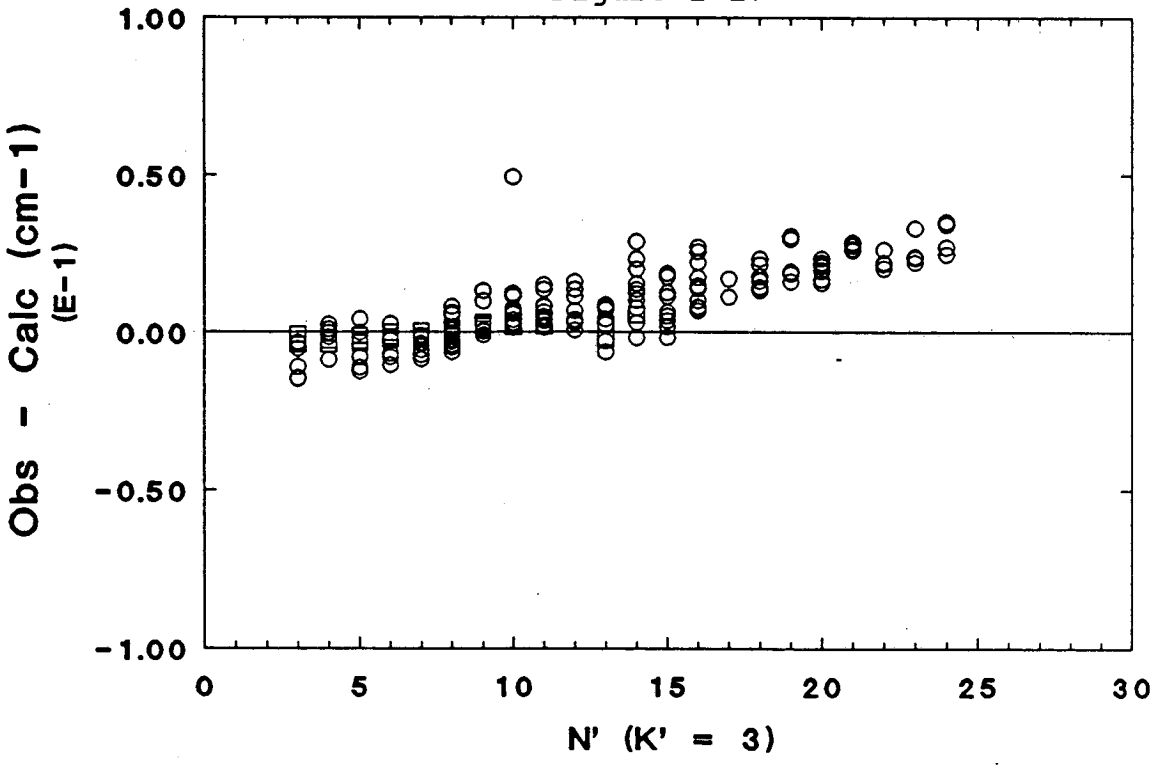

Figure I-18

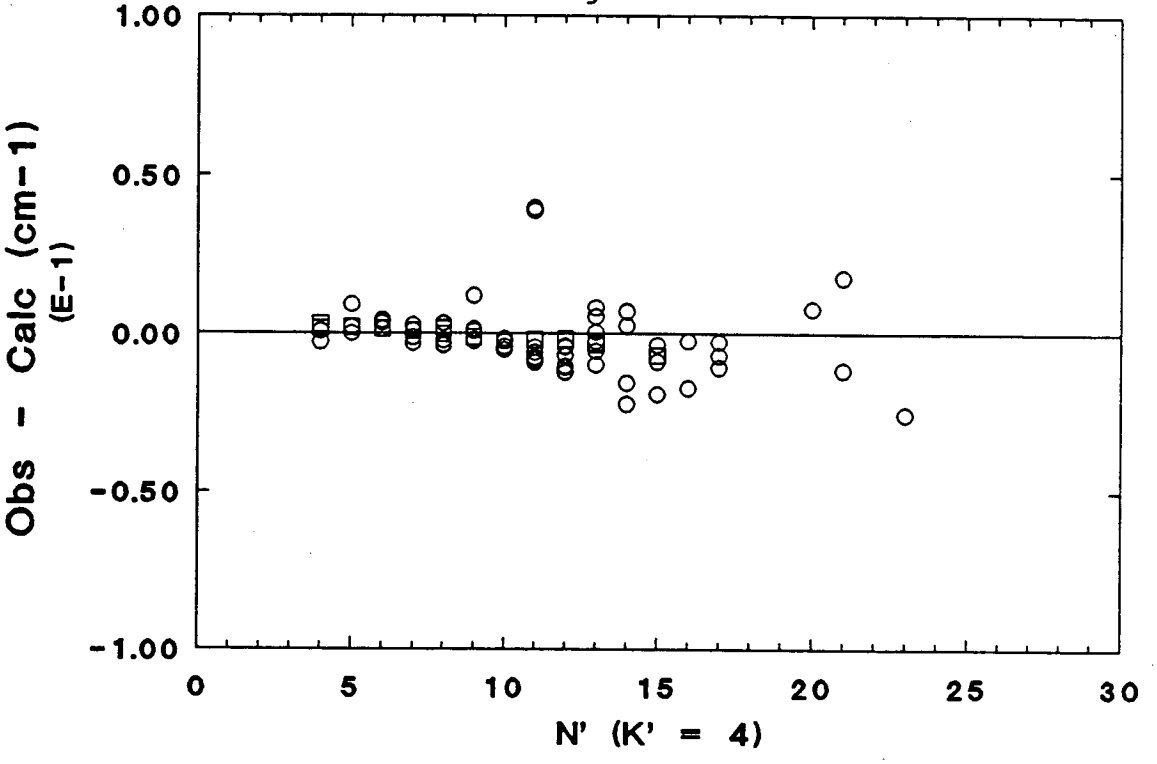

Figure I-19

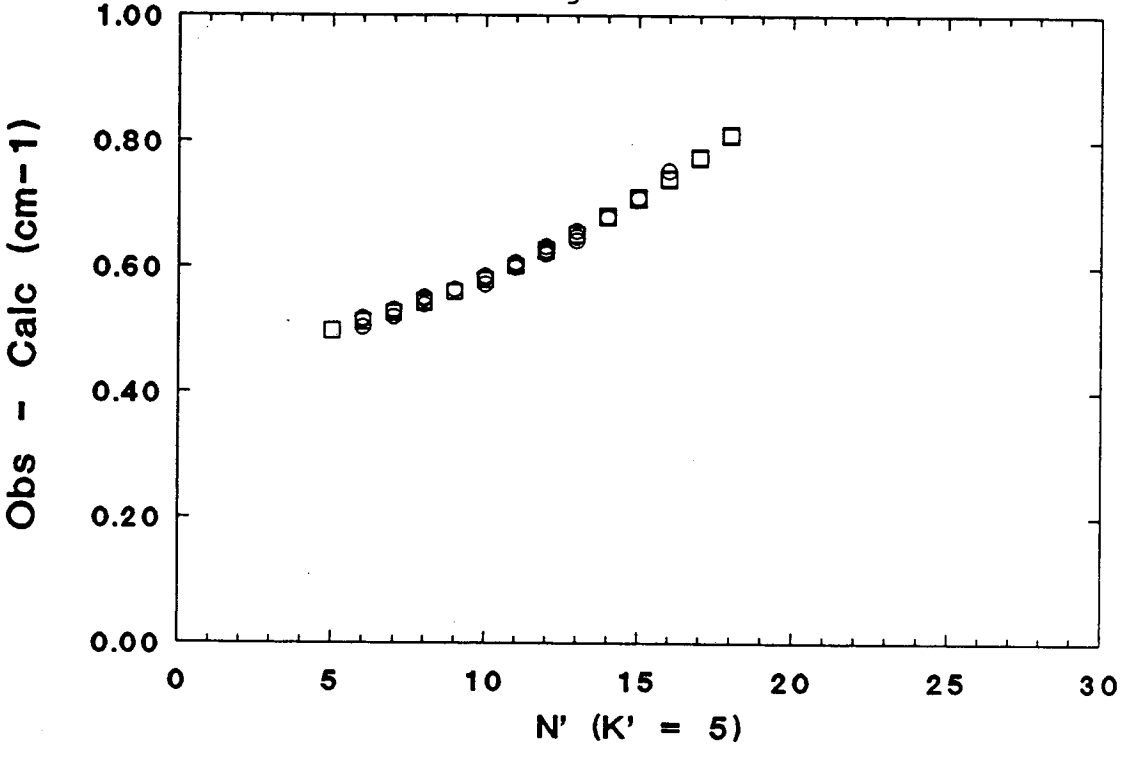

References

1. See for example J.S. Levine, the photochemistry of Atmospheres (Academic, New York, 1985).

2. See for example D.J. Hucknall, CHemistry of Hydrocarbon Combustion (Chapman and Hall, London, 1985).

3. W.M. Vaidya, Proc. Phys. Soc. A, 147, 513 (1934).

4. A.G. Gaydon, Spectroscopy and Combustion Theory (Chapman and Hall, London, 1934).

5. G.A. Handbook and R.C. Herman, Industr. Engng. Chem. 43, 2739 (1951).

6. R.N. Dixon, Trans. Faraday Soc. 65, 3141 (1969).

7. D. E. Milligan and M.E. Jacox, J. Chem. Phys. 51, 277 (1969).

8. M.E. Jacox, Chem. Phys. Lett. 56, 43 (1978).

9. D.A. Ramsay, J. Chem. Phys. 21, 960 (1953).

10. G. Herzberg and D.A. Ramsay, Can. J. Phys. 53, 2232 (1975).

11. J.W.C. Johns, S.H. Priddle, and D.A.Ramsay, Discuss. Faraday Soc. 35, 90 (1963).

12. J.M. Brown and D.A. Ramsay, Can. J. Phys. 41, 3032 (1964).

13. D.E. Ewing, W.E. Thompson and G.C. Pimentel, J. Chem. Phys. 32, 927 (1960).

14. D.E. Milligan and M.E. Jacox, J. Chem. Phys. 41, 3032 (1964).

15. B.M. Landsberg, A.J. Merer, and T. Oka, J. Mol. Spectrosc. 67, 459 (1977).

16. J.W.C. Johns, A.R.W. McKellar, and M. Riggin, J. Chem. Phys. 67, 2427 (1977).

17. C. Freed, L.C. Bradley and G.R. O'Donnell, J. Quant. Elect., QE-16, 1195 (1980).

18. J.M. Brown, J. Buttenshaw, A. Carrington, K. Dumper,

and C.R. Parent, J. Mol. Spectrosc. 79, 47 (1980).

19. A.R.W. McKellar, Faraday Discuss. Chem. Soc., 71, 63 (1981).

20. J.M. Brown, K. Dumper, and R.S. Lowe, J. Mol. Spectrosc. 97, 441 (1983).

21. S. Saito, Astrophs. Lett. 178, L95 (1972).

22. J.A. Austin, D.H. Levy, C.A. Gottlieb and H.E. Radford, J. Chem. Phys. 60, 207 (1974).

23. J.M. Cook, K.M. Evenson, C.J. Howard and R.F. Curl, Jr., J. Chem. Phys. 64, 1381 (1976).

24. B.J. Boland, J.M. Brown and A. Carrington, Mol. Phys. 34, 453 (1977).

25. H.M. Pickett and T.L. Boyd, Chem. Phys Lett. 58, 446 (1978).

26. G.A. Blake, K.V.L.N. Sastry, and F.C. Delucia, J. Chem. Phys. 80, 95 (1984).

27. T.J. Sears, Comput. Phys. Rep. 2, 1 (1984).

28. E. Hirota, J. Mol. Struct. 146, 237 (1986).

29. J.S. Shirk and G.C. Pimentel, J. Am. Chem. Soc. 90, 3349 (1968).

30. R.N. Dixon, J. Mol. Spectrosc. 30, 248-252 (1969).

31. See, for example, Section 3.1, Part II of this work.

32. See, for example, R.J. Gill, W.D. Johnson and G.H. Atkinson, Chem. Phys, 58, 29-44 (1981).

33. P.J.H. Tjossem, P.M. Goodwin, and T.A. Cool, J. Chem. Phys. 84, 5334 (1986).

34. R. Vasudev and R.N. Zare, J. Chem. Phys. 76, 5267 (1982).

35. M.-C. Chuang, M.F. Foltz and C.B. Moore, J. Chem. Phys. 87, 3855 (1987).

36. B.M. Stone, M. Noble, and E.K.C. Lee, Chem. Phys. Lett. 118, 83 (1985).

37. K.K. Murray, T.M. Miller, D.G. Leopold, and W.C.

Lineberger, J. Chem. Phys. 84, 2520 (1986).

38. H. Petek, Ph.D. Thesis, U.C. Berkeley, 1985.

39. A.O. Langford, Ph.D. Thesis, U.C. Berkeley, 1983.

40. Section 2.4, Part II of this work.

41. A. Horowitz and J.G. Calvert, Int. J. Chem. Kinet. Vol. X, 805-819 (1978).

42. S. Gerstenkorn and P. Luc, "Atlas du spectre d'absorption de la molecule d'iode," Edition du Centre National de la Recherche Scientifique, Paris, 1980.

43. R. Spence and W. Wild, J. Chem. Soc. 338 (1935).

44. J. Chem. Eng. Data, II, 124 (1966).

45. H. Petek, D.J. Nesbitt, P.R. Ogilby, and C.B. Moore, J. Phys. Chem. 87, 5367 (1983).

46. J.K.G. Watson in "Vibrational Spectra and Structure, A Series of Advances," (J.R. Durig, Ed.), Vol. VI, Elsevier, Amsterdam, 1977.

47. J.M. Brown and T.J. Sears, J. Mol. Spectosc. 75, 111 (1979).

48. T.J. Sears, Comput. Phys. Commun. 34, 123 (1984).

49. T.J. Sears, Comput. Phys. Commun. 2, 1-32 (1984).

50. W. Gordy and R.L. Cook, Microwave Molecular Spectra (2nd edition), John Wiley & Sons, 1984.

51. J.M. Flaud and C. Camy-Peyret, J. Mol. Spectrosc. 51, 142 (1974).

52. D.L Albritton, W.J. Harrop, A.L. Schmeltekopf, R.N. Zare, and E. L. Crow, J. Mol. Spectrosc. 46, 67 (1973).

53. R.F. Curl and C.B. Dane, J. Mol. Spectrosc. 128, 406-412 (1988).

54. R.F. Curl, J. Comput. Phys. 6, 367 (1970). D.L. Albritton, A.L. Schmeltekopf, and R.N. Zare, Molecular Spectroscopy: Modern Research, Vol.II, pp1-67 (1976).

55. T. Oka and Y. Morino, J. Mol. Spectros. 6, 472 (1961).

56. C.E. Barnes, J. M. Brown, A. Carrington, J. Pinkstone, T.J. Sears, and P.J. Thistlethwaite, J. Mol. Spectrosc. 72, 86 (1978).

57. R.S. Lowe and A. R. W. McKellar, J. Chem. Phys. 74, 2686 (1981).

58. J.M. Bowman, J.S. Bittman, and L.B. Harding, J. Chem. Phys. 85, 911 (1986).

Part II.

Kinetics and Product Branching Ratios for the Reaction HCO + NO_2

1. Introduction

The reaction of HCO with NO_2 is important in atmospheric and combustion chemistry. It is involved in nitration and oxidation reactions,[1-3] and pyrolysis of organic nitrates and nitrites.[4] Learning about the reaction rate, products, and reaction mechanism is essential for quantitative modeling of those processes. There are four possible product channels in the reaction between HCO and NO_2:

$$\begin{aligned} HCO + NO_2 &\rightarrow OH + NO + CO \\ &\rightarrow H + CO_2 + NO \\ &\rightarrow HONO + CO \\ &\rightarrow HNO + CO_2 \end{aligned}$$

Recently Gutman's group has measured the rate constant for this reaction using laser photolysis with photoionization mass spectrometry detection. However, they failed to detect the reaction products.[5] Morrison and Heicklen studied the products of the HCO + NO_2 reaction by photolyzing a gaseous mixture of H_2CO and NO_2 at room temperature.[1,6] They used gas chromatography to analyze the stable molecules after the reaction proceeded. The results were interpreted as indicating that H + CO_2 + NO is the only product channel and that perhaps some adducts

were formed, but the investigation was inconclusive.

Theoretical calculation[7], Figure II-1, shows that two possible collision complexes can be formed in the HCO + NO_2 reaction. The calculated heat of formation of HCO(ONO) at 298 K is lower than that of HCO(NO_2) by 10 kcal/mole. Whether the collision complexes can be stabilized in this system is an interesting and important issue. Morrison and Heicklen have tentatively assigned an IR absorption band between 700 and 800 cm^{-1} to the complexes.[6] HCO(ONO) has been postulated as a reaction intermediate in organic synthesis,[8] although it has not been independently isolated.

In this work, the rate constant and product branching ratios for the HCO + NO_2 reaction have been determined using laser flash kinetic spectroscopy. The rate constant has been demonstrated to be independent of SF_6 buffer gas pressure up to 700 torr. The reaction products, HNO, CO_2, and HONO, corresponding to three different product channels, were directly monitored as the reaction proceeded. The results provide valuable information not only for quantitative modeling, but also for understanding the reaction mechanism.

Figure II-1. Potential energy diagram of the reaction between HCO and NO_2 calculated by C. Melius.[7] Solid lines are ab initio calculated heats of formation at 285 K by using the BAC-MP4 method. The connecting dashed lines are merely estimated.

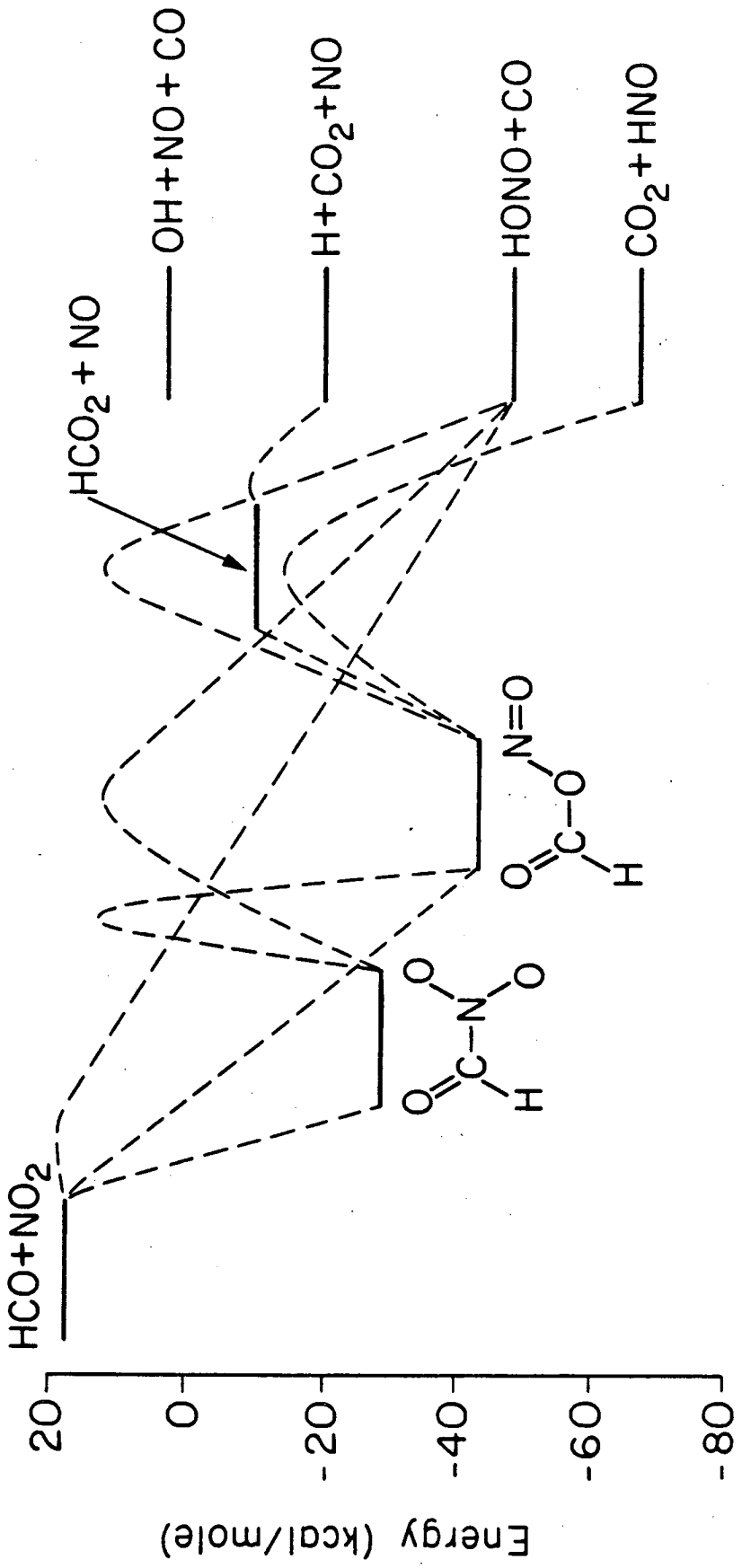
HCO+NO2
HCO2 + NO
OH+NO+CO
H+CO2+NO
HONO+CO
CO2+HNO
20
0
-20
-40
-60
-80
Energy (kcal/mole)

2. Experimental

2.1 Visible Laser Monitoring of HCO Decay

The rate constant for the reaction between HCO and NO_2 was measured by monitoring the decay of the HCO concentration as the reaction proceeds. The schematic diagram of the experimental setup is shown in Figure II-2. CH_3CHO and NO_2 were continuously flowed through the photolysis cell (156 cm long, 2.5 cm in diameter, with quartz windows). HCO radical was produced by photolysis of the CH_3CHO with a 308 nm excimer laser (Lambda Physik/103E). The pulse width of the excimer laser was 8 ns and the energy was about 60 to 80 mJ per pulse. The visible probe laser was an Ar^+ laser (Spectra Physics/2030-18) pumped ring dye laser (Spectra Physics/380A). The photolysis laser beam (7 mm in diameter) was combined with the probe laser beam (3 mm in diameter) before entering the photolysis cell using a UV-reflecting and visible-transmitting mirror (M1 in Figure II-2). Both UV and visible lasers were then colinearly directed through the photolysis cell. A portion of the visible laser output was split off with a beam splitter (transmittance $\approx$ 70%) prior to combining with the photolysis laser to provide a reference beam. The

Figure II-2. The experimental set-up for visible laser monitoring of HCO decay.

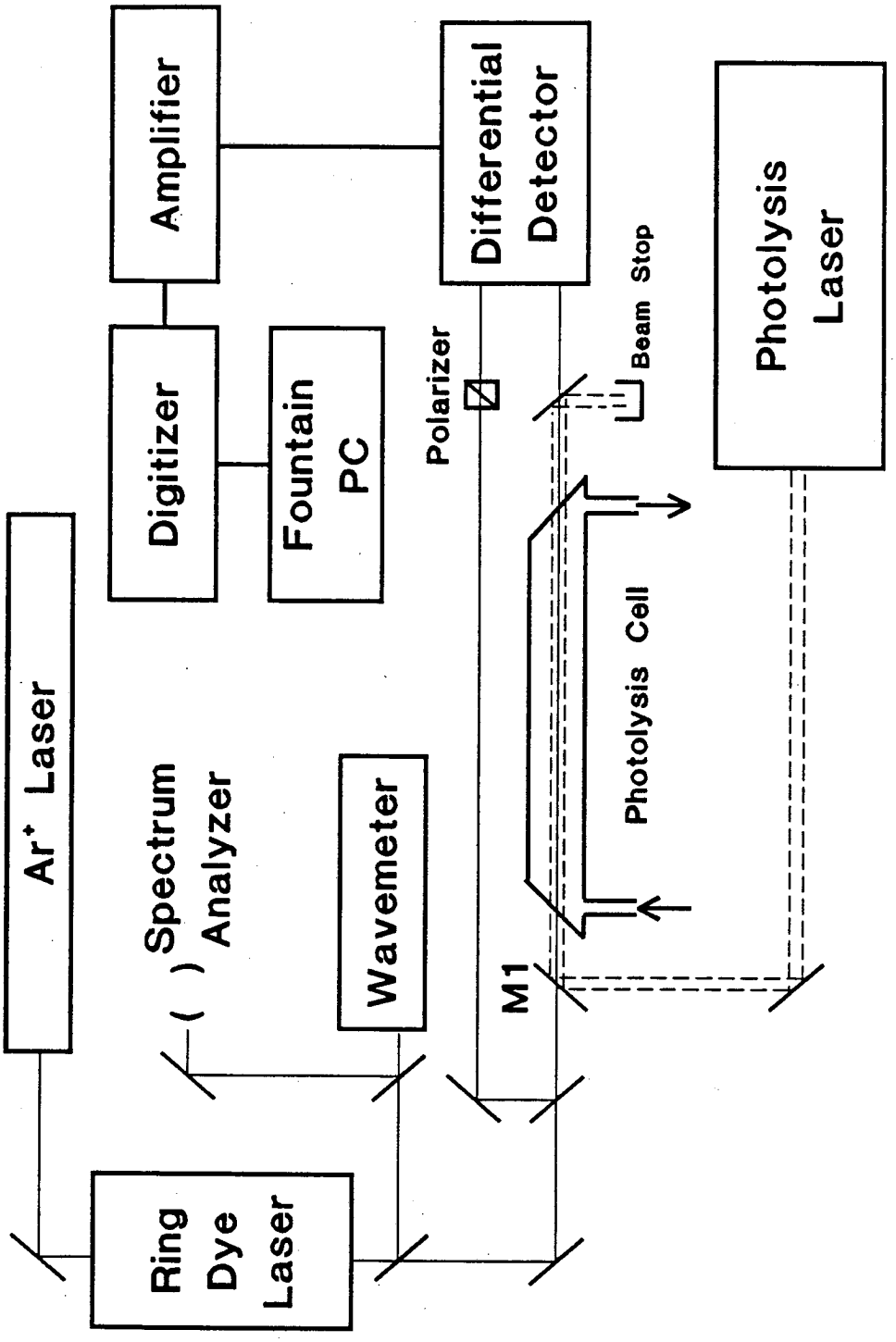
Amplifier
Differential Detector
Photolysis Laser
Digitizer
Fountain PC
Polarizer
Beam Stop
Ar+ Laser
Spectrum Analyzer
Wavemeter
Photolysis Cell
M1
Ring Dye Laser

intensities of the two beams were balanced with a polarizer placed in the reference beam.

Photodiodes (RCA/C30810) with large sensitive area and fast response time were used for detecting both the probe and the reference beams. The difference between the probe signal and the reference signal was amplified, and then digitized (Tektronix/7912AD) with a 20 MHz low pass filter at the input. The data were stored and analyzed with a personal computer (Fountain/XT).

The advantage of using the subtraction scheme in the visible detection and the detailed features of the apparatus have been discussed in References 9 and 10. The diodes used in this experiment are different from the ones (EG&G/SGD100A) previously described. The sensitive area of the RCA diodes is 100 mm^2 (11.4 mm in diameter) rather than 5.1 mm^2 of the SGD100A. The rise time of the RCA diode is 12 ns while that of SGD100A is 5 ns. Although the detection time constant was limited by the photodiode rise time, it was not a problem because the decay rate of HCO due to the reaction with NO_2 was on the order of a microsecond. Since the photodiode used in this experiment has such a big sensitive area, deflection of the probe beam by shock waves has been eliminated. As a result, larger UV laser flux can be used to photolyze the

precursor, and a better signal-to-noise ratio was obtained with fewer photolysis shots. The detection limit (S/N = 1) for HCO radical is 1.5 X 10^{12} molec cm^{-3} for a single photolysis shot; previously the limit was 2 X 10^{11} molec cm^{-3} averaging over 512 shots.[9] Under the experimental conditions, without the presence of NO_2 the recombination reaction HCO + HCO → H_2CO ($k = 3.0 \times 10^{-11}$ cm^3 $molec^{-1}$ sec^{-1})[11] was mainly responsible for the loss of HCO. The quoted detection sensitivity was obtained with the decay of HCO due to the recombination reaction less than 2%, 5 μs after the photolysis pulse and a detection time constant of 50 ns.

2.2 Infrared Difference Frequency Laser Detection of Reaction Products

The experimental apparatus used for detecting the reaction products is illustrated in Figure II-3. CH_3CHO and NO_2 were continuously flowed through the photolysis cell. The same photolysis cell (with infrasil windows) and photolysis laser were used as described in Section 2.1. The probe laser was an IR difference frequency laser system, which has been described in detail before,[10,12] and some improvements made in the system during the last few years are discussed in Appendix I. The same Ar^+

Figure II-3. Schematic diagram of the experimental apparatus for the detection of the reaction products.

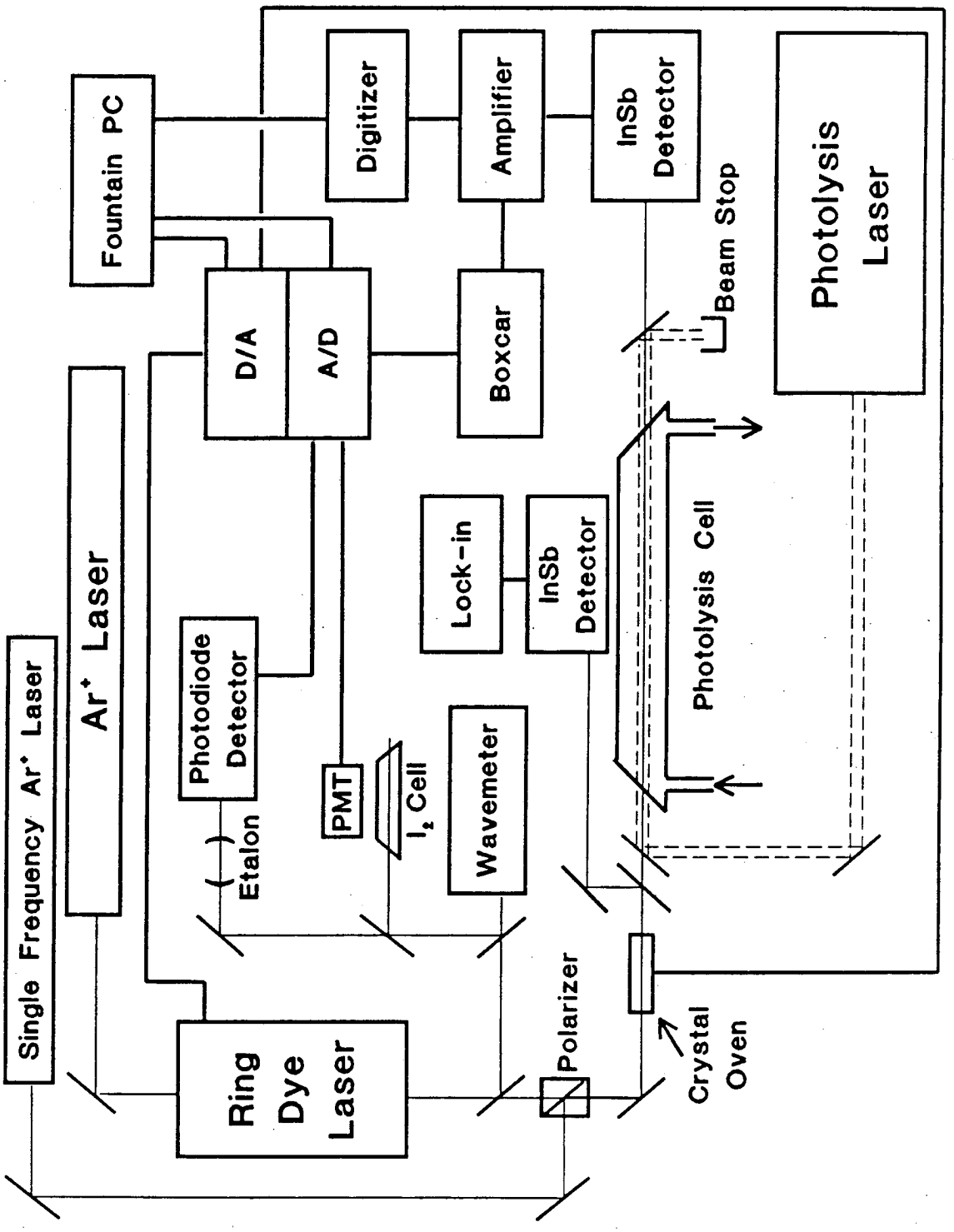
Fountain PC
Digitizer
Amplifier
InSb Detector
Photolysis Laser
Beam Stop
D/A
A/D
Boxcar
Ar+ Laser
Lock-in
InSb Detector
Photolysis Cell
Photodiode Detector
PMT
I2 Cell
Wavemeter
Etalon
Single Frequency Ar+ Laser
Ring Dye Laser
Polarizer
Crystal Oven

laser pumped ring dye laser as described in the previous section was used, and the single frequency Ar^+ laser (Lexel/94-5) was operated either at 514.5 nm or 488 nm depending on the absorption frequency of the species being studied.

The photolysis laser beam (7 mm in diameter) and the probe laser beam were colinearly directed down the photolysis cell by using a UV-reflecting and IR-transmitting dichroic mirror. The IR laser beam was focused at the center of the cell; the beam diameter at each end of the cell was less than 5 mm. Special attention was paid to ensure that the probe laser is overlapped with the center part of the photolysis beam over the entire length of the photolysis cell. This is especially important in quantitatively measuring the yields of reaction products.

The uniformity of the UV laser beam was tested by measuring the power of the laser beam going through the center of a 1 mm diameter aperture while moving the aperture over the cross section of the laser beam. The aperture was mounted on a X-Y stage. Over the whole area of the UV beam, the measured laser power was constant within 90%. Unstable resonator optics were used in the excimer laser cavity and the output was used without

further focusing. The divergence of the UV laser beam was less than 5% over the whole length of the photolysis cell.

Both UV photolysis and IR probe laser power were monitored during the experiments. A small portion of the UV beam split with a piece of quartz plate prior to entering the photolysis cell was directed onto a pyroelectric detector (Molectron/J3-09) for UV power normalization. The signal was then integrated with a boxcar integrator. The IR beam was split with an IR beam splitter before it was combined with the photolysis beam. An InSb detector (Santa Barbara/E292) and a lock-in amplifier were used for signal detection and processing. The fluctuation of each laser beam was less than 15% of its total power during the course of the experiments. The absolute UV power was measured with a calibrated UV power meter (Scientech/38-0105).

Two InSb detectors were used in this experiment. One (Santa Barbara/E292) has fast time response (20 ns) but small sensitive area (0.25 cm in diameter). The other (Infrared Associates/H-313-IS) has large sensitive area (0.8 cm in diameter) but relatively slow response time (about 1 μs). The quantitative yield of CO_2 was measured with the Infrared Associates detector (borrowed from Saykally's group) in order to eliminate the shock wave

problem. The signal was amplified, and then either digitized (Tektronics/7912AD) or integrated with a boxcar integrator (PAR/164/162).[13] The data were stored and analyzed with a personal computer (Fountain/XT). The detection limit (S/N = 1) for measuring CO_2 is 3.3 X $10^{13}(N)^{-1/2}$ molec cm^{-3} (N = number of photolysis shots) when the R(18) line of the (1,0,1) ← (0,0,0) band was monitored, which corresponds to a fractional absorption of 2.6%.

2.3 Sample Preparation and Handling

Acetaldehyde (Mallinckrodt, min 99%) was purified by several freeze-pump-thaw cycles and kept at 0 °C. NO_2 (Matheson, min 99.5%) was fractionally distilled from -29 °C (o-Xylene/liquid nitrogen slush) to -78 °C (dry ice/ethanol bath) and was stored at liquid nitrogen temperature. NO (Matheson,99%) was distilled through a dry ice/ethanol trap. SF_6 (Matheson, 99.99%) and CO_2 (Matheson,99.998%) were used without further purification.

The flow rates of CH_3CHO and NO_2 through the photolysis cell were monitored with calibrated flow meters (Hasting/LF-100 and ALL-5). The calibration was done by measuring the amount of time it takes for a certain

pressure increase in a known volume. Table I depicts the calibration of the Hasting/LF-100 flow meter used to measure the flow rate of CH_3CHO and that of the Hasting/ALL-5 flow meter used to measure the flow rate of NO_2. The flow rates were typically 8.5 sccm* for CH_3CHO and 0.5 sccm for NO_2, and at 6 torr it takes ≈ 40 sec to replace the gas in the photolysis cell.

The gas pressure in the photolysis cell was measured with Baratron pressure gauges. MKS/310BHS-1, -10, and -1000 were used for 0-1 torr, 1-10 torr, and over 10 torr total pressure measurements. Since the gas flow rates were relatively slow, there was no noticeable pressure gradient along the photolysis cell.

2.4 Photolysis of CH_3CHO and NO_2 at 308 nm

CH_3CHO absorbs from 350 to 235 nm UV light continuously[14], corresponding to the $\pi^* \leftarrow n$ transition. There are some observable vibronic features between 290 nm and the long wavelength end of the absorption spectrum.

---

* sccm = standard cubic centimeter per minute

Table II-1. Flow meter calibrations

Hasting/LF-100 (CH_3HCO)		Hasting/ALL-5 (NO_2)	
Flow Meter Reading	Calibrated Flow Rate (sccm)*	Flow Meter Reading	Calibrated Flow Rate (sccm)
7.5	3.68	0.31	0.202
13.5	6.77	0.50	0.339
15.8	7.72	0.63	0.410
18.0	8.79	0.80	0.517
20.0	9.38	1.42	0.982
22.0	10.29	1.97	1.317
24.5	11.72	2.45	1.664
30.7	15.76	3.46	2.175

* scmm = standard cubic centimeter per minute

The absorption coefficient of CH_3CHO has been measured in this experiment in order to obtain the quantitative yield of HCO radical from the 308 nm UV photolysis. Figure II-4 depicts the measured absorbance ($A = -\ln(I/I_0)$) of CH_3CHO versus its pressure between 1.174 to 9.425 torr. The slope of the linear least-squares fit is 0.167 ± 0.003 $torr^{-1}$. The length of the photolysis cell was 156 cm. Therefore the absorption coefficient of CH_3CHO at 308 nm is (1.07 ± 0.02) X 10^{-3} $torr^{-1}$ cm^{-1}. The photolysis laser under the normal experimental conditions was the light source.

In order to take the NO_2 absorption into account, its absorption coefficient at 308 nm was also measured. Figure II-5 shows the absorbance of NO_2 versus its pressure between 0.338 to 2.092 torr. The absorption coefficient of NO_2 is (5.41 ± 0.14) X 10^{-3} $torr^{-1}$ cm^{-1}.

Typically the total pressure of CH_3CHO and NO_2 in the photolysis cell was around 6 torr with the ratio of CH_3CHO to NO_2 greater than 10 to 1. The flux of the UV photolysis laser was about 15 mJ/cm^2 per pulse. Each data trace was an average over 5 to 10 photolysis shots. The total quantum yield for photodissociation of CH_3CHO and NO_2 at 308 nm are 0.925[15] and 0.97[16]. Less than 0.1% of the total CH_3CHO and 1% of the total NO_2 molecules in the

Figure II-4. Aborbance of CH_3CHO ($A = -\ln(I/I_0)$) versus pressure measured with 308 nm excimer laser. The solid line is the linear least-squares fit. The resulting slope is 0.167 ± 0.003 $torr^{-1}$.

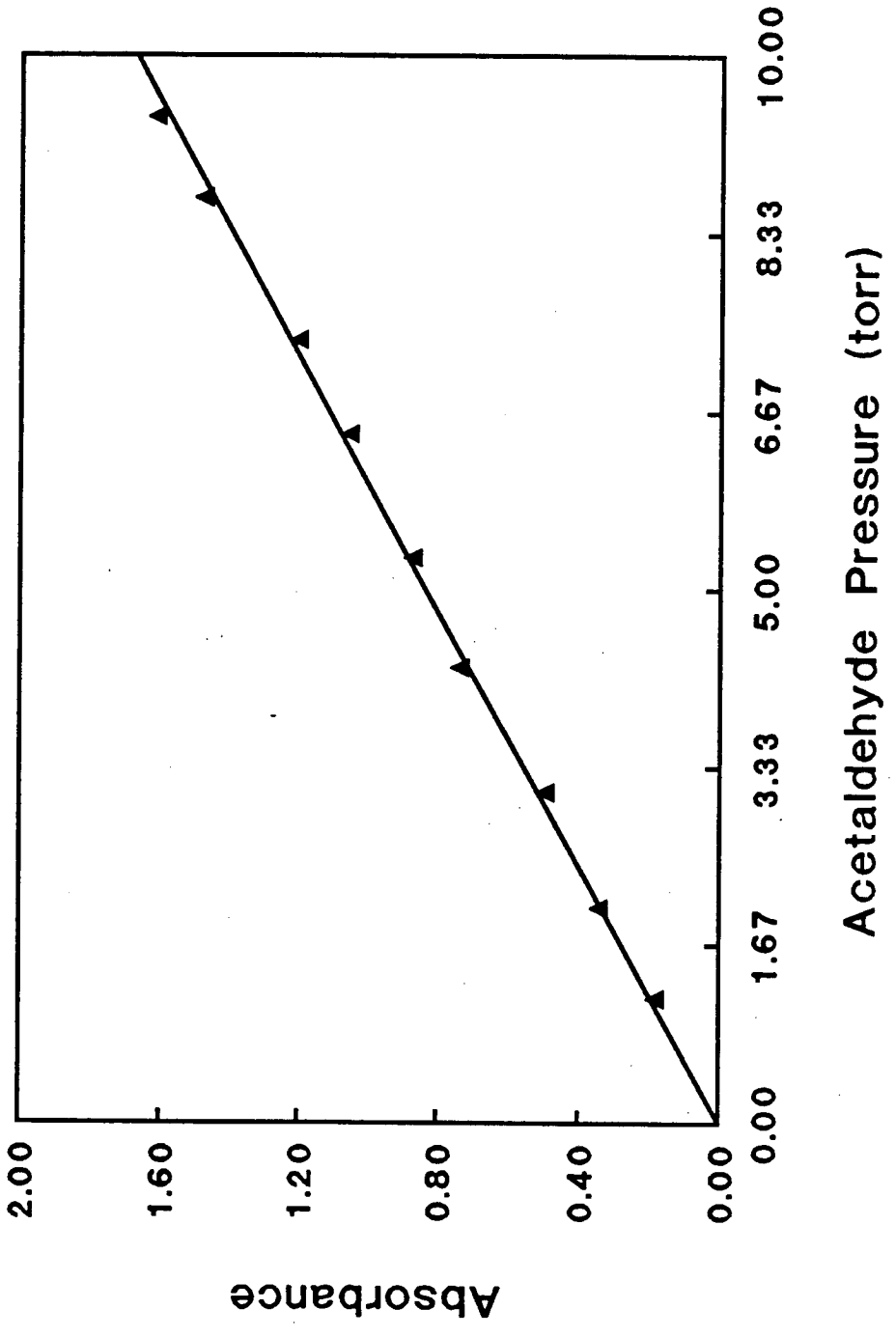
Absorbance
2.00
1.60
1.20
0.80
0.40
0.00
0.00
1.67
3.33
5.00
6.67
8.33
10.00
Acetaldehyde Pressure (torr)

Figure II-5. Absorbance of NO_2 ($A = -\ln(I/I_0)$) versus pressure measured with 308 nm excimer laser. The solid is the linear least-squares fit which gives the slope of 0.844 ± 0.022 $torr^{-1}$.

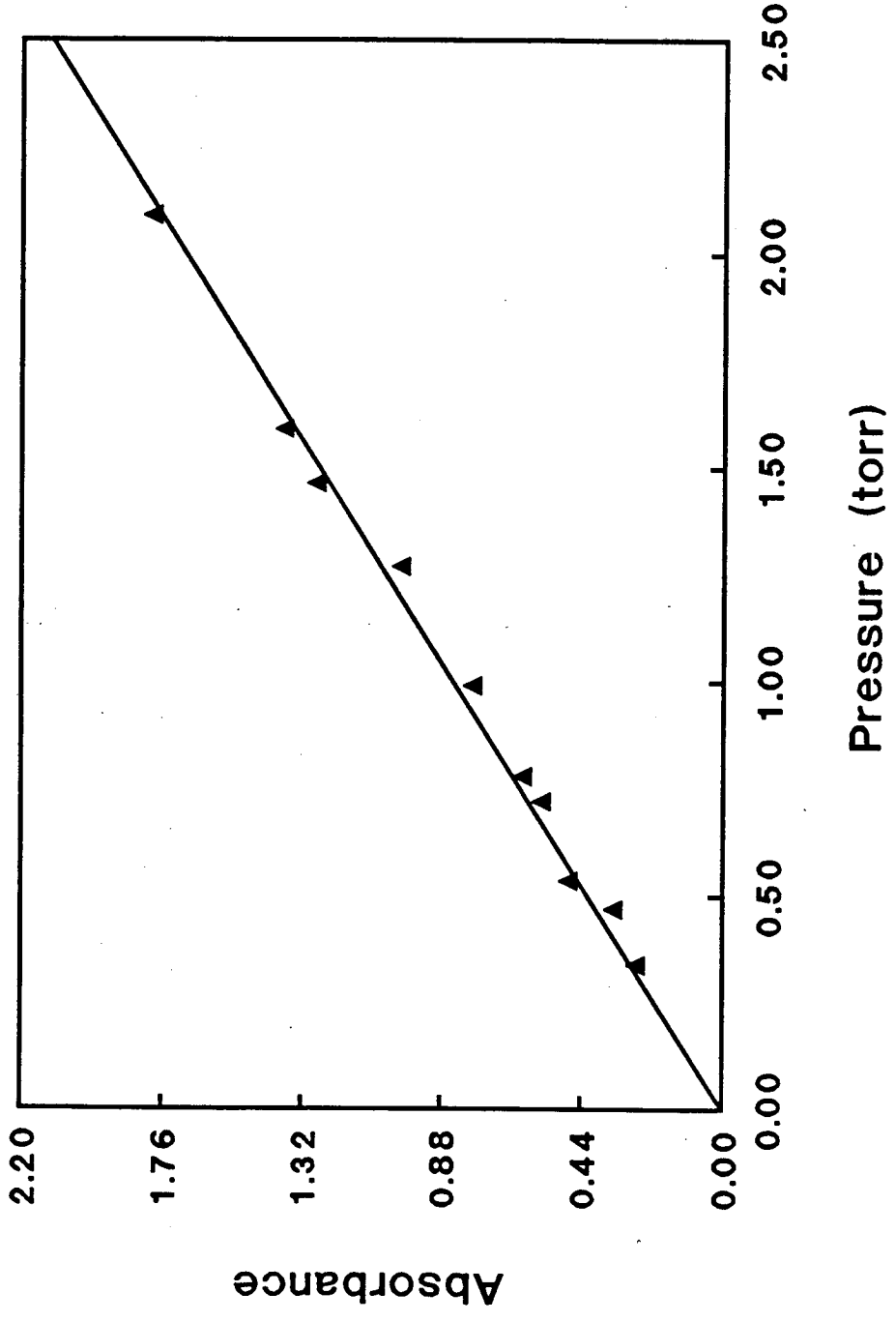
Absorbance
2.20
1.76
1.32
0.88
0.44
0.00
0.00
0.50
1.00
1.50
2.00
2.50
Pressure (torr)

beam path volume were photolyzed during the signal averaging (10 shots).

The branching ratio for photodissociation of CH_3CHO has been studied by Horowitz and Calvert.[17,18] The quantum yields for the following three channels

$$CH_3CHO \rightarrow CH_3 + HCO \qquad (I)$$
$$\rightarrow CH_4 + CO \qquad (II)$$
$$\rightarrow CH_3CO + H \qquad (III)$$

at 300 nm and 313 nm are 0.903, 0.010, 0.053, and 0.837, 0.016, 0.046, respectively*. The interpolated values of

---

* According to Horowitz and Calvert's experimental results[17,18], the quantum yields for (I), (II), and (III) processes are pressure dependent. At 300 nm, their mathematical fits to the experimental measurements of quantum yields for the above three processes are:

$$1/\phi_I = 1.075 + 5.17 \times 10^{-3}\ P(CH_3CHO)^{**} + 2.87 \times 10^{-3}\ P(CO_2) + 2.17 \times 10^{-3}\ P(O_2 \text{ or } N_2)$$

$$1/\phi_{II} = 94 + 0.54\ P(CH_3CHO) + 0.30\ P(CO_2) + 0.23\ P(O_2 \text{ or } N_2)$$

$$1/\phi_{III} = 17.0 + 0.308\ P(CH_3CHO) + 0.137\ P(CO_2) + 0.13\ P(O_2 \text{ or } N_2)$$

At 308 nm, the results are: (see next page)

the branching ratio at 308 nm are 0.862, 0.014, 0.049. The density of HCO produced by the photolysis thus can be calculated. It is typically on the order of 10^{14} molec/cm^3 per pulse.

$1/\phi_I = 1.082 + 1.84 \times 10^{-2}\ P(CH_3CHO) + 1.03 \times 10^{-2}\ P(CO_2) + 0.79 \times 10^{-2}\ P(O_2 \text{ or } N_2)$

$1/\phi_{II} = 55 + 1.15\ P(CH_3CHO) + 0.64\ P(CO_2) + 0.49\ P(O_2 \text{ or } N_2)$

$1/\phi_{III} = 18.3 + 0.493\ P(CH_3CHO) + 9.59 \times 10^{-3}\ P(CH_3CHO)^2 + 0.71\ P(CO_2) + 0.54\ P(O_2 \text{ or } N_2)$

The quantum yields at 300 nm and 313 nm are calculated here for $P(CH_3CHO) = 6.000$ torr and $P(NO_2) = 0.300$ torr, assuming the efficiency of collisional quenching of the excited precursors by NO_2 is the same as by CO_2.

** P = pressure in torr at 25 °C.

3. Results

3.1 Reaction Rate Constant

HCO was monitored through the $^{P}Q_{1}(10)$ line of the (0,9,0) ← (0,0,0) band ($\tilde{A}^{2}A'' \leftarrow \tilde{X}^{2}A'$) at 16,262.25 cm^{-1}.[19] The bottom trace (dotted plot) in Figure II-6 shows the rise of the HCO absorption following the UV photolysis and its decay as the reaction of HCO + NO_2 proceeds. The energy threshold for HCO (0,0,0) formation from the photodissociation of CH_3CHO is 320 nm (89.3 kcal mol^{-1}).[20] The formation of vibrationally excited HCO from photolyzing CH_3CHO at 308 nm is energetically possible. With more than 5 torr of CH_3CHO, the time for the relaxation of vibrationally hot HCO should be shorter than 0.35 μs;[21] it would be observed as a delay in the rise of the trace in Figure II-6(a). The rise of HCO was much faster than its removal by the HCO + NO_2 reaction under the present experimental conditions, as seen by comparing the traces in Figure II-6. The loss of HCO due to diffusion or reactions in the absence of NO_2 is shown in the top trace of Figure II-6; This loss is less than 2% in 5 μs.

The decay of HCO was least-squares fitted with a

Figure II-6. Absorption of HCO following the photolysis pulse with (the top trace) and without (the bottom trace) the presence of NO_2. The probe laser was set at 16262.25 cm^{-1} which corresponds to the $^{P}Q_1(10)$ line in the (0,9,0) ← (0,0,0) band ($\tilde{A}^2A'' \leftarrow \tilde{X}^2A'$) of HCO absorption. The signals were averaged over 5 photolysis shots. $P(CH_3CHO)$ = 6.000 torr for both top and bottom traces. $P(NO_2)$ = 0.330 torr for the bottom trace. UV laser power ≈ 15 $mJ \cdot cm^{-2}$ per pulse. The solid line in the bottom trace is the single exponential fit.

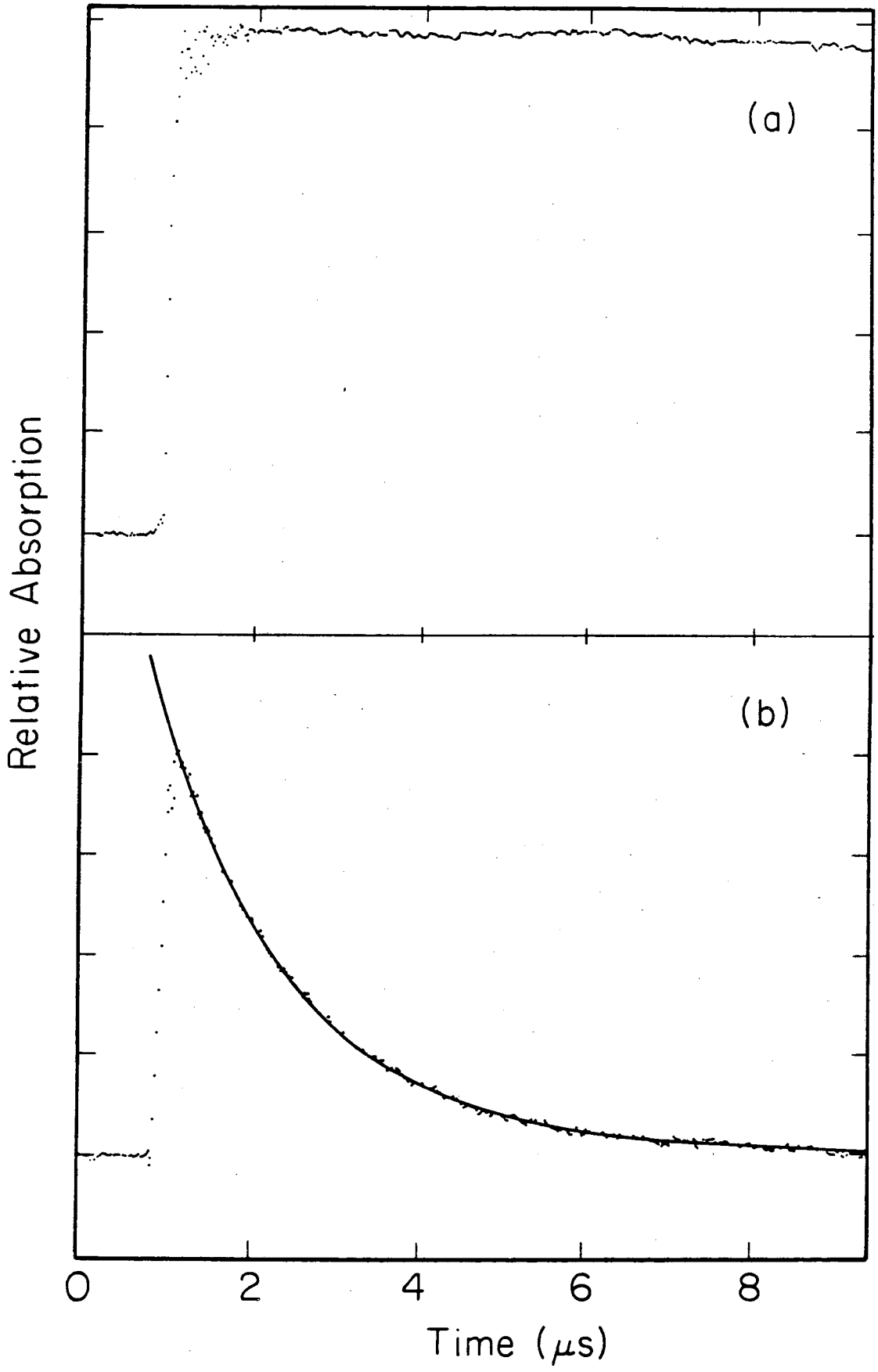
(a)
(b)
Relative Absorption
0
2
4
6
8
Time (μs)

single exponential function. Since the absorption of HCO produced by a single photolysis shot was less than 5%, the measured absorption signal (I_0 - I) was considered to be proportional to the absorbance. The solid line in Figure II-6(b) is the single exponential fit. The resulting pseudo-first-order reaction rates versus NO_2 pressure are plotted in Figure II-7. The slope derived from the linear least-squares fit (the solid line in Figure II-7) gives (5.7 ± 0.4) X 10^{-11} cm^3 $molec^{-1}\cdot sec^{-1}$ for the rate constant of the HCO + NO_2 reaction at 296 K. The quoted error is 2 σ. Considering the possible systematic errors resulting from the gas pressure and the flow rate measurements, and the decrease of NO_2 concentration due to UV photolysis and the side reactions (see Section 3.3.2 (3)) the overall estimated error for the reaction rate determination is ±15%, which means that the rate constant is (5.7 ± 0.9) X 10^{-11} cm^3 $molec^{-1}\cdot sec^{-1}$. This measured value of the rate constant is in excellent agreement with the recent published reaction rate measurement by Timonen et al.[5]. Timonen et al. also used CH_3CHO as the precursor and 308 nm excimer laser photolysis. Their total pressure was typically less than 1 torr with 0.05% of CH_3CHO, 0 - 0.35% of NO_2, and >99% of He. Their reported reaction rate constant is (5.6 ± 1.1) X 10^{-11} cm^3 $molec^{-1}\cdot sec^{-1}$.

Figure II-7. The pseudo-first-order reaction rate vs. NO_2 pressure. The slope of the linear least-square fit gives the rate constant of 5.70×10^{-11} cm^{-3} $molec^{-1} \cdot sec^{-1}$ for the reaction of HCO + NO_2 at 296 K.

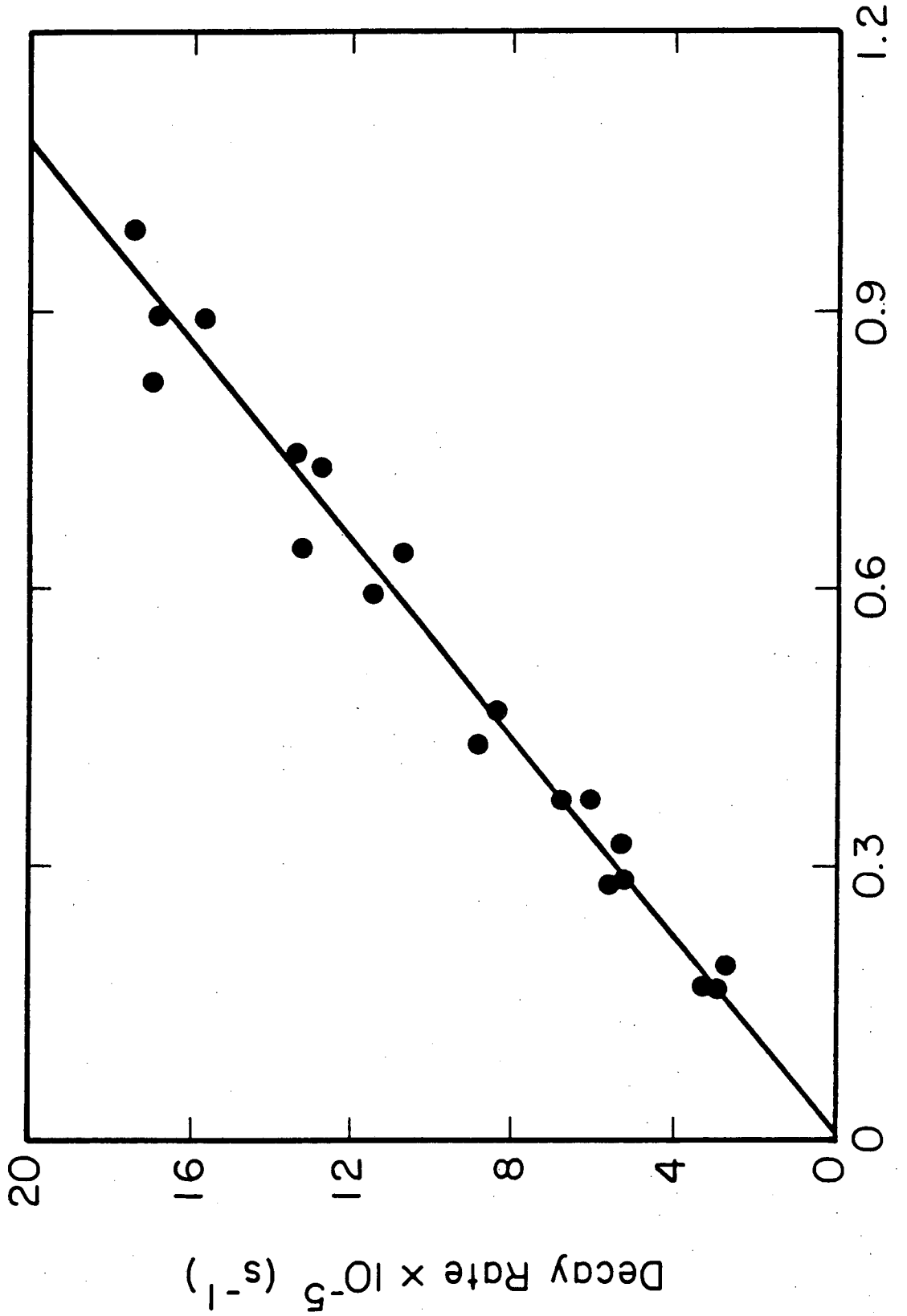
Decay Rate x 10^{-5} (s^{-1})
20
16
12
8
4
0
0
0.3
0.6
0.9
1.2
NO_2 Pressure (torr)

3.2 Pressure Dependence of the Rate Constant

SF_6 was used as a buffer gas in an attempt to collisionally stabilize $HCONO_2$ or HCOONO intermediates. SF_6 does not absorb 308 nm UV or 16,265.25 cm^{-1} visible light. CH_3CHO, NO_2, and SF_6 gases were premixed in a large bulb and then transferred through the vacuum line to the photolysis cell. The vacuum line and the photolysis cell were passivated with the gas mixture in order to avoid loss of NO_2 from the static gas mixture due to wall absorption. Fresh gas mixture was used for each data trace. The decay rate of HCO was measured at various SF_6 pressures at 296 K, Figure II-8. Since the HCO resonance absorption decreased due to pressure broadening when SF_6 was added, up to 18 torr of CH_3CHO was used in order to increase the HCO absorption signal. The measured rate constant is about 5% larger than reported above since at this high concentration some of the HCO was destroyed by the recombination reaction of HCO + HCO → H_2CO + CO (see Section 2.1). The observed rate constant is independent of total pressure from 6 torr up to 700 torr. The estimated error for each measurement is less than ±20%.

Figure II-8. The plot of the reaction rate constant without correcting for the HCO recombination effect (see text) versus SF_6 buffer gas pressure.

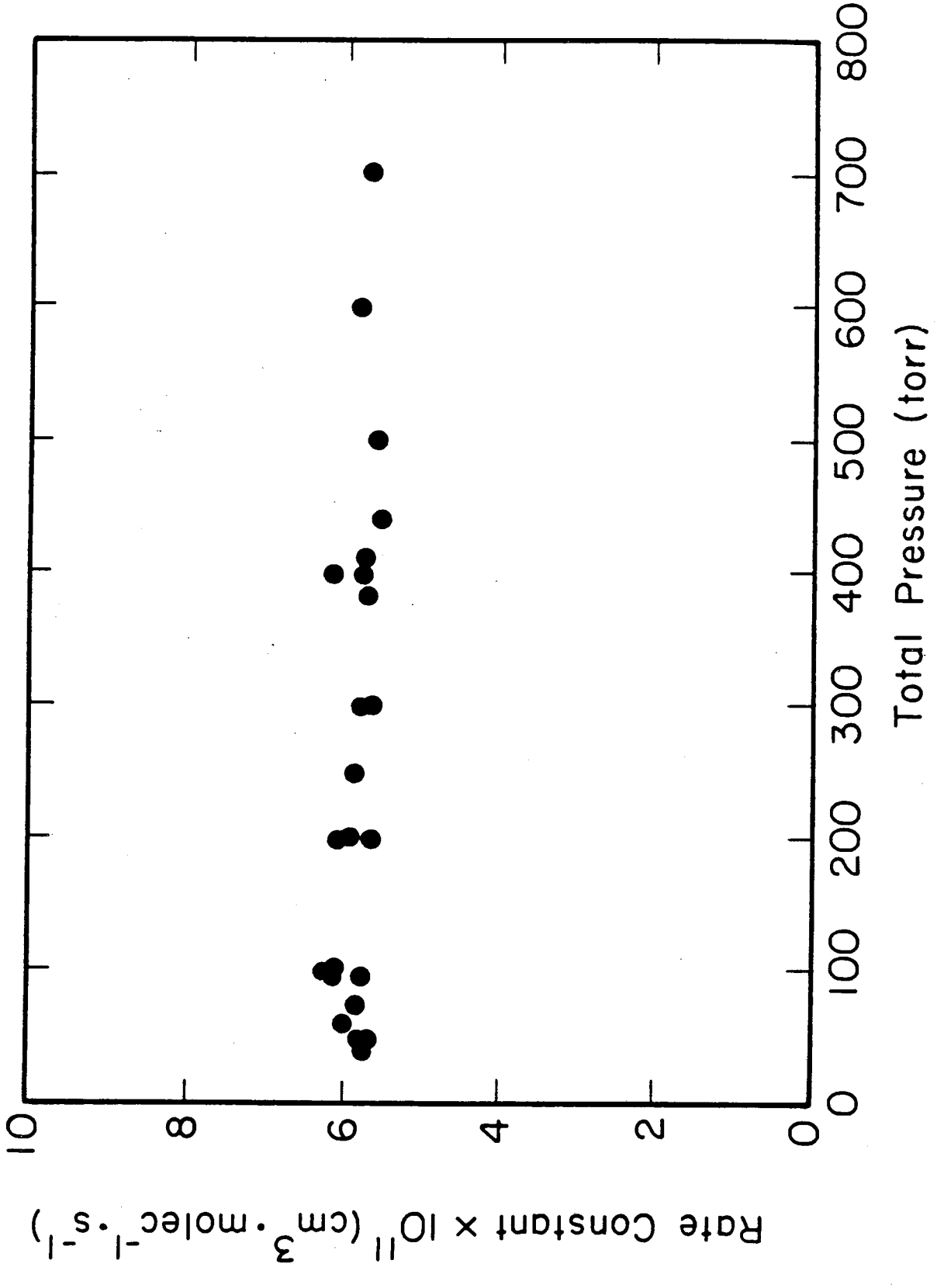
Rate Constant x 10^{11} ($cm^3 \cdot molec^{-1} \cdot s^{-1}$)
0
2
4
6
8
10
0
100
200
300
400
500
600
700
800
Total Pressure (torr)

3.3 Reaction Products

3.3.1 HNO Detection

The most exothermic product channel possible for the HCO + NO_2 reaction is HNO + CO_2 (ΔH = 87.2 kcal mol^{-1},[22]). The high resolution N-H stretching spectrum[23] providing accurate line positions for monitoring the HNO concentration. Observation of HNO as a reaction product was attempted using the IR flash kinetic spectrometer. However, no HNO absorption was observed when the probe laser was scanned through the frequency region where HNO absorbs.

In order to determine the system sensitivity for detecting the transient HNO species, the absorption signal of HNO as a product of the HCO + NO reaction was used as a reference. It has been established that the only product channel for HCO + NO reaction is HNO + CO.[24] Traces (a) and (b) in Figure II-9 depict the absorption signals of HNO obtained under the same experimental conditions for the HCO + NO and the HCO + NO_2 reactions, respectively. The delay and the gate settings of the boxcar were 5 μs and 50 μs, respectively. The frequency at the line center is 2665.88 cm^{-1} corresponding to the $^{p}Q_{1}(6)$ line in the

Figure II-9. HNO was monitored for both HCO + NO and $HCO + NO_2$ reactions at 2665.884 cm^{-1} which is the $^{p}Q_1(6)$ line of the (1,0,0) ← (0,0,0) band of HNO absorption. HNO + CO is known to be the only product channel for the HCO + NO reaction (trace (a))[17]. No HNO signal was observed for the reaction between HCO and NO_2 (trace (b)). The boxcar had a 50 μs gate, and 10 μs input time constant. The delay of the gate relative to the photolysis pulse was 5 μs.

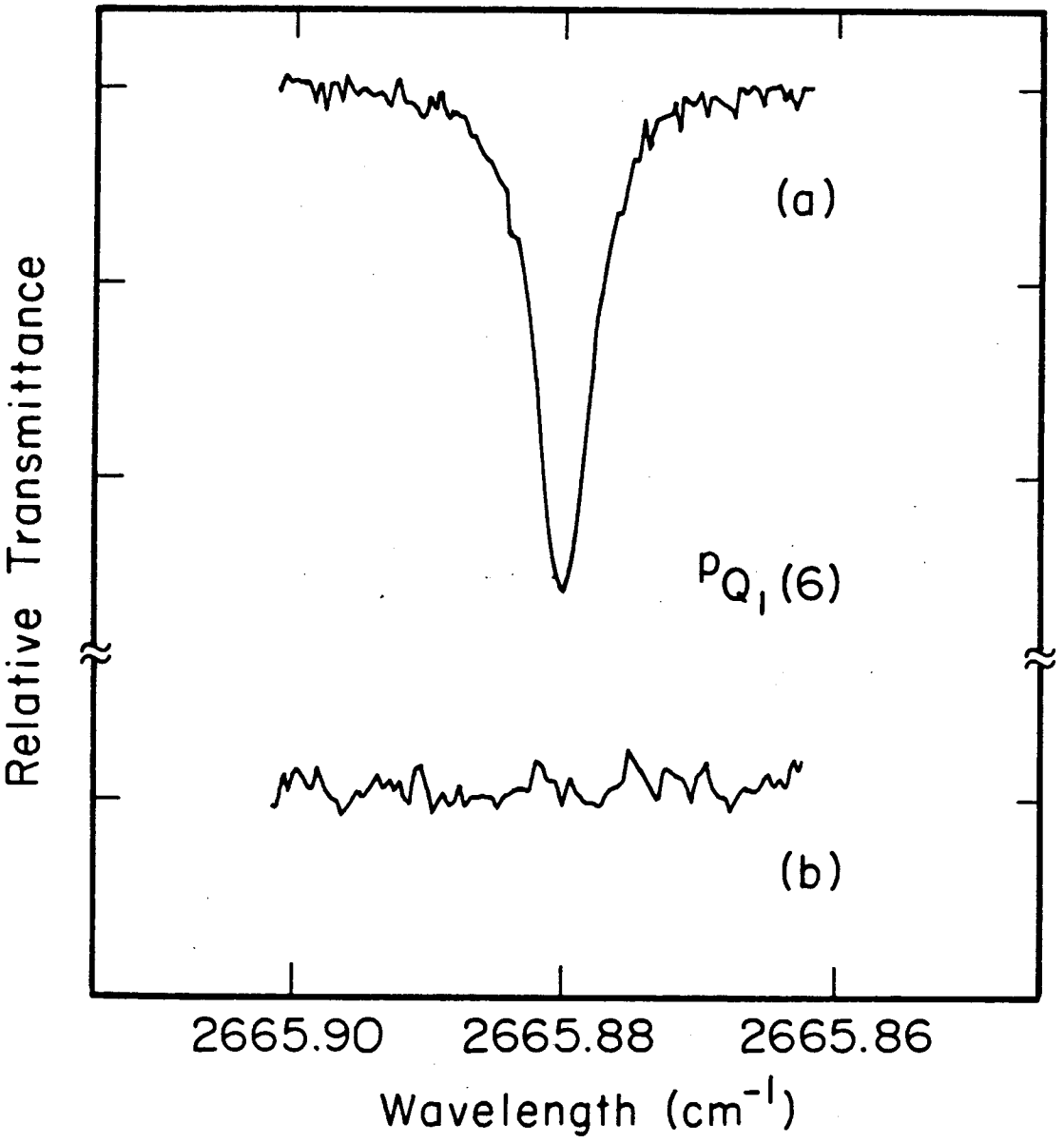
Relative Transmittance
(a)
$P_{Q_1}(6)$
(b)
2665.90
2665.88
2665.86
Wavelength (cm^{-1})

(1,0,0) ← (0,0,0) HNO absorption band. HNO was observed as a product in the reaction of HCO + NO, but not in that of HCO + NO_2. A conservative estimate based on the signal-to-noise ratio of the measurement shows that less than 10% of the HCO yields HNO.

There is a possibility that HNO produced from the HCO + NO_2 reaction was removed by the secondary reaction of HNO + NO_2. However, the reaction between HNO and NO_2 is expected to be slower than the HCO + NO_2 reaction. No HNO was observed as a product of the HCO + NO_2 reaction in this experiment with the delay of the boxcar gate relative to the photolysis pulse varied from 2 to 10 μs.

3.3.2 CO_2 Detection

As shown in the potential energy diagram of Figure 1, CO_2 can be a product of the reaction between HCO and NO_2 via the unstable intermediate HCO_2. The barrier preventing the dissociation of HCO_2 to form H and CO_2 is only about 1.5 kcal/mole.[7] HCO_2 should not be stable under the current experimental conditions. The exothermicity of the H + CO_2 + NO product channel is 37.3 $kcal \cdot mol^{-1}$.[22] Figure II-10 shows the appearance of CO_2 in the system monitored through the R(18) line of the (1,0,1)

Figure II-10. The appearance of CO_2 was monitored through the R(18) line in the (1,0,1) ← (0,0,0) vibration band at 3728.41 cm^{-1}. The signal was averaged over 5 photolysis shots. $P(CH_3CHO)$ = 6.049 torr. $P(NO_2)$ = 0.281 torr. UV laser power = 14.6 mJ cm^{-2} per pulse.

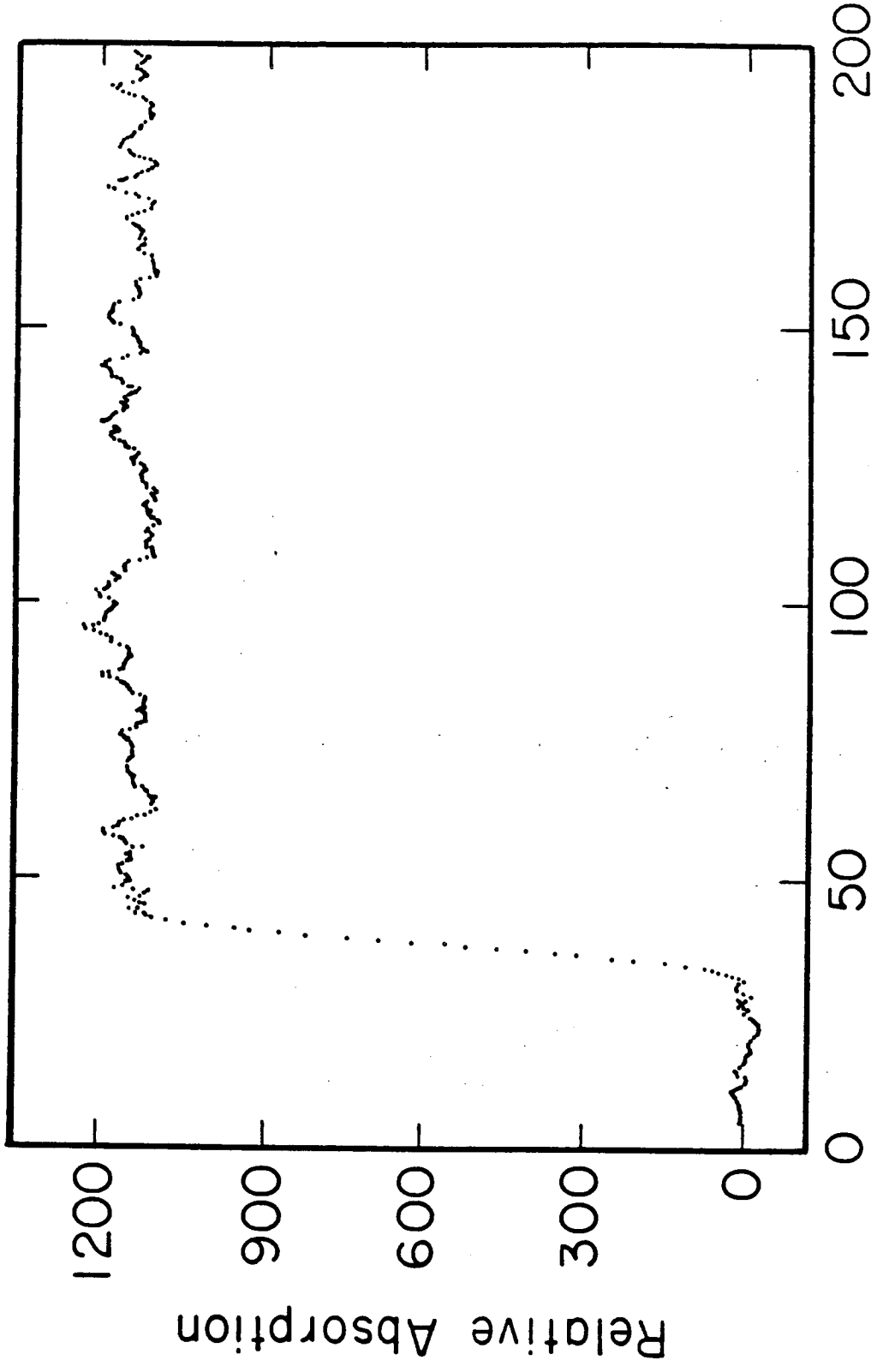
Relative Absorption
1200
900
600
300
0
0
50
100
150
200
Time (μs)

← (0,0,0) combination band at 3728.41 cm^{-1}.[25] The CO_2 yield was quantitatively determined by calibrating the transient CO_2 absorption against the absorption of pure CO_2.

(1). Calibration of the Transient CO_2 Absorption

The CO_2 produced when the mixture of CH_3CHO and NO_2 was photolyzed with the 308 nm excimer could accumulate in the photolysis cell since the flow rate was slow. As a result the IR laser power would be attenuated due to the absorption of the accumulated CO_2 if many photolysis shots were used. In order to avoid this problem, the transient absorption of CO_2 was measured using the transient digitizer instead of using the kinetic spectroscopy method described for the HNO absorption. The result was then calibrated with the measured cw absorption coefficient of CO_2. The accuracy in setting the IR laser frequency on the peak of the CO_2 absorption line is obviously very important in this measurement. A test on that was carried out and is described below.

Figure II-11 shows the cw absorbance of CO_2 vs. CO_2 pressures measured by two methods. In the first method, with the IR laser beam being chopped (block and unblocked)

Figure II-11. Peak absorbance of CO_2 versus CO_2 pressure (see section 3.3.2. (1).).

▼ - measured with the transient digitizer.

▽ - measured with the lock-in amplifier.

The solid and the dashed lines are the linear least-squares fits. The resulting slopes are $(3.89 \pm 0.10) \times 10^{-2}$ and $(3.64 \pm 0.16) \times 10^{-2}$ $torr^{-1}$, respectively.

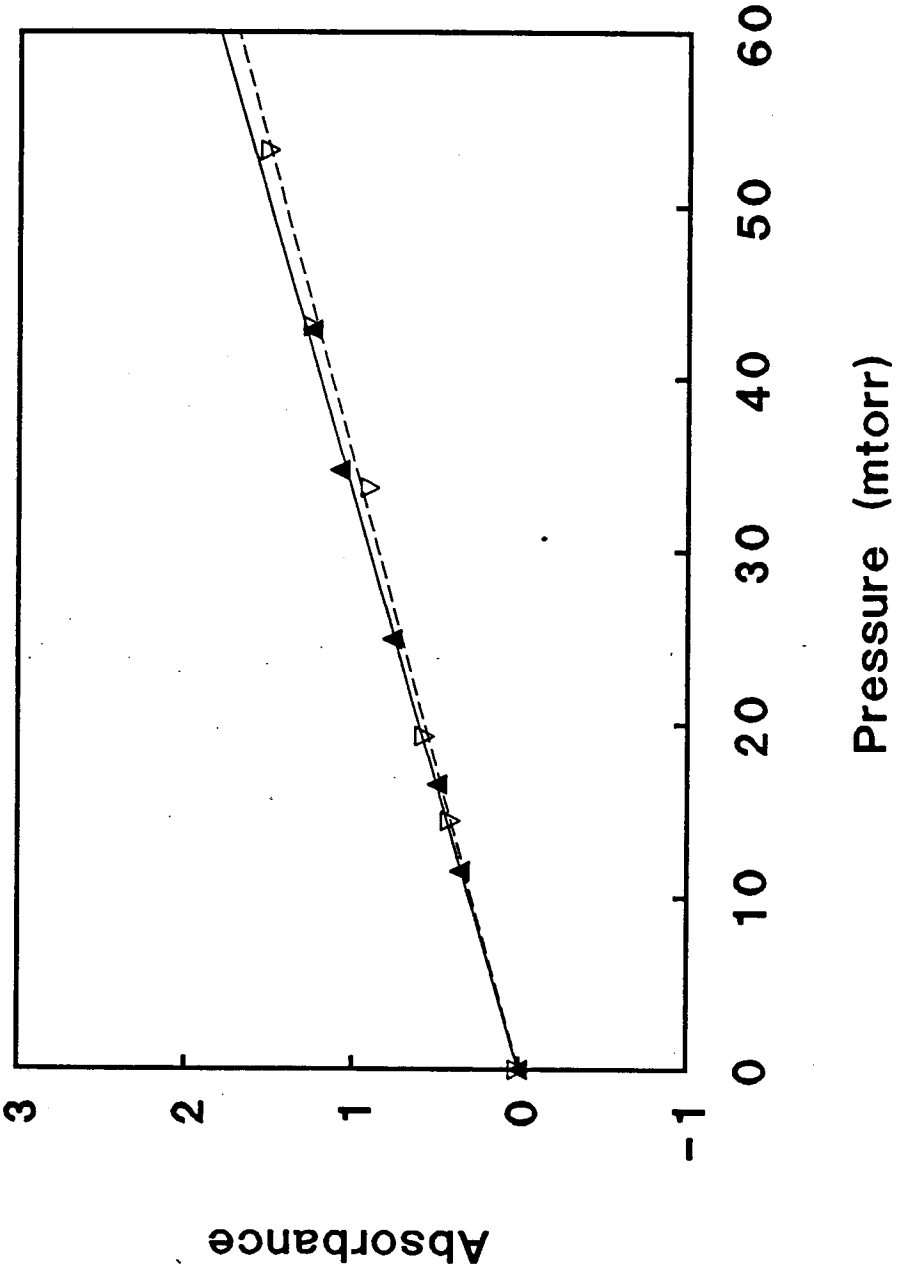
Absorbance
3
2
1
0
-1
0
10
20
30
40
50
60
Pressure (mtorr)

using an electrical chopper (mechanical), the transient digitizer was used to record the signal of IR transmittance through the photolysis cell with a known pressure of CO_2. The IR laser was either tuned off the CO_2 absorption line for measuring the total amplitude of IR laser power or tuned to the peak of the CO_2 line for measuring the amplitude of the transmittance at the resonance absorption of CO_2. The absorbance of CO_2 then was calculated. In the second method, the IR laser was tuned through the frequency range of CO_2 absorption line and a lock-in amplifier was used to record the spectrum and the peak absorbance determined. The solid and dashed lines in Figure II-11 are the linear least-squares fits to the results of the two sets of the measurements. The difference between the derived slopes is 2.6 $torr^{-1}$ which is 6.8% of the average value of 37.6 ± 1.0 $torr^{-1}$. The quoted error is the 2σ value. The measured absorbance in terms of the integrated line strength is 6% lower than the published literature value.[26] It is concluded that the error of the CO_2 absorbtion measurement resulting from the uncertainty of setting the IR laser at the peak resonance absorption frequency of CO_2 is less than 10%.

It was noticed that the absorption line width of CO_2 was broadened by CH_3CHO and NO_2. The measured absorption coefficients of CO_2 without and with CH_3CHO and NO_2 are

shown in Figure II-12. With 0.350 torr of NO_2 and 6.000 torr of CH_3CHO, and CO_2 pressures from 11.5 to 53.2 mtorr, the measured CO_2 absorption coefficient is 0.187 ± 0.005 $torr^{-1}$ cm^{-1}. The absorption coefficient of pure CO_2 with no pressure broadening is 0.241 $torr^{-1}$ cm^{-1}.

The absorption of CO_2 summed over 5 photolysis pulses, shown in Figure II-10, is 1154 counts*, which is the average of all the data points from 20 to 120 μs after the photolysis shot. Thus the absorption for each laser pulse is 230.8 counts. The total IR power was 2600 counts. The IR power normalization factors were 2.638 and 2.652 respectively (see Section 2.2). The absorbance ($-\ln(I/I_0)$) was then calculated to be 0.0935. Therefore, the column density of CO_2 formed for each photolysis shot was 1.62×10^{16} cm^{-2}.

(2). Calculation of the CO_2 Yield

There are reactions in the system other than HCO + NO_2 which can lead to the production of CO_2. The complete

---

* The number of counts is linearly proportional to the absorption signal amplitude.

Figure II-12. Peak absorbance of CO_2 versus its pressure measured with and without pressure broadening using the transient digitizer.
▼ - with 6.000 torr of CH_3HCO and 0.350 torr of NO_2.
▽ - only CO2.
The slopes of the linear least-squares fits (the solid and the dashed lines) are $(3.01 \pm 0.16) \times 10^{-2}$ and $(3.89 \pm 0.10) \times 10^{-2}$ $torr^{-1}$ respectively.

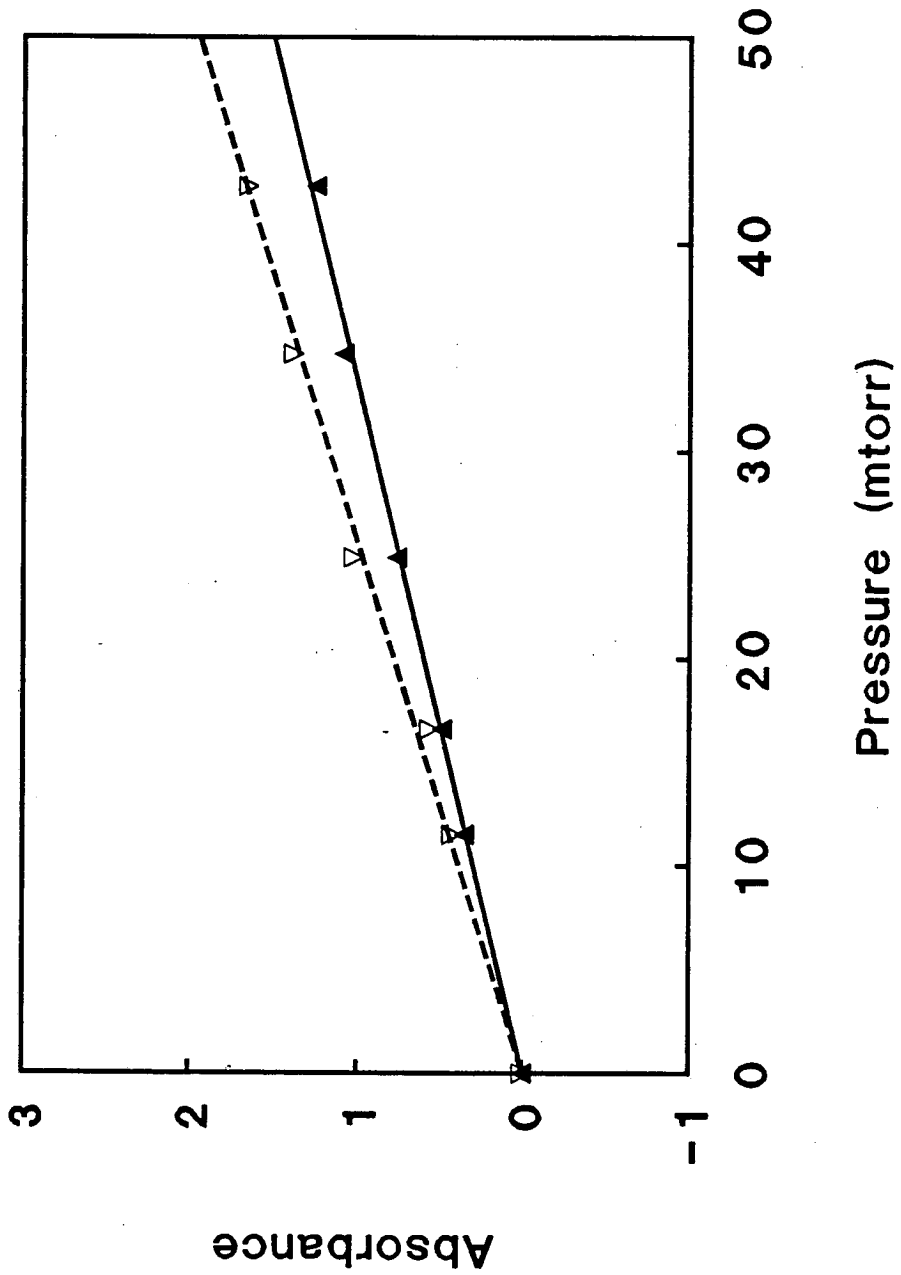
Absorbance
3
2
1
0
-1
0
10
20
30
40
50
Pressure (mtorr)

reaction scheme is*:

$CH_3CHO + h\nu \rightarrow HCO + CH_3$ (I)

$\rightarrow CH_4 + CO$ (II)

$\rightarrow H + CH_3CO$ (III)

$HCO + NO_2 \rightarrow H + CO_2 + NO$ (1a) $k_1 = 5.70 \times 10^{-11}$

$\rightarrow HONO + CO$ (1b)

$\rightarrow HNO + CO_2$ (1c)

$H + NO_2 \rightarrow OH + NO$ (2) $k_2 = 1.25 \times 10^{-10}$ [27]

$H + CH_3CHO \rightarrow H_2 + CH_3CO$ (2') $k_{2'} = 9.80 \times 10^{-14}$ [28]

$OH + CH_3CHO \rightarrow CH_3CO + H_2O$ (3) $k_3 = 1.60 \times 10^{-11}$ [29]

$CH_3CO + NO_2 \rightarrow CO_2 + CH_3 + NO$ (4) $k_4 = 2.5 \times 10^{-11}$ [30]

$NO_2 + h\nu \rightarrow NO + O$

$O + CH_3CHO \rightarrow OH + CH_3CO$ (5) $k_5 = 4.82 \times 10^{-13}$ [31]

$O + NO_2 \rightarrow NO + O_2$ (6) $k_6 = 9.50 \times 10^{-12}$ [32]

$CH_3 + NO_2 \rightarrow CH_3O + NO$ (7a) $k_{7a} = 2.51 \times 10^{-11}$ [33]

$CH_3 + NO_2 + M \rightarrow CH_3NO_2 + M$ (7b) $^{**}k_{7b} = 9.87 \times 10^{-28}$ [34]

$\rightarrow CH_3ONO + M$ (7c) $k_{7c}/k_{7b} = 2.17$ [35]

---

* Units of the rate constants(k): $cm^3\ molec^{-1}\ sec^{-1}$.

** The unit of k_{7b} is: $cm^6\ molec^{-2}\ sec^{-1}$; M = Ar.

$CH_3 + CH_3CHO \rightarrow CH_4 + CH_3CO$ (8) $k = 5.61 \times 10^{-18}$ [36]

$CH_3O + NO_2 \rightarrow CH_3ONO_2$ (9) $k = 3.18 \times 10^{-12}$ [37]

According to the mechanism described above, CH_3CO and H radicals formed from the photodissociation of CH_3CHO, and O atom from NO_2, eventually all lead to CO_2 production via reaction (4). Since the concentration ratio of CH_3CHO and NO_2 is greater than 10:1, reaction (2) is about 100 times faster than reaction (2'). Thus only reaction (2) is considered to be responsible for the removal of H atoms. On the other hand the removal rates of O atoms by reactions (5) and (6) are comparable under the experimental conditions. The fraction of O atoms removed through reaction (5) was calculated as $k_5 \cdot [CH_3CHO]/(k_5 \cdot [CH_3CHO] + k_6 \cdot [NO_2])$.

When the UV photon flux was 2.26×10^{16} cm^{-2} (14.6 mJ cm^{-2}), and CH_3CHO and NO_2 pressures were 6.049 and 0.281 torr, the column densities of HCO, H, and O radicals formed from UV photolysis were 1.13×10^{16}, 0.0642×10^{16}, and 0.297×10^{16} cm^{-2}. The column density of CH_3CO generated by photolysis was the same as that of H atom (reaction (III)). While each H and CH_3CO radical produced one CO_2, each HCO reacted with NO_2 via reaction (1a) produced two CO_2. The column density of CO_2 produced due to reaction (5) was 0.310×10^{16} cm^{-2}. The total column

density of CO_2 measured in the experiment was 1.62×10^{16} cm^{-2}. After correcting for the CO_2 production from reactions initiated by CH_3CO, H and O radicals, it is concluded that 52.5% of HCO which reacts with NO_2 formed CO_2.

Five sets of experimental data using various CH_3CHO and NO_2 pressures give the result that 52% of the HCO + NO_2 reaction goes to the H + CO_2 + NO product channel. Considering the upper limit of 10% for CO_2 production from the HNO + CO_2 channel, the HCO + NO_2 → H + CO_2 + NO channel is responsible for 45% to 52% of the reaction.

(3). Error Estimation

The errors arising from the measurements involved in this experiment all made contributions to the uncertainty in the determination of CO_2 yield. The estimated error of each measurement is given below:

(1) gas pressure, 1%; gas flow, 3% each;
(2) UV absorption coefficients of CH_3CHO and NO_2, 3% each;
(3) UV and IR laser power normalization, 5 % each;
(4) absolute UV power, 10%;
(5) cw absorption coefficient of CO_2, 10%;

(6) transient CO_2 absorption intensity, 5%;

The estimated error considering contributions from the uncertainties listed above is less than 15% of the CO_2 yield obtained. Since the calculation for the final yield of CO_2 is also directly related to the quantum yields of the photodissociation processes of CH_3CHO at 308 nm, and rate constants of reaction (5) and (6), the overall uncertainty in determining the CO_2 yield is larger than 15%. The quoted errors of the rate constant measurements for reactions (5) and (6) are ±14%[30] and ±12%[31]. Assuming the error of the quantum yield measurements for the photodissociation of CH_3CHO at 308 nm is ±10%, then the total CO_2 yield from the reaction of HCO + NO_2 should be 0.52 ± 0.14.

(4). Detection of Vibrationally Excited CO_2

It has been noticed that the rise of the (0,0,0) state CO_2 is slower than the reaction rate. Some CO_2 in the (0,1,0) state has been observed by monitoring the R(16) line in the (1,1,1) ← (0,1,0) hot band at 3735.63 cm^{-1}.[25] Strong infrared emission has also been observed when H_2CO and NO_2 were photolyzed at 308 nm. The emission signal was weaker when CH_3CHO was used as the HCO

precursor, most likely due to the energy transfer between CO_2 and CH_3CHO being more efficient than that between CO_2 and H_2CO. The emission signal was identified to be from vibrationally excited CO_2 by using narrow band IR filters and by using room temperature CO_2 as collision buffer gas. About 70% of the observed emission was from the CO_2 whose asymmetric stretching mode was excited. The other about 30% of the emission signal was at higher frequency (>2450 cm^{-1}). It is possible that the excited HONO (O-H stretching mode) was responsible for that. The emission signal gradually disappeared when 1 to 10 torr of room temperature CO_2 were added.

3.3.3 CO and HONO Detection

An attempt was made to measure transient CO as a reaction product by monitoring its absorption at 4285.009 cm^{-1}, corresponding to the R(6) line in the 2-0 overtone band.[38] This experiment failed due to limited detection sensitivity. At room temperature, the absorption strength of CO at 4285.009 cm^{-1}, which corresponds to one of the strongest absorption lines of CO in the 2-0 band, is about 17 times weaker than that of CO_2 at 3728.41 cm^{-1}.[26,39]

HONO is relatively unstable at room temperature, but

it can be generated in a mixture of NO, NO_2, and H_2O through the reaction $NO + NO_2 + H_2O = 2HONO$, with the equilibrium constant $K = 1.36\ atm^{-1}$.[40] HONO has two isomeric forms, cis and trans. HONO exists 33.5% in the cis form and 66.5% in the trans form at 296 K.[41] The high resolution absorption spectrum of the O-H stretching in HONO has been recorded.[42] Small portions of the Q branch absorption spectrum of the O-H stretching in trans-HONO were measured in the present work, as shown in Figure II-13. All together 10 torr of NO, 0.5 torr of NO_2, and 0.3 torr of H_2O were added into the photolysis cell to produce HONO through the equilibrium reaction. Transient HONO produced by the reaction of $HCO + NO_2$ was then measured by setting the probe laser at a HONO resonance absorption frequency. In Figure II-14, the transient absorption HONO was first averaged over 80 photolysis shots with the IR laser tuned at 3590.41 cm^{-1}, then a total of 80 shots were subtracted from the trace with the IR laser tuned off the resonance to 3590.20 cm^{-1}, in order to eliminate the shock wave signal.

Since the signal-to-noise ratio is relatively low for detecting transient HONO absorption as shown in Figure II-14, it is quite difficult to measure the yield of HONO quantitatively. Moreover unlike the case of HNO detection, here it is not obvious that a good reference

Figure II-13. HONO cw absorption spectrum recorded with the IR difference frequency laser system. HONO was generated through the reaction $NO + NO_2 + H_2O \rightleftharpoons 2HONO$, with 10 torr of NO, 0.5 torr of NO_2, and 0.3 torr of H_2O. The peak at 3590.41 cm^{-1} corresponds to 57% absorption of the total IR light.

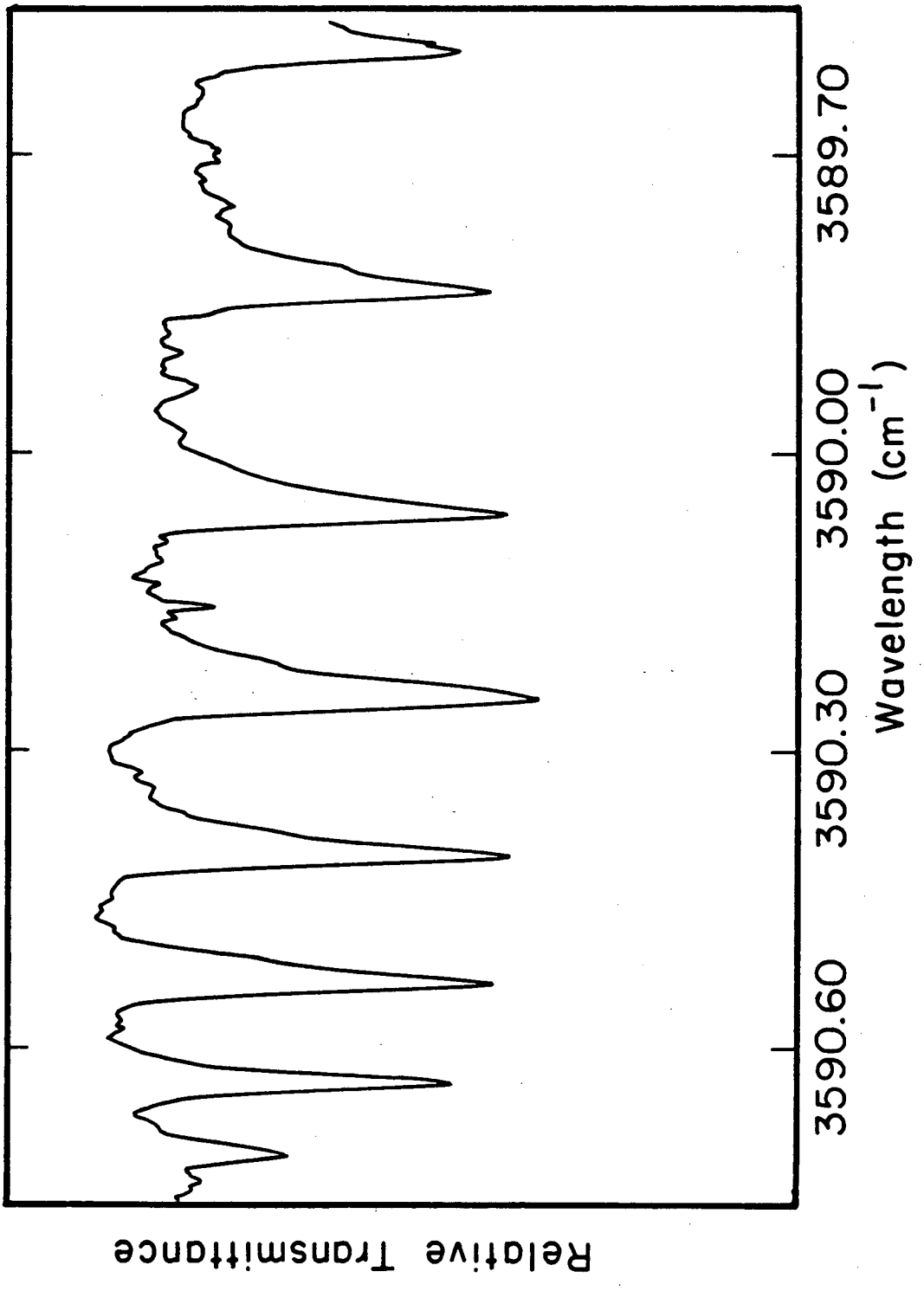
Relative Transmittance
3590.60
3590.30
3590.00
3589.70
Wavelength (cm^{-1})

Figure II-14. HONO produced by the reaction of HCO + NO_2 was monitored at 3590.41 cm^{-1}. The signal was averaged over 80 photolysis shots with $P(CH_3CHO)$ = 6.200 torr, and $P(NO_2)$ = 0.285 torr.

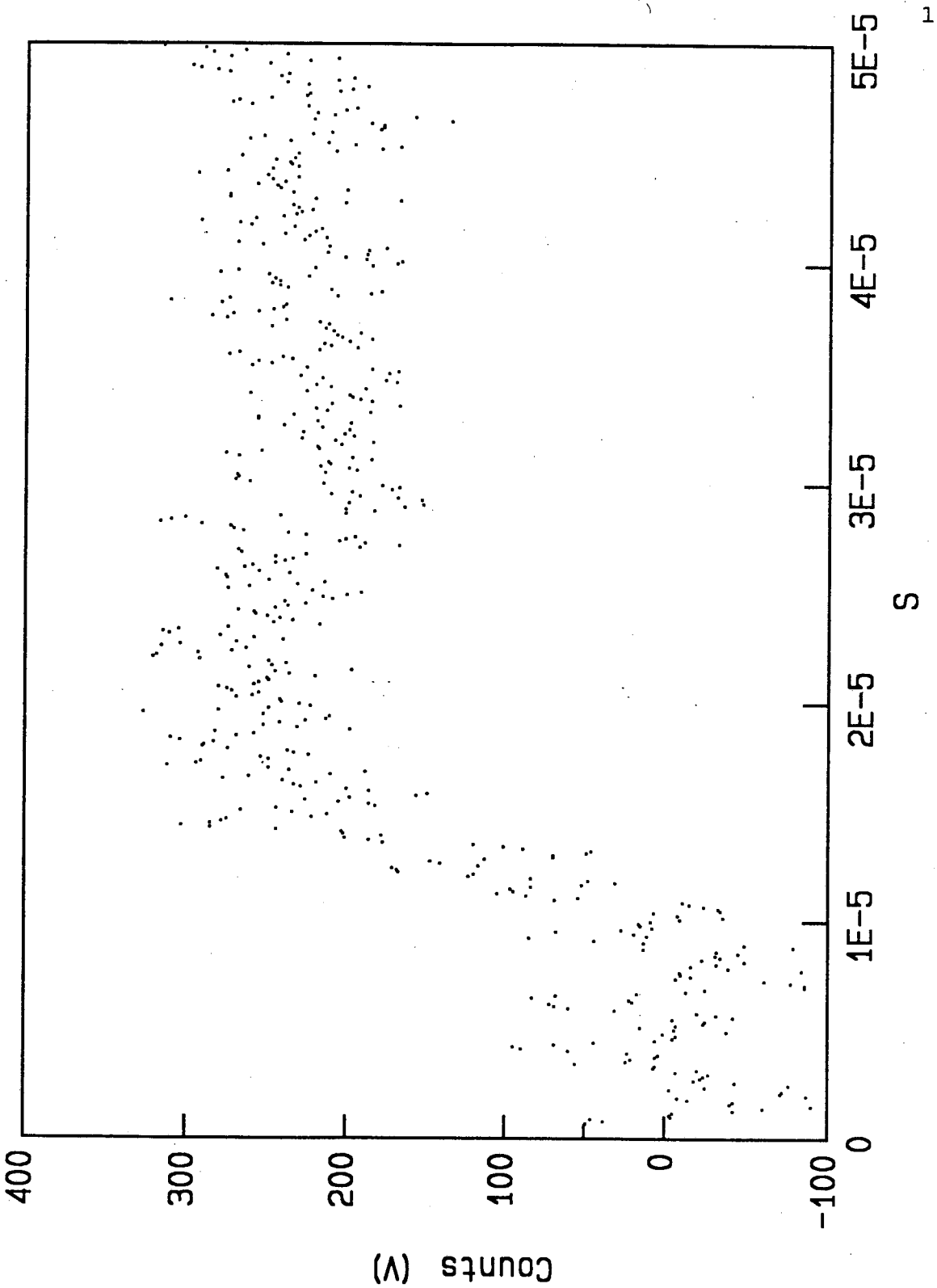
Counts (V)
400
300
200
100
0
-100
0
1E-5
2E-5
3E-5
4E-5
5E-5
S

system can be easily chosen. Although the absorption of HONO produced by the equilibrium reaction NO + NO_2 + H_2O = 2HONO can be used as a reference for the HONO transient absorption calibration, extrapolation of the absorption intensity to eliminate pressure broadening is necessary. Since NO_2 and especially H_2O adsorb strongly to the cell wall at room temperature, it is difficult to measure the pressure of NO_2 and of H_2O in the cell, therefore the concentration of HONO cannot be accurately determined. No attempt has been made to measure the HONO yield from the reaction of HCO + NO_2 quantitatively.

4. Discussion

Timonen et al.[5] have shown that the reaction rate constant for the HCO + NO_2 reaction is inversely related to the temperature. The negative apparent activation energy indicates that complex formation is the first step in this reaction, although the measurement of the pressure dependence of the rate constant up to 700 torr does not provide evidence for the stabilization of the complex. Complex formation rather than direct hydrogen abstraction has been established as the mechanism of the reaction between HCO and NO.[24] It is indicated in Figure II-1 that the H + CO_2 + NO product channel is only correlated with the HCOONO complex. On the other hand, HONO can be formed via both HCOONO and $HCONO_2$ complexes. If HCOONO is formed, it is more likely to dissociate into H + CO_2 + NO than to form HONO + CO, since the former dissociation process has a much lower exit barrier than the latter. Therefore, it is possible that only reaction via the $HCONO_2$ complex leads to HONO formation. In any case, the dissociation of HCOONO to form H + CO_2 + NO should be much faster than other processes because of the low exit barrier. Consequently the dependence of the decay rate of HCO on buffer gas pressure should be small since the reaction complex has a very short life time. The mechanism for formation and collisional stabilization of

reaction intermediates has been discussed in detail in Reference 24.

The exothermicities for the H + CO_2 + NO and the HONO + CO channels are 37.3 and 62.4 kcal·mole^{-1}, respectively.[22] These excess energies should be partitioned among the vibrational, rotational, and translational degrees of freedom of the products in each channel. The observation of CO_2 in the (0,1,0) state and that of CO_2 IR emission indicate that some of the CO_2 produced in the reaction are vibrationally excited. However, it is possible that some of these excited CO_2 molecules are from the reaction between CH_3CO and NO_2.[30] The rise of the ground state HONO is not single exponential indicating that the initial HONO produced in the reaction is also vibrationally excited.

The dissociation energy of HONO to form OH + NO is 49.9 kcal mole^{-1}.[22] There is a 12.5 kcal mole^{-1} exothermicity for the OH + NO + CO product channel, which corresponds to 20% of the total amount of energy released when HONO and CO are formed. However, the amount of energy distributed among the CO vibrational and rotational, and the translational degree of freedom is expected to be larger than 12.5 kcal mole^{-1}, preventing significant dissociation of HONO to form OH + NO. This is

supported by the direct observation of HONO as a reaction product in this experiment. Unless the internal energy of HONO is less than or very close to its dissociation threshold, the dissociation rate of HONO to form OH + NO should be too fast to allow the transient absorption of HONO to be observed. Moreover, the rise of the ground state HONO is comparable to the reaction rate, indicating that HONO produced by the HCO + NO_2 reaction was not highly vibrationally excited, although it does not fit to a single exponential function well. However, since the HONO yield from the reaction was not quantitatively measured, it is still possible that some of the HONO molecules dissociated to form OH + NO, which in turn will affect the CO_2 yield measurement. The OH + NO + CO product channel may become significantly accessible for the reaction between HCO and NO_2 at high temperature as in combustion processes.

Several groups have studied the thermal reaction of H_2CO and NO_2 in the temperature range of 118-203 °C.[43-46] Since the primary products of this reaction were proposed to be HCO and HONO,[47] the reaction between HCO and NO_2 was also investigated as a secondary reaction in some of those studies.[45,46,48] The most recent work was carried out by M.C. Lin et al..[46] By modeling the concentration-time profiles of H_2CO, CO, CO_2, and NO as the reactant and

products of the related reactions, recorded using FTIR, they derived the rate constants for forming HONO + CO and H + CO_2 + NO products from the HCO + NO_2 reaction; they are 2.8 X 10^{-11} and 1.4 X 10^{-11} cm^3 $mole^{-1}$ sec^{-1} between 393 to 476 K, respectively. Lin et al.'s result in terms of CO_2 quantum yield is 33% - compared to 52% reported in this work. The two studies were carried out at significantly different temperatures; nonetheless, the results are in agreement within the experimental errors. It has been reported by Calvert et al.[49] that at least some of the HCO produced by the reaction of H_2CO + OH is vibrationally excited and dissociates spontaneously to form H + CO. This reaction (HCO† → H + CO) was not considered in the reaction mechanism used by Lin and coworkers in their kinetic modeling. Depending on the extent of this dissociation process occurs, it may change the rate constants corresponding to HONO + CO and H + CO_2 + NO channels resulting from the kinetic modeling reported by Lin and coworkers.

Appendix

Upgrading the Difference Frequency Laser Spectrometer

The IR difference frequency laser system used in this work has been described in detail in Reference 10. Some modifications made on the system in the last few years are discussed in the following three sections.

(1). Reconstruction of the Temperature-Phase-Matching Oven

The oven used for temperature phase matching in the difference frequency laser set-up consists of an oven core placed inside of a stainless steel jacket, a heating system, and an electronic controller. It was originally built by Chromatix Co. which does not exist any more. The oven core was made of two pieces of nickel-coated copper which were brazed together. Copper has high heat conductivity; nickel is relatively inert. Two pieces of heating wire, one for main heating, the other for gradient heating, were wound around the core. Two thermocouples with the joints buried under the two pieces of heating wire were used as temperature sensors. A small piece of mica was placed between the oven core and each

thermocouple joint to prevent the thermocouple being shorted out on the oven core.

Since the oven was heated constantly in an oxygen rich atmosphere to as high as 450 °C, the heating wire and the thermocouples were gradually oxidized. As a result the temperature of the oven could not be well regulated by the controller. The heating wire was rewound following the instructions available from people who formerly worked for Chromatix Co. and the thermocouples were replaced. The resistance of the main heater wire and the gradient heater wire were 2.8 and 6.19 Ω per feet, respectively. In the present version of the oven, Gauge 27 and 30 nichrome 80 (Pelican) heater wire with double fiberglass sleeving are used for main and gradient heating, respectively. Iron/constantan thermocouples (Omega Engineering, Inc./Type J/AWG-30) were used. Size 22 and 24 fiberglass sleevings made for high temperature application to 1200 °F were bought from Daburn Electronics and Cable Corp.

Each dimension of the cross section of the oven cavity is about 0.01" larger than that of the crystal. This allows the crystal to be easily slid in and out of the oven cavity. However oxidized material gradually comes out of the thin groove where the two pieces of

nickel-coated copper are joined together, and can reduce the cavity size to the extent that the crystal could be squeezed to crack. Therefore it is important to take the crystal out and check the cavity every few months or so. The oxidized material can be polished off using fine silicon carbide paper. It is possible to make an oven core out of a whole piece of metal by broaching or electrical discharging. Both machine shops at the Physics Department (UCB) and LBL have electrical discharge machines.

(2). Present Design and Performance of the IR Difference Frequency Laser Spectrometer

An upgraded Ar^+ laser (Spectra Physics/2030-18) has been used to pump the ring dye laser. With 4 W Ar^+ laser pumping, at least 800 mW of dye laser power can be obtained at the peak of the R6G dye lasing wavelength. The single frequency Ar^+ laser (Lexel/94-5) can be operated either at 514.5 or 488 nm depending on the absorption frequency of the species being studied. The typical IR power generated was on the order of 10 μw. With the crystal presently used, the phase matching temperature for 3730 cm^{-1} is 292 °C. The IR light can be generated over a frequency range of 6 to 9 wavenumbers at

a fixed oven temperature.

House oxygen was used for providing an oxygen rich environment for the $LiNbO_3$ crystal. Instead of having oxygen flow through the metal tube placed between the oven core and the jacket, an external flowing scheme was designed which allows the oxygen flow to be checked easily. Two pieces of thin metal tube were connected to the teflon tubing conducting oxygen, and then each was placed at one end of the oven. Some oxygen also flowed through the heater shields placed one at each end of the oven.

The frequency range covered by the present difference frequency system using the $LiNbO_3$ crystal is about 2,450 to 4,400 cm^{-1}. Although most O-H, N-H, and C-H stretching fundamental bands fall into this frequency range, a wider tuning range is definitely useful and sometimes it is necessary as discussed in both parts of this work. A new type of crystal, $LiIO_3$ (Cleveland Crystals Inc./$2756), can be used as a nonlinear mixing element to generate IR light from 1,850 to 5,300 cm^{-1}. However, since the indices of refraction in $LiIO_3$ are almost temperature independent, the phase matching condition has to be achieved by angle tuning. Oka's group has built such a system using Volkov et al.'s work as a

guide.[43] They used two crystals in a mirror image configuration to compensate the "walk off" arising because of the $LiIO_3$ crystal has to be angle tuned. The total IR power they got is on the order of 10 times lower than what they got out of their $LiNbO_3$ system.

(3). New Data Acquisition System

A Fountain/XT personal computer has been interfaced to control the temperature of the crystal oven and the dye laser scanning, and to store the data. The new interface system (Keithley/System 500-570) has a standard channel capacity of 32 single-ended or 16 differential analog inputs, 2 analog outputs (12-bit), 16 digital outputs, and 16 digital inputs. In addition, one 16-bit one-channel high resolution analog output board was purchased. This 16-bit analog output (ETALON RAMP) and one of the 12-bit analog outputs (XTAL RAMP) were used to provide 0 to 10 Volt ramps for scanning the ring dye laser and for tuning the temperature of the oven. Other detailed information about the interface system can be found in the manual of the System 570.

A total of 10 differential analog input channels have been brought out to the front pannel of the

difference-frequency-laser interface box. These channels are labled: BOX1 IN; BOX2 IN; BOX3 IN; ETALON IN; IODINE IN; REF IN; LASER POWER IN; AUX1 IN; AUX2 IN; AUX3 IN. The digital outputs are TTL pulses. The output from the BOXCAR TRIGGER was used to trigger the excimer laser after the pulse being converted into 15 V (to 50 Ω) by a amplifier (DWG 1314).

The software package (Keithley/Soft500) which came with the interfacing system has a number of subroutines which can be used very conveniently. However, since the subroutines can only be used with Basic programming and they are not optimized for any particular task, the running speed is relatively slow. The version of the program which can handle 2 digital outputs, 2 analog outputs, and 4 analog inputs was written in Turbo Basic (DIFF_SPC.BAS). It can be used to operate the present data acquisition system with the excimer laser running up to 20 Hz. For even faster repetition rates, a higher level computer language is needed. For example, with Turbo C language, a factor of ten could be gained for the running speed.[44]

References

1. B. M. Morrison, Jr., and J. Heicklen, J. Photochem. 15, 131-145 (1981).

2. A.V. Topchiev, A.P. Ballod, T.V. Fedorova, and V.Y. Shtern, Pet. Chem. USSR, 2, 150 (1962).

3. D. Barton, J. Phys. Chem. 65, 1831 (1961).

4. R.A. Fifer, 17th International Symposium on Combustion (The Combustion Institute, Pittsburg, 1979) p.587.

5. R. S. Timonen, E. Rarajczak, and D. Gutman, J. Phys. Chem. 92, 651-655 (1988).

6. B.M. Morrison, Jr., and J. Heicklen, J. Photochem. 13, 189-199 (1980).

7. C. F. Melius, Private communication.

8. H. C. Hamann and D. Swern, Tetrahedron Letter No.28, pp.3303-3308 (1966).

9. A.O. Langford, Ph. D. thesis, U.C. Berkeley, 1983.

10. H. Petek, Ph. D. thesis, U.C. Berkeley, 1985.

11. J.E. Baggott, H.M. Frey, P.D. Lightfoot and R. Walsh, Chem. Phys. Lett. 132, 225 (1986).

12. Part I, Section 2.1 of this work.

13. Part I, Section 2.2 of this work.

14. D.A. Hansen and E.K.C. Lee, J. Chem. Phys. 63, 3272 (1975).

15. The sum of the quantum yields for processes (I), (II), and (III).

16. Chemical Kinetics and Photochemical Data for Use in Stratospheric Modeling (JPL publication 83-62), Sept. 15, 1983.

17. A. Horowitz, C.J. Kershner, and J.G. Calvert, J. Phys. Chem. 86, 3094-3105 (1982).

18. A. Horowitz and J.G. Calvert, J. Phys. Chem. 86, 3105-3114 (1982).

19. Canadian National Research Council Depository for Unpublished Data.

20. R.J. Gill, and G.H. Atkinson, Chem. Phys. Lett. 64, 426 (1979).

21. B.M. Stone, M. Noble and E.K.C. Lee, Chem. Phys. Lett. 118, 83 (1985).

22. Kinetic and photochmical data for atmospheric chemistry, J. Phys. Chem. Ref. Data, Vol. 9, No.2, 1980.

23. J.W.C. Johns, A.R.W. McKellar, and E. Weinberger, Can. J. Phys. 61 (7) 1106-1119 (1983).

24. A.O. Langford and C.B. Moore, J. Chem. Phys. 80, 4211 (1984).

25. H.R. Gordon and T.K. McCubbin, Jr., J. Molec. Spectrosc. 19, 137-154 (1966).

26. C.M. Deeley and J.W.C. Johns, J. Molec. Spectrosc. 129, 151-159 (1988).

27. B.S. Agrawalla, A.S. Manocha, and D.W. Setser, J. Phys. Chem. 85, 2873 (1981).

28. J.V. Michael and J.H. Lee, Chem. Phys. Lett. 51, 303 (1977).

29. R. Atkinson and J.H. Pitts, Jr., J. Chem. Phys. 68, 2992 (1978).

30. I.R. Slagle and D. Gutman, J. Am. Chem. soc. 104, 4741-48 (1982).

31. S. Mori, Bull. Inst. Chem. Res., Kyoto Univ. 59, 116 (1981).

32. P.P. Bemand, M.A.A. Clyne, and R.T. Watson, J. Chem. Soc. Faraday Trans. 270, 564 (1974).

33. F. Yamada, I.R. Slagle, and D. Gutman, Chem. Phys. Lett. 83, 409 (1981).

34. K. Glaenzer, and J. Troe, Ber. Bunsenges. Phys. Chem. 78, 182 (1974).

35. A.M. Davis, and W.H. Corcoran, Ind. Eng. Chem., Fund. 11, 431 (1972).

36. J.A. Kerr and S.J. Moss, Handbook of Bimolecular and Termolecular Gas Reactions, Vol. 1, CRC Press, 1981.

37. J.M. Caulley, S.M. Anderson, J.B. Jeffries, and F. Kaufman, Chem. Phys. Lett. 115, 180 (1985). H.A. Wiebe, A. Villa, T.M. Hellman, and J. Heicklen, J. Am. Chem. soc. 95, 7 (1973).

38. C.R. Pollock, F.R. Peterson, D.A. Jennings, J.S. Wells, and A.G. Maki, J. Molec. Spectros. 99, 357-368 (1983).

39. C.L. Korb, R.H. Hunt, and E.K. Plyler, J. Chem. Phys. 48, 4252 (1968).

40. P.G. Ashmore and B.J. Tyler, J. Chem. Soc. 1017 (1961).

41. R.H. Kagann and A.G. Maki, J. Quant. Spectrosc. Radiat. Transfer, 30, pp.37-44 (1983).

42. A.G. Maki and T.R. Todd, private communication.

43. F.H. Pollard and R.M.H. Wyatt, Trans. Faraday Soc. 45, 760 (1949).

44. F.H. Pollard and P. Woodward, Trans. Faraday Soc. 45, 767 (1949).

45. D. Barton, J. Phys. Chem. 65, 1831 (1961).

46. Y. He, E. Kolby, P. Shumaker, and M.C. Lin, to be published.

47. J.H. Thomas, Trans. Faraday Soc. 49, 630 (1953).

48. R. Show, J. Chem. Soc. 1517 (1964).

49. A. Horowitz, F. Su, and J.G. Calvert, Int. J. Chem. Kinet. X, 1099-1117 (1978).

50. S.Yu. Volkov, D.N. Kozlov, P.V. Nikles, A.M. Prokhorov, V.V. Smirnov, and S.M Chuksin, Sov. J. Quantum Electronics, 11, 135 (1981).

51. Henry Chen, Electronic Shop, Chemistry Department, UCB.

LAWRENCE BERKELEY LABORATORY
TECHNICAL INFORMATION DEPARTMENT
1 CYCLOTRON ROAD
BERKELEY, CALIFORNIA 94720